

TD
224
T4
T38
no.177

TR-177

SPATIAL WATER BALANCE IN TEXAS

Seann Reed
David Maidment
Jérôme Patoux

TEXAS WATER RESOURCES INSTITUTE

TEXAS A&M UNIVERSITY

AUGUST 1997

Spatial Water Balance of Texas

Seann Reed
David R. Maidment
Jérôme Patoux

Project Number UTA-94-1
September 1, 1994 - August 31, 1995
Grant Number 14-08-001-G2048

The research on which this report is based was financed in part by the U.S. Department of the Interior, U.S. Geological Survey, through the Texas Water Resources Institute. Non-Federal matching funds were provided by the University of Texas at Austin and the Texas Water Development Board.

Contents of this publication do not necessarily reflect the views and policies of the Department of the Interior, nor does mention of trade names or commercial products constitute their endorsement by the United States Government or the Texas A&M University System.

Technical Report No. 177
Texas Water Resources Institute
The Texas A&M University System
College Station, TX 77843-2118

August 1997

All programs of the Texas Water Resources Institute and the Texas Agricultural Experiment Station are available to everyone regardless of socioeconomic level, race, color, sex, religion, handicap, national origin or age.

TD
224
T4
T38
no. 177

TABLE OF CONTENTS

1. INTRODUCTION	6
2. LITERATURE REVIEW	9
2.1 <i>Atmospheric Water Balance Studies</i>	9
2.2 <i>Soil Water Balance Studies</i>	10
2.3 <i>Surface Water Balance Studies</i>	11
2.3.1 <i>Water Balances of Texas</i>	11
2.3.2 <i>Runoff Mapping</i>	12
3. ATMOSPHERIC WATER BALANCE	14
3.1 <i>Atmospheric Data</i>	14
3.2 <i>Methodology</i>	15
3.2.1 <i>Water Balance Equations</i>	15
3.2.2 <i>A Control Volume over Texas</i>	17
3.2.3 <i>Direct Computation and Flux Integration Approaches to Estimate Divergence</i>	18
3.2.3.1 <i>Divergence approach</i>	18
3.2.3.2 <i>Flux integration approach</i>	21
3.3 <i>Results and Discussion</i>	23
3.3.1 <i>Results</i>	23
3.3.2 <i>Sources of error</i>	29
3.3.3 <i>Summary and Discussion</i>	31
4. SOIL-WATER BALANCE	33
4.1 <i>Methodology</i>	33
4.1.1 <i>Model Description</i>	33
4.1.2 <i>Description of input data</i>	34
4.1.2.1 <i>Climate data</i>	34
4.1.2.2 <i>Water-holding capacity data</i>	34
4.1.2.3 <i>Open Water Evaporation Estimates</i>	36
4.1.2.4 <i>Radiation Data</i>	39
4.1.3 <i>Water-holding capacity of the soil</i>	39
4.1.4 <i>Estimating Actual Evapotranspiration</i>	40
4.1.5 <i>Budgeting soil moisture to yield surplus</i>	41
4.1.6 <i>Balancing Soil Moisture</i>	42
4.2 <i>Potential Evapotranspiration</i>	43
4.2.1 <i>Potential evaporation vs. potential evapotranspiration</i>	43
4.2.2 <i>Penman combination method</i>	44
4.2.3 <i>Simpler Methods</i>	45
4.2.3.1 <i>Pan coefficients</i>	45
4.2.3.2 <i>Priestley-Taylor Method</i>	46
4.2.3.3 <i>Comparison of Pan and Priestley-Taylor Methods</i>	47
4.3 <i>Results</i>	51
4.4 <i>Summary</i>	55
5. SURFACE WATER BALANCE	56

5.1 Overview	56
5.2 Methodology	57
5.2.1 Digital Elevation Model Processing	57
5.2.2 Selecting Gaging Stations for Analysis	62
5.2.3 Watershed Delineation	63
5.2.4 Compiling Watershed Attributes	66
5.2.4.1 <i>Determining Mean Precipitation and Net Inflow</i>	66
5.2.4.2 <i>Reservoir Evaporation</i>	68
5.2.4.3 <i>Urban Land Use</i>	69
5.2.4.4 <i>Recharge</i>	69
5.2.4.5 <i>Springs</i>	70
5.3 Results and Discussion	71
5.3.1 Expected Runoff	71
5.3.2 Mapping Actual Runoff and Evaporation	77
5.3.3 Mapping the Bowen Ratio	88
5.3.4 Summary Tables	91
5.3.5 Summary and Discussion	93
6. CONCLUSIONS	96
7. ACKNOWLEDGEMENT	99
8. REFERENCES	100
9. APPENDIX	104

LIST OF TABLES

Table 3-1: Comparison of Netflux and Throughflux in 1977	30
Table 4-1 : Typical Values for Soil-water Parameters by Texture	40
Table 5-1: Summary of Annual Hydrologic Cycle Fluxes by River Basin	91
Table 5-2: Examining the Influence of Reservoirs on Runoff	93

LIST OF FIGURES

Figure 1-1: Mean Annual Rainfall in Texas from Oregon State PRISM Study (Daly, 1994)	8
Figure 3-1: 2° Cells Overlaid on the Texas Border	17
Figure 3-2: Dimensions of a 2° Atmospheric Column in South Texas	18
Figure 3-3: Computational Mesh for Divergence Calculations	20
Figure 3-4: Computational Cells Intersected with the Generalized Boundary of Texas	20
Figure 3-5: Vector Cross Product	21
Figure 3-6: Monthly Divergence of Water Vapor Over Texas for 22 Years	24
Figure 3-7: Yearly Mean Divergence of Water Vapor Over Texas (1973 - 1994)	24
Figure 3-8: Net Influx of Water to the Atmosphere Above Texas, June 1991 - July 1993	25
Figure 3-9 : Evaporation Estimates from Bradley Divergence + Precipitation in 1992	26
Figure 3-10: Evaporation Estimates from NMC Divergence + Precipitation	26
Figure 3-11: Moisture Flux Vectors in January, 1973	27
Figure 3-12: Moisture Flux Vectors in July, 1973	28
Figure 3-13: Moisture Flux Vectors in July, 1993	29
Figure 4-1: Soil-water Holding Capacity (mm)	35
Figure 4-2: One Degree Quadrangle Index Map	37
Figure 4-3: Mean Annual Reservoir Evaporation (mm), TWDB, 1995	38
Figure 4-4: Mean Annual Temperature in Texas from Legates and Willmott Climatology	48
Figure 4-5: Mean Annual Net Radiation Estimates from the ERBE Program	49
Figure 4-6: Priestley-Taylor Potential Evaporation (mm/year)	50
Figure 4-7: Annual Surplus from Soil-water Balance	52
Figure 4-8: Soil-water Balance Monthly Results for Two Cells	53
Figure 4-9: Mean Annual Soil Moisture (mm)	54
Figure 4-10: Mean Annual Saturated Fraction of Soil-water Holding Capacity	54
Figure 5-1: Drainage Network Delineation	58
Figure 5-2: Processed Digital Elevation Model	60
Figure 5-3: EPA River Reach File 1 Streams	61
Figure 5-4: USGS Flow Gaging Stations	63
Figure 5-5: 166 Delineated Watersheds	65
Figure 5-6: Watershed Areas Reported By USGS versus Areas Defined by DEM for All But 16 Watersheds	66
Figure 5-7: Grid of Mean Annual Precipitation	67
Figure 5-8: Average Annual Recharge (mm/year) Based Upon DRASTIC Ratings	70
Figure 5-9: Runoff vs. Rainfall for All Watersheds	72
Figure 5-10: 90 Selected Watersheds	74
Figure 5-11: Runoff vs. Rainfall for Selected Watersheds	75
Figure 5-12: "Expected" Annual Runoff Coefficient	76
Figure 5-13: "Expected" Mean Annual Runoff	78
Figure 5-14: Actual - "Expected" Runoff	79
Figure 5-15: Actual Mean Annual Runoff	80
Figure 5-16: "Expected" Accumulated Runoff	82
Figure 5-17: Actual - "Expected" Accumulated Runoff	83
Figure 5-18: Actual Accumulated Runoff	84
Figure 5-19: Accumulated Runoff in the San Antonio and Guadalupe Basins	85
Figure 5-20: Deviations from "Expected" Accumulated Runoff in the Guadalupe and San Antonio Basins	86
Figure 5-21: Annual Losses: Rainfall - Runoff	87
Figure 5-22: Expected Annual Evaporation Computed as Precipitation Minus Expected Runoff	89
Figure 5-23: Map of Bowen Ratios Computed from Equation 5.4	90

1. INTRODUCTION

Water availability is critical to the economy in the state of Texas. Numerous reservoirs and conveyance structures have been constructed across the State to meet the water supply needs of farmers, municipalities, industries, and power generating facilities. Despite this extensive water management system, water supply remains a concern because of increasing populations and uncertainties about climate stability. The rainfall map of Texas shown in Figure 1.1 clearly shows that water management is a spatial problem. The State as a whole receives about 711 mm year⁻¹ of rainfall, while the area of the State east of the 100th meridian receives 890 mm year⁻¹ and the area west of the 100th meridian receives only 457 mm year⁻¹. In addition to water supply concerns, the assessment of non-point source pollution is another important issue that is largely dependent on the spatial distribution of runoff. Although, the focus of this report is not to address water supply or pollution issues directly, an improved understanding of the spatial water balance – the partitioning of precipitation between evaporation, runoff, and groundwater recharge at different points in space – will directly benefit those who wish to assess water resource availability and non-point source pollution potential across the State.

The goal of this study was to gain an improved understanding of the stocks of water in different components (air, soil, water bodies) of the hydrologic cycle and the fluxes between these components. A basic approach for determining stocks and fluxes involves the calculation of a water balance. A water balance, applied to a particular control volume, is an application of the law of conservation of mass which states that matter cannot be created or destroyed. To achieve a balance, the rate of change of storage of water within the control volume must be equal to the difference between its rates of inflow and outflow across the control surface.

In this study, three independent water balance models were constructed to model different components of the hydrologic cycle – an atmospheric water balance, a soil-water balance, and a surface water balance. These models were constructed using a geographic information system (GIS). A GIS provides a framework for storing and manipulating spatial data and facilitates modeling on control volumes of various sizes and shapes. In all three cases, the choice of modeling unit was driven by the resolution and characteristics of the input data. The control volumes for the atmospheric, soil, and surface water balance models respectively are (1) an

imaginary column confined horizontally by the boundary of Texas and extending to the 300 mb pressure level, (2) 0.5° cells with a depth equal to the plant-extractable water capacity of the soil, and (3) 166 gaged watersheds of differing sizes and shapes. Neither the atmospheric nor the surface water balance involve any simulation of physical processes and are simply mass balances based on empirical data. The soil-water balance does attempt to simulate evaporation from the soil through the use of a soil-moisture extraction function. Both the atmospheric and soil-water balance models are time-varying models, while the surface water balance model is steady-state and uses an empirical relationship to estimate mean annual runoff and evaporation in ungaged areas. One advantage of making three independent water balance calculations is that checks for consistency can be made among the three models. For example, all three models yield an estimate of *actual* evapotranspiration which is a difficult quantity to estimate, particularly at the regional scale. Previous studies at the scale of Texas have estimated only evaporation from open water surfaces and *potential* evapotranspiration from the land surface (TDWR, 1983; Dugas and Ainsworth, 1983).

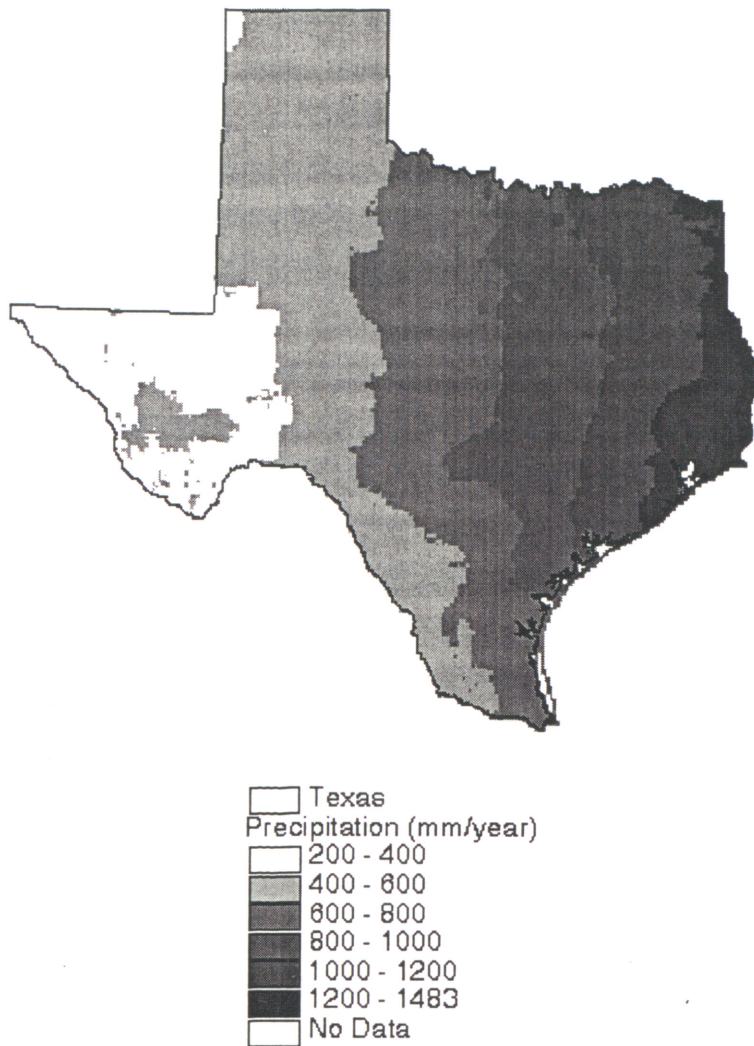


Figure 1-1: Mean Annual Rainfall in Texas from Oregon State PRISM Study (Daly, 1994)

2. LITERATURE REVIEW

2.1 *Atmospheric Water Balance Studies*

A number of researchers have used the atmospheric water balance to estimate hydrologic fluxes. Among these researchers, Rasmusson, 1967, Brubaker *et al.*, 1994, and Oki *et al.*, 1995, describe atmospheric water balance studies at river basin, continental, and global scales. Rasmusson, 1967, analyzes the characteristics of total water vapor flux fields over North America and the Central American Sea. A noteworthy observation made by Rasmusson is that a large diurnal wind system covering the central United States, part of Mexico, and the Central American Sea produces significant diurnal variations in the transport of water vapor. By decomposing the vertically integrated vapor flux term into mean motion and transient eddy terms, where the mean motion term is at a time scale of one month and the transient eddy term describes motion at a time scale of less than one month, Brubaker *et al.* also observe important vapor flux transport at sub-monthly time scales. Brubaker *et al.* note that poleward eddy flux transport from the Gulf of Mexico is significant, particularly during the winter months. From these observations, Brubaker *et al.* surmise that the use of monthly-averaged or sparse data may significantly underestimate the eddy flux component of vapor transport. These observations are relevant to the interpretation of our results, as discussed in Section 3.3. Brubaker *et al.* also note that the accuracy of runoff estimates made using atmospheric data increases with the size of the study area and cite a recommendation by Rasmusson, 1977, that a minimum area of 10^6 km^2 should be used. The area of Texas is about $0.7 \times 10^6 \text{ km}^2$. Improvements in observational networks and general circulation models may justify runoff estimation on smaller areas in the future.

If the annual change in atmospheric water storage and surface water storage are both negligible, runoff estimates can be obtained from the vertically integrated vapor flux convergence ($-\nabla \cdot \bar{Q}$). Using four years of data from the European Centre for Medium-Range Weather Forecasts (1985-1988), Oki *et al.* compared convergence values with the observed annual runoff for 70 river basins throughout the world. Differences between vapor flux convergence and measured runoff varied widely, although larger river basins tended to show smaller differences. On average, the vapor flux convergence was about 2/3 of the measured

runoff. Oki *et al.* also made a more detailed study of the Chao Phraya River basin in Thailand which drains 178,000 km². Oki *et al.* estimated annual runoff, monthly evaporation, and monthly storage for the Chao Phraya from 1985 to 1988. The evaporation and river basin storage values were estimated by augmenting atmospheric data with precipitation and runoff data. In the Chao Phraya basin, the vapor flux convergence was consistently higher than observed runoff; however, the temporal variations of vapor flux convergence and runoff were comparable. This was illustrated by applying a reduction factor to the convergence values.

Significant uncertainties in runoff estimation using atmospheric data still exist even at the continental scale. Both Brubaker *et al.* and Oki *et al.* compare their continental runoff estimates with those given by Baumgartner and Reichel, 1975, for river runoff. For North America, Brubaker *et al.* estimate annual runoff as 84.6 mm/year while Oki *et al.* estimate 263 mm/year and Baumgartner and Reichel give 223 mm/year. Both Brubaker *et al.* and Oki *et al.* make note of the fact that poorly defined continental or basin boundaries may contribute to inaccuracies in runoff estimation. This problem is solved in the current study of Texas by using a geographic information system in which any arbitrarily defined boundary can be used to compute the water balance, although the problem remains that atmospheric soundings are sparse.

2.2 *Soil Water Balance Studies*

Where detailed data about soil layers, depth to groundwater, and vegetation are not available, hydrologists have often resorted to simple bucket models and budgeting schemes to model near-surface hydrology. Despite numerous uncertainties associated with the simple soil-water budget model like the one used in this study, many researchers have applied this type of model to problems ranging from catchment scale studies to the global water balance and climate change scenarios (Thornthwaite, 1948; Shiklomanov, 1983; Manabe, 1969; Mather, 1978; Alley, 1984; Willmott *et al.*, 1985; Mintz and Walker, 1993; Mintz and Serafini, 1992). This approach is attractive because of its simplicity. The simple "bucket" model used here requires minimal input data: precipitation, potential evapotranspiration, and soil-water holding capacity. The studies by Willmott *et al.*, Mintz and Walker, and Mintz and Serafini, are climatological studies that present the global distributions of precipitation, evapotranspiration, and soil moisture. Mintz and Serafini compare their evapotranspiration estimates for sixteen major river basins throughout the

world with those derived from river runoff analysis made by Baumgartner and Reichel, 1975, and the values show reasonable agreement.

At a smaller scale, Mather, 1978, (Chapter 4) describes the application of a soil-water budget model to several watersheds in the coastal plains of Delaware, Maryland, and Virginia. Comparisons between measured and computed runoff values are rather poor for monthly data, but better for annual data, although Mather suggests further refinement of the method even for annual values. In its simplest form, the soil-water budget model does not account for situations where the precipitation rate is greater than the infiltration capacity of the soil. Mather describes one approach to remedy this problem, that is, to first use the SCS method to estimate direct overland runoff and subtract this amount from the precipitation before it is allowed to enter the soil "bucket." This approach appears to yield better results (Mather, Chapter 4). A similar approach of taking an initial rainfall abstraction before allowing precipitation to enter the soil column for climatological budgeting was used in a study of the Niger Basin described by Maidment *et al.*, 1996 (further description available at <http://www.ce.utexas.edu/prof/maidment/gishydro/africa/africa.htm>). In the Niger Basin study, the surplus from the soil-water budget is passed to a surface and groundwater routing model which is in turn calibrated with observed runoff.

2.3 *Surface Water Balance Studies*

2.3.1 **Water Balances of Texas**

The surface water balance, a commonly used method in hydrologic studies, relies on the fact that with the exception of coastal areas, the landscape can be divided into watershed units from which there is only one surface water outflow point. Provided that the average watershed precipitation and runoff can be measured with reasonable accuracy, the annual evaporative losses from a watershed can be estimated. Of course this assumes that change in storage is negligible and that there are no significant inter-watershed transfers via groundwater or man-made conveyance structures. Empirical relationships are often used to estimate mean annual or mean monthly flows in ungaged areas; this approach is used in this study.

Two water balance studies that are particularly relevant to Texas are those by Ward, 1993, and the Texas Board of Water Engineers, 1961. Ward presents a water balance similar to that described here in which he estimates precipitation, evapotranspiration, runoff, recharge, and

water demands for four different hydroclimatological regions in Texas and for the State as a whole. To estimate annual runoff, Ward uses an empirical relationship between rainfall and runoff. A similar approach is used in this study, although the rainfall-runoff relationship derived here is used in conjunction with a large database of measured values to develop spatially distributed maps of runoff. The Texas Board of Water Engineers (TBWE; now Texas Water Development Board) Bulletin 6001 is a study of surface runoff (1940-1956) from the major basins and sub-basins in Texas that uses measured flow data. To estimate runoff in ungaged watersheds or watersheds with insufficient streamflow records, the authors of Bulletin 6001 used a proportion of the observed runoff in a watershed with similar characteristics and an additional factor to account for the difference in precipitation if necessary. One product of Bulletin 6001 is a map of Texas sub-basins with printed values of runoff. Improvements in computer technology since 1961 allow for more detailed electronic maps to be generated in this study, although the idea of mapping runoff values is similar.

2.3.2 Runoff Mapping

Three recently published articles by Arnell, 1995; Lullwitz and Helbig, 1995; and Church *et al.*, 1995, describe studies of runoff mapping. All three use a geographic information system (GIS) to manage spatial data at a regional or continental scale. The paper by Arnell summarizes five approaches for deriving gridded runoff maps at a 0.5° grid resolution including (1) simply averaging the runoff from all stations within each grid cell, (2) statistically interpolating runoff between gages, (3) using an empirical relationship that relates runoff to precipitation, potential evaporation, and temperature, (4) using a soil-water balance type model, and (5) overlaying grid cells onto catchment runoff maps to derive area-weighted runoff estimates. Arnell evaluates all but method (4) by mapping runoff onto 0.5° grid cells over a large portion of western Europe, and then intersecting the results with seven gaged river basins to validate the results. The results show that method (5) produces the most reasonable estimates. In a study similar to that of Arnell, Lullwitz and Helbig created 0.5° runoff maps for the Weser River in Germany. Both Arnell and Lullwitz and Helbig note that 0.5° runoff maps can be useful for validating general circulation models (GCM's). Church *et al.* present maps of evapotranspiration (ET) and runoff/precipitation (R/P) ratios for the northeastern United States. Church *et al.* use an interpolation method to create runoff maps. Church *et al.* found their results to be useful in assessing the effects of acidic deposition.

The approach used for runoff mapping in this study is different from any of the methods described above, although it is most similar to Arnell's method 5. The approach taken here combines an empirical rainfall-runoff relationship and watershed runoff balancing.

3. ATMOSPHERIC WATER BALANCE

An atmospheric water balance is an accounting of the inflow and outflow of water vapor flowing over a region, coupled to the rate at which water is being added to or removed from the atmosphere by means of evaporation and precipitation. The percentage of the moisture flowing over a region which is involved in the region's hydrologic cycle can thus be assessed, and it may even be possible to estimate the rate of regional evaporation using measured atmospheric moisture flow and precipitation data.

3.1 *Atmospheric Data*

Two sources of atmospheric data were used in this study. One data set was provided by Allen Bradley at the University of Iowa Institute for Hydraulic Research and the other by the National Meteorological Center (NMC). The data provided by Bradley originate from rawinsonde soundings. These rawinsondes are launched twice daily (0 and 12 Coordinated Universal Time (UTC)) to measure temperature, humidity, and wind profiles at several levels in the atmosphere. Using these data, Bradley estimated the specific humidity at each measurement level and used the following equations to estimate the vertically integrated vapor flux:

$$Q_u = -\frac{1}{g} \int_{p_s}^{p_t} q \bar{u} dp \quad (3.1a)$$

$$Q_v = -\frac{1}{g} \int_{p_s}^{p_t} q \bar{v} dp \quad (3.1b)$$

In these equations, Q_u is the zonal (east-west) component of vapor flux in [$\text{kg m}^{-1} \text{s}^{-1}$], Q_v is the meridional (north-south) component of vapor flux in [$\text{kg m}^{-1} \text{s}^{-1}$], q is the specific humidity [gm gm^{-1}], u is the zonal component of wind velocity [m s^{-1}], v is the meridional component of wind velocity [m s^{-1}], p is the pressure [Pa], and g is the gravitational constant (9.81 m s^{-2}). The negative sign arises due to the fact that the hydrostatic assumption was used to convert from elevation to pressure. The limits of integration are the surface pressure (p_s) and the pressure at the "top" of the atmosphere (p_t). Strictly speaking, the top of the atmosphere does not exist since there is no physical boundary constraining the atmosphere below a certain level; however, the

transport of water vapor across the 300 mb (30.3 kPa) level is considered negligible so 300 mb was defined as the top of the atmosphere in these computations.

Bradley provided mean monthly integrated vapor flux values for October 1972 to December 1994. The mean monthly values for 0 and 12 Coordinated Universal Time were provided separately. These two values were averaged to estimate mean monthly flux. The data files from Bradley were provided in two formats: integrated flux estimates interpolated to a 2° grid using a standard meteorological method for interpolation called the Barnes objective analysis, and flux estimates interpolated to points on the Texas border from the 2° grid using bilinear interpolation. These two data formats facilitate computation of the atmospheric water balance using either a divergence approach or a flux integration approach as described below. Computations were made using both approaches as a check, and the two methods yielded consistent results.

Another data set, containing monthly atmospheric moisture divergence estimates on a 2.5° grid, was obtained from the National Meteorological Center (NMC) for the 26 month period from June 1991 to July 1993. At NMC, a general circulation model (GCM) is run two to four times per day to predict atmospheric conditions a few hours in advance. After these few hours have passed, observational data including rawinsonde data, satellite temperature and moisture data, and surface observations, are used to adjust the predictions and the next simulation is run. A general circulation model fills gaps in regions with sparse observations and creates atmospheric data sets on regular grids. The NMC monthly divergence estimates used in this study are outputs from the general circulation model. These values are the results of a simulation only and were not modified after the fact to fit actual measurements (Patoux, 1994). No computations were required to determine the divergence on the NMC grid because these values were provided; therefore, the calculations described below refer only to the Bradley data.

3.2 *Methodology*

3.2.1 **Water Balance Equations**

The mass conservation equation for water vapor in the atmosphere can be written as

$$\frac{\partial W}{\partial t} = -\nabla \cdot \bar{Q} + E - P \quad (3.2)$$

where W is the amount of water vapor stored in the atmospheric column, $\nabla \cdot \bar{Q}$ is the divergence or net outflow of water vapor across the sides of the atmospheric column, Q is the vapor flux, E is evaporation, and P is precipitation. The quantity W is also referred to as the precipitable water and may be expressed in units of mass per unit surface area [$M L^{-2}$] or converted to an equivalent depth of liquid water [L] by dividing by the density of liquid water (1000 kg m^{-3}). The divergence is represented mathematically by $\nabla \cdot \bar{Q} = \frac{\partial Q_u}{\partial x} + \frac{\partial Q_v}{\partial y}$ and measures the difference between inflow and outflow to a region. A positive divergence means that outflow is greater than inflow, and a negative divergence (or convergence) means that inflow is greater than outflow. The units of divergence are [$M L^{-2} T^{-1}$] but may also be expressed as depth of liquid water per time [$L T^{-1}$] – results in this paper are presented in these units. To show how the atmospheric water balance can be used to estimate the runoff from a river basin, a similar equation can be written for the surface water balance.

$$\frac{\partial H}{\partial t} = R_{in} - R_{out} - E + P \quad (3.3)$$

In Equation 3.3, H is the depth of liquid water storage in the basin, R_{in} and R_{out} are the inflow and outflow of surface or subsurface runoff, E is evaporation, and P is precipitation. Combining Equations 3.2 and 3.3 yields the expression:

$$-\frac{\partial W}{\partial t} - \nabla \cdot \bar{Q} = \frac{\partial H}{\partial t} + (R_{out} - R_{in}) = P - E \quad (3.4)$$

In mean annual water balance computations, the change in atmospheric storage ($\partial W / \partial t$) and surface water storage ($\partial H / \partial t$) are often assumed to be negligible so that the negative of the divergence provides an estimate of runoff.

$$-\nabla \cdot \bar{Q} = R_{out} - R_{in} = P - E \quad (3.5)$$

It is seen in Equation 3.5 that if the divergence ($\nabla \cdot \bar{Q}$) in a region is positive, then evaporation is greater than precipitation ($P - E < 0$), while a negative divergence or "convergence" indicates

that precipitation is greater than evaporation ($P-E > 0$). One goal of this study was to estimate the divergence or net influx of water to the atmosphere above Texas.

3.2.2 A Control Volume over Texas

To define an atmospheric column for vapor flux calculations, the boundary of Texas was generalized by dividing it into straight segments, each with a length of approximately 100 km, and this boundary was extended vertically to the top (300 mb level) of the atmosphere. In visualizing this control volume, it is important to keep in mind that the height of the atmosphere (8-10 km) is thin compared to the horizontal extent of Texas. Figure 3.1 shows that only 42 2° cells are required to cover the state of Texas and surrounding areas, while Figure 3.2 shows the thickness of the atmosphere relative to the horizontal extent of a 2° grid cell.

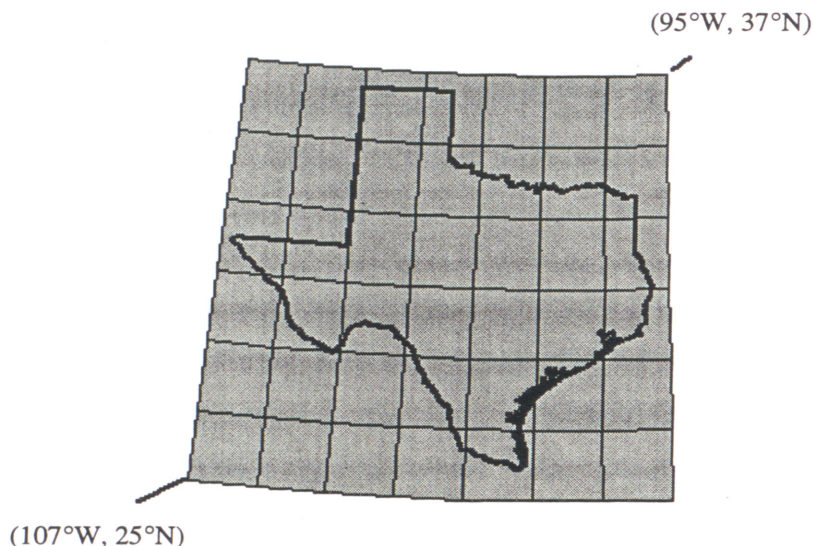


Figure 3-1: 2° Cells Overlaid on the Texas Border

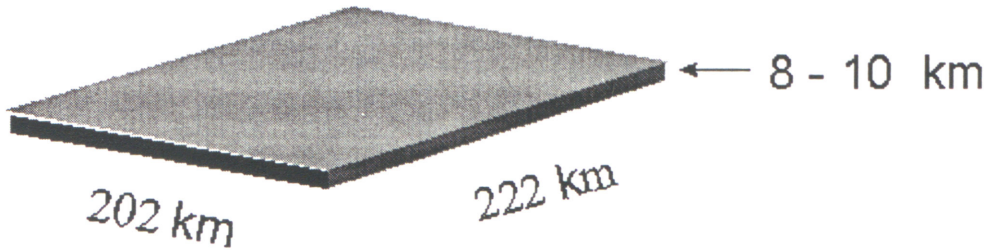


Figure 3-2: Dimensions of a 2° Atmospheric Column in South Texas

3.2.3 Direct Computation and Flux Integration Approaches to Estimate Divergence

3.2.3.1 Divergence approach

Two methods for computing divergence ($\nabla \cdot \bar{Q}$) were applied to the Bradley data set and, as expected, both methods gave consistent results. In the first method, the divergence was computed directly from the 2° grid by using a finite difference approximation to the divergence equation in spherical coordinates. Equation 3.6 gives an expression for divergence in both Cartesian and spherical coordinates.

$$\nabla \cdot \bar{Q} = \frac{\partial Q_u}{\partial x} + \frac{\partial Q_v}{\partial y} \quad (3.6a)$$

$$\nabla \cdot \bar{Q} = \frac{1}{R_e \cos \phi} \left(\frac{\partial Q_\lambda}{\partial \lambda} + \frac{\partial (Q_\phi \cos \phi)}{\partial \phi} \right) \quad (3.6b)$$

R_e is the radius of the model earth taken as 6371.2 km, Q_λ and Q_ϕ are the zonal and meridional components of vapor flux (previously denoted as Q_u and Q_v respectively), λ is longitude in radians, and ϕ is latitude in radians. The spherical form of the divergence equation can be derived following the methodology given by Kreyszig, 1993, Section 8.12. The following centered difference approximation was used to calculate divergence directly from the 2° gridded data.

$$\nabla \cdot \bar{Q}(i, j) = \frac{1}{R_e \cos(\phi_j)} \left(\frac{Q_{\lambda(i+1,j)} - Q_{\lambda(i-1,j)}}{(\lambda_{i+1} - \lambda_{i-1})} + \frac{\cos(\phi_{j+1})Q_{\phi(i,j+1)} - \cos(\phi_{j-1})Q_{\phi(i,j-1)}}{(\phi_{j+1} - \phi_{j-1})} \right) \quad (3.7)$$

The 10 x 9 computational mesh used for the Bradley data is shown in Figure 3.3. For points on this mesh in columns 1 and 10 ($i = 1$ and 10) and rows 1 and 9 ($j = 1$ and 9), Equation 3.7 was modified to use a forward or backward difference approximation as appropriate, because data values outside of this mesh were not provided. The use of a forward or backward difference approximation did not affect any of the cells intersecting the boundary of Texas.

The units of the divergence computed with Equation 3.7 are [$\text{kg m}^{-2} \text{s}^{-1}$]. To estimate the net divergence in the atmosphere above Texas, cells centered on the mesh points depicted in Figure 3.3 were intersected with the Texas boundary as shown in Figure 3.4. The boundary of Texas shown in Figure 3.4 is the same generalized boundary use in the flux integration calculations described in the next section. Intersection is a GIS term that describes an overlaying of two spatial data sets. In this case, the border of Texas was intersected with the 2° cell layout of atmospheric data to determine the area of each cell lying within the State. By summing up the divergence estimates and using these included areas as weights, an estimate of the divergence for the State as a whole was made. This intersection was made in a projected plane; the projection used was an Albers equal-area projection.

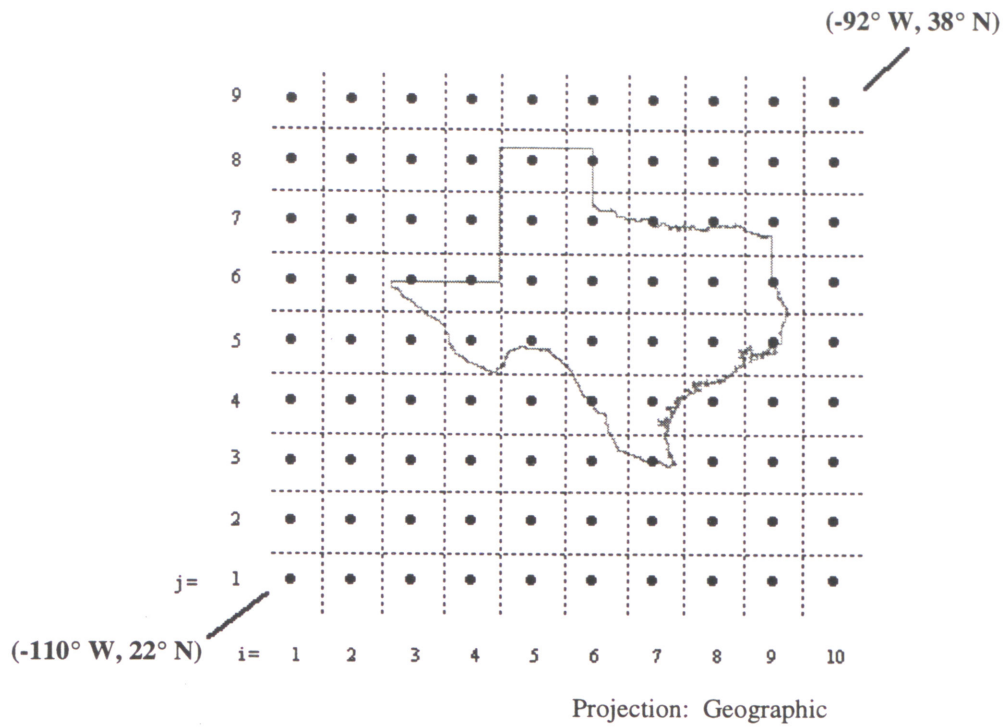


Figure 3-3: Computational Mesh for Divergence Calculations

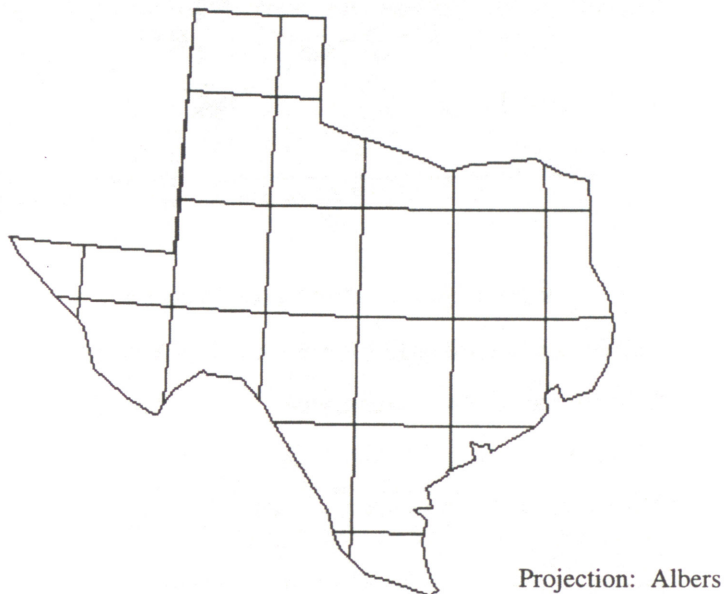


Figure 3-4: Computational Cells Intersected with the Generalized Boundary of Texas

3.2.3.2 Flux integration approach

Thanks to the divergence theorem of Gauss (Kreyszig, 1993, p. 545, 551), an alternative method for calculating divergence is available that involves calculating the moisture flux across line segments that make up the Texas border. This approach is interesting because the flux across any arbitrary boundary line can be estimated. Because a three dimensional problem was reduced to a two dimensional problem through vertical integration of the vapor flux, the divergence theorem in two dimensions can be applied:

$$\nabla \cdot \bar{Q} = \frac{1}{A} \oint \bar{Q} \cdot \bar{n}_l dl \quad (3.8)$$

Rather than using a vector dot-product as in Equation 3.8, the right hand side of this equation can be evaluated by applying a vector cross-product to each border segment and summing the result for each to determine the net flux into the Texas atmosphere. This concept is illustrated in Figure 3.5.

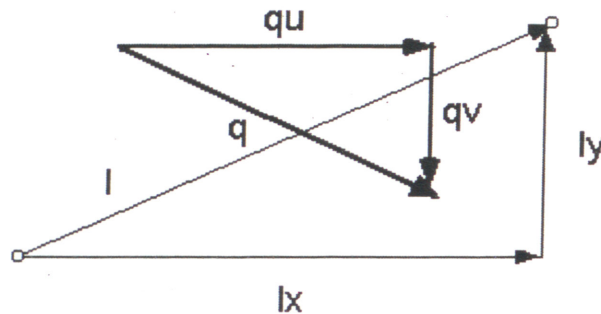


Figure 3-5: Vector Cross Product

The vector $\bar{l} = (l_x, l_y)$ defines the boundary line where x is in the direction of parallels of latitude and y is in the direction of meridians of longitude. As before, the vector $Q = (Q_u, Q_v)$ is the atmospheric moisture flux in $[\text{kg m}^{-1} \text{s}^{-1}]$ where Q_u is in the x direction and Q_v is in the y direction. The mass flow rate across a boundary segment in $[\text{kg s}^{-1}]$ can be obtained from the vector cross-product as follows:

$$\bar{Q}_l = \bar{l} \times \bar{Q} = \bar{k}(l_x Q_v - l_y Q_u) \quad (3.9)$$

In this problem, the boundary segments that make up the border of Texas are defined so that they all point in a clockwise direction, the interior of the region is to the right of each boundary vector and the exterior to the left. The result of the vector cross product is a vector oriented in the vertical direction. If this vector is positive, this indicates mass leaving the region and if this vector is negative, this indicates mass entering the region. For net flux calculations, only the magnitude of the resulting vector \bar{Q}_i is needed. The total outflow is determined by summing the magnitudes of all \bar{Q}_i vectors pointing in the positive \bar{k} direction and the total inflow by summing the magnitudes of all \bar{Q}_i vectors pointing in the negative \bar{k} direction. The net flux or divergence is outflow minus inflow.

In these calculations, the directions of the vector flux components are defined in geographic space and the geometric relationships between the flux vectors and border segments are also determined in geographic space; however, the lengths of the border components $|l_x|$ and $|l_y|$ correspond to the length of these segments as measured along the surface of the earth. To estimate $|l_x|$ and $|l_y|$ given the latitude and longitude of segment endpoints, the length of a radian of longitude and a radian of latitude on the earth's surface (with the earth represented as an ellipsoid) were multiplied by the difference between the longitude and latitude of the two segment endpoints as follows:

$$|l_x| = \frac{a \cos \phi}{(1 - e^2 \sin^2 \phi)^{0.5}} \Delta \lambda \quad (3.10a)$$

$$|l_y| = \frac{a(1 - e^2)}{(1 - e^2 \sin^2 \phi)^{1.5}} \Delta \phi \quad (3.10b)$$

The equations for the length of a radian along a meridian of longitude and the length along a parallel of latitude were taken from Snyder, 1987, p. 25. The parameters for the Clarke 1866 ellipsoid were used to evaluate Equation 3.10 because this was the ellipsoid used to define the Texas border. In Equation 3.10, a is the radius of curvature for the ellipse in the plane of the Equator ($a=6378206.4$ m), e is the eccentricity ($e=0.000045815$), $\Delta \lambda$ is the longitudinal difference between segment end points [radians], and $\Delta \phi$ is the latitudinal difference between segment end points [radians].

3.3 *Results and Discussion*

3.3.1 **Results**

Figure 3.6 shows the results of the monthly divergence calculations for 1973 to 1994 using the Bradley data. These are the results from a direct divergence calculation on a spherical grid (Section 3.2.3.1). Although not shown here, the flux integration results (Section 3.2.3.2) are nearly identical (within 2% on average) as expected. Figure 3.7 presents the same data of Figure 3.6 averaged by year. Figure 3.8 provides a comparison of Bradley and NMC divergence for the 26 month period when the NMC data were available (June 1991 - July 1993). There are significant differences between these two estimates, both in variation of divergence throughout the year and the average divergence magnitudes. Assuming that the mean annual change in atmospheric storage is negligible, the 22 year average runoff (P-E) from the Bradley data is $1206 \text{ mm year}^{-1}$ and the 2 year average runoff predicted from the NMC data is 379 mm year^{-1} . Both of these estimates are much higher than observed surface runoff. A 30 year mean annual runoff of $78.4 \text{ mm year}^{-1}$ was estimated from the surface water balance described in Section 5 below. Such large errors in predicting runoff using the atmospheric water balance are not uncharacteristic for this type of study. Although Oki *et al.* found good agreement between convergence and observed runoff for several basins in the analysis of 70 basins worldwide, they also reported a wide range of errors in which the vapor flux convergence may be up to 80 times the observed runoff or the vapor flux convergence may predict a net evaporation 28 times greater than observed runoff. Several sources of error in making atmospheric flux calculations are discussed in Section 3.3.2.

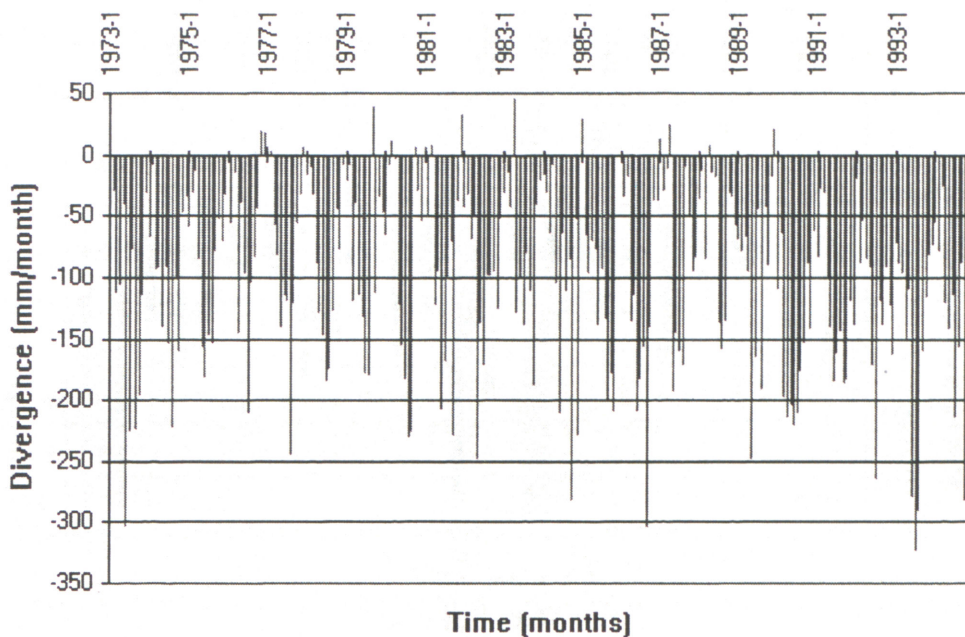


Figure 3-6: Monthly Divergence of Water Vapor Over Texas for 22 Years

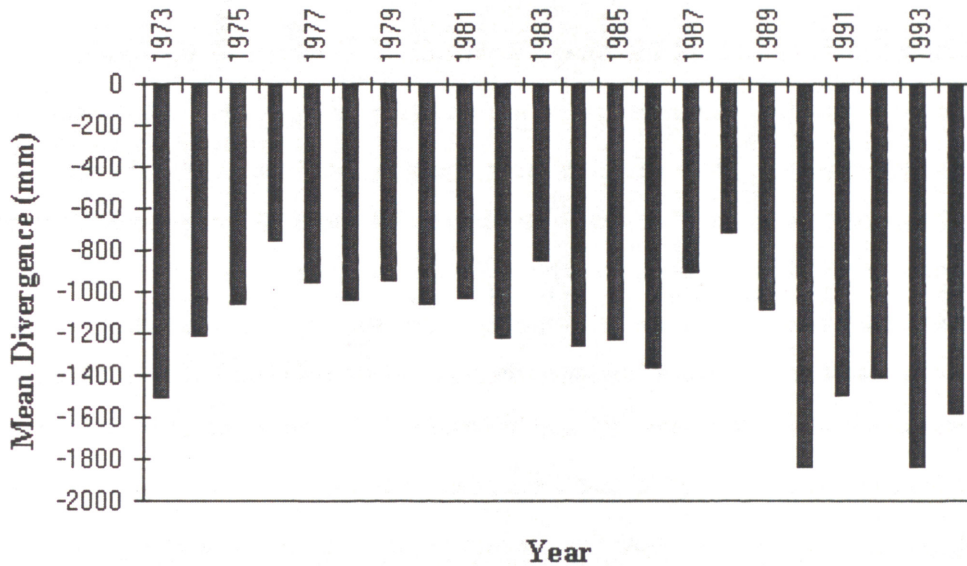


Figure 3-7: Yearly Mean Divergence of Water Vapor Over Texas (1973 - 1994)

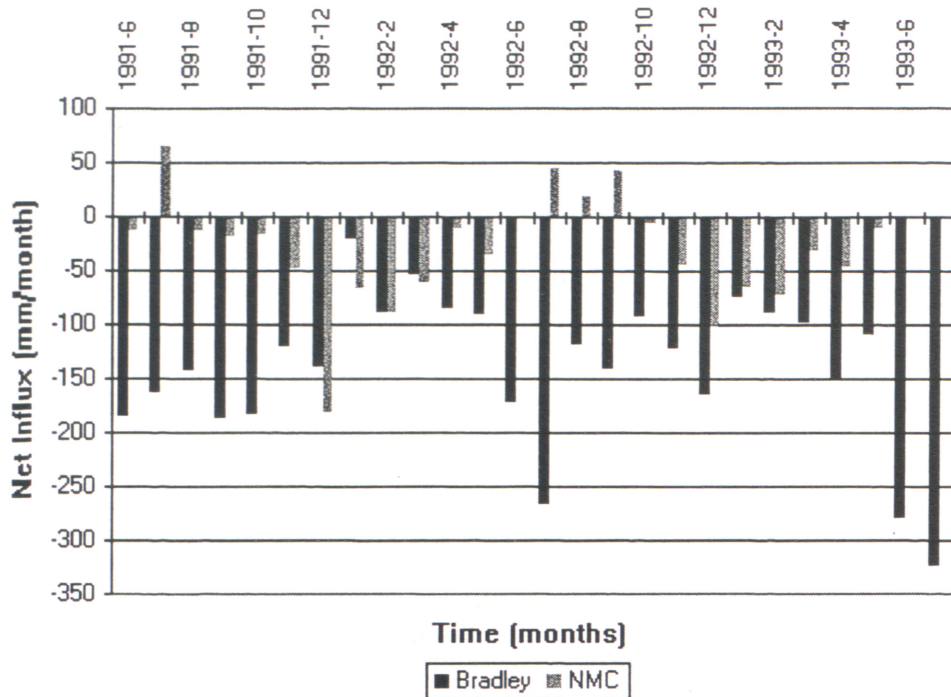


Figure 3-8: Net Influx of Water to the Atmosphere Above Texas, June 1991 - July 1993

If it is assumed that the change in storage from month to month in the atmosphere is negligible, monthly evaporation estimates can be made as $(E = \nabla \cdot \bar{Q} + P)$. Taking statewide average monthly precipitation estimates for 1992 from the study of Patoux, 1994 (Figure 4.2.7), rough monthly evaporation estimates are shown in Figures 3.9 and 3.10 using the Bradley and NMC data respectively. The average precipitation estimates for Texas were made using Thiessen polygons built from the locations of precipitation stations and computing the areal average using an intersection procedure similar to that described in Section 3.2.3.1. Clearly the evaporation estimates shown in Figure 3.9 are unreasonable because negative evaporation estimates don't have physical meaning. Using the Bradley data, the total $\nabla \cdot \bar{Q}_{1992}$ is -1417 mm and the total P_{1992} is 860 mm, which means that the atmosphere must increase its storage by 557 mm in order for a net positive evaporation to occur over the year. These numbers, again, show that the divergence estimates derived in this study are much too high. Using NMC data, the total $\nabla \cdot \bar{Q}_{1992}$ is -310 mm, P_{1992} is 860 mm, giving $E_{1992} = 550$ mm if the annual change in storage is negligible. Figure 3.10 shows the more reasonable NMC monthly evaporation estimates; however, the annual divergence estimate (-309 mm) is still quite high relative to annual runoff

and changes in atmospheric storage may not be an adequate explanation for the relatively large negative evaporation estimates in January, February, and March.

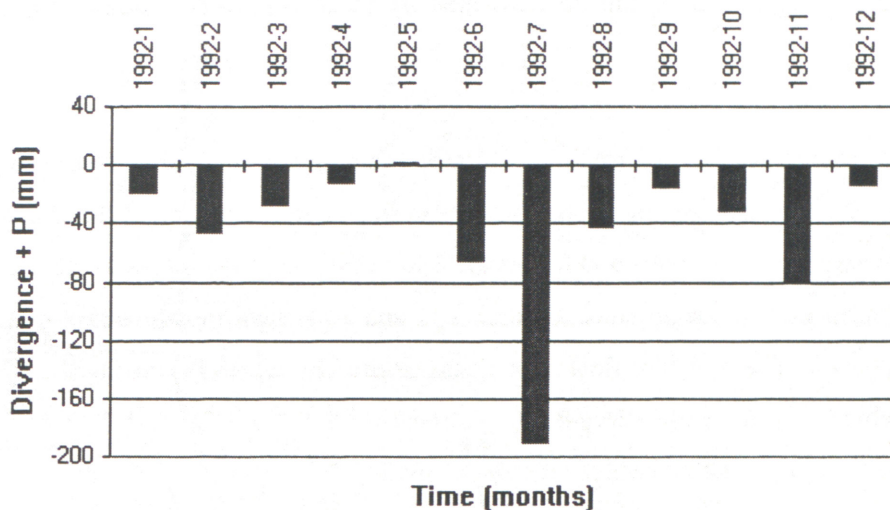


Figure 3-9 : Evaporation Estimates from Bradley Divergence + Precipitation in 1992

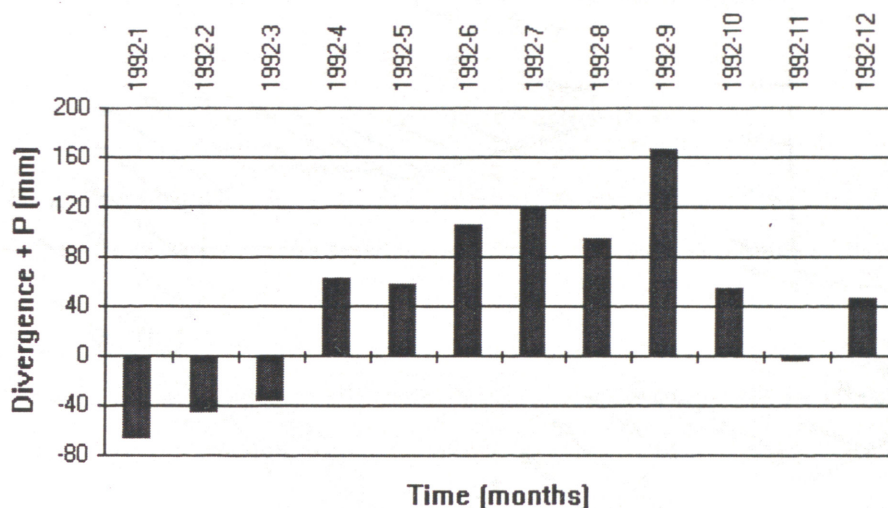


Figure 3-10: Evaporation Estimates from NMC Divergence + Precipitation

Unfortunately, very little data on atmospheric storage were available for this study. In unpublished follow-up work to the study by Patoux, 1994, Patoux estimated the moisture content of the atmosphere over Texas for the first 6 months of 1991. The moisture content increased from about 17.1 mm in January to 54.7 mm in June, with increases of 3.6 mm, 2.4 mm, 3.4 mm,

7.8 mm, and 20.4 mm in the intervening months. This trend simply shows that the atmosphere holds more moisture in the warm summer months. It doesn't appear that large discrepancies illustrated in Figures 3.9 and 3.10 can be explained by these relatively modest atmospheric moisture changes.

In addition to making net flux calculations, a simple program for displaying flux vectors in a geographic information system was developed for use in this study. Looking at the flux vectors gives a sense of where moisture enters and leaves the State, and also gives a feel for seasonal and annual trends in moisture flux magnitudes. Figures 3.11 and 3.12 show moisture flux vectors for January and July 1973. The moisture flow over Texas drastically increased during the Midwest flood of 1993 which is shown in Figure 3.13. Comparing Figures 3.12 and 3.13 shows the difference in summer moisture flux between 1973 and 1993.

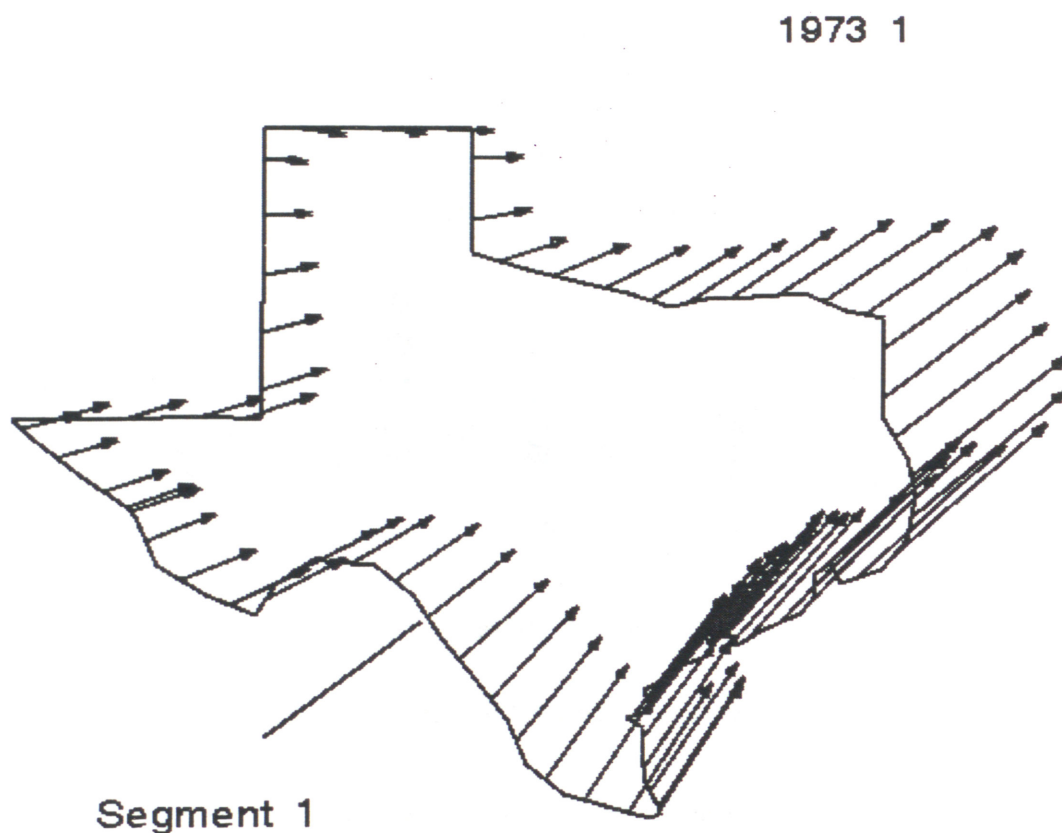


Figure 3-11: Moisture Flux Vectors in January, 1973

1973 7

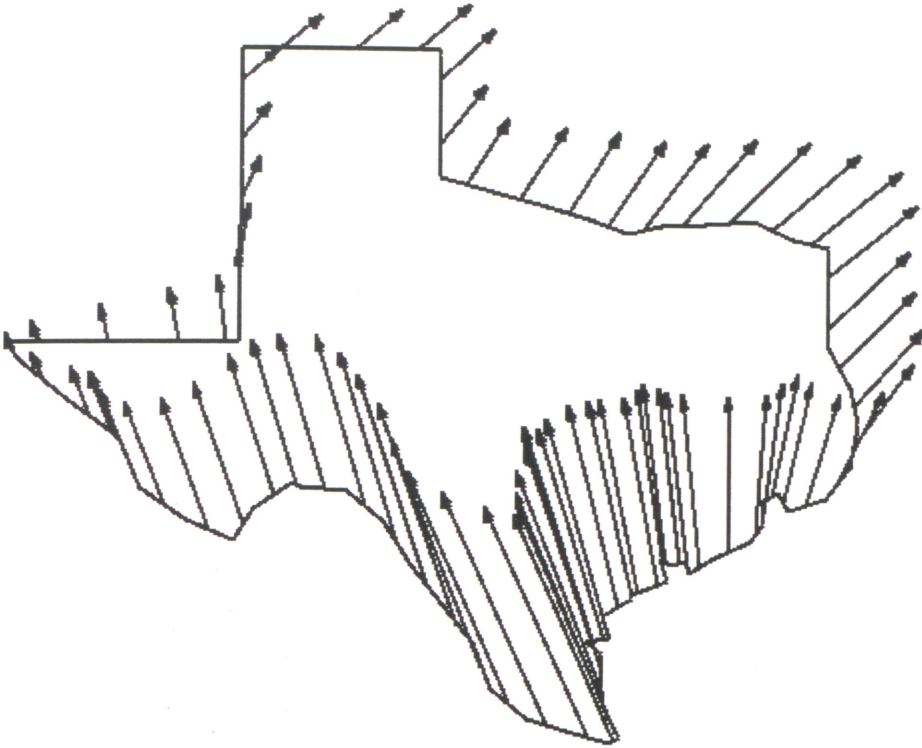


Figure 3-12: Moisture Flux Vectors in July, 1973

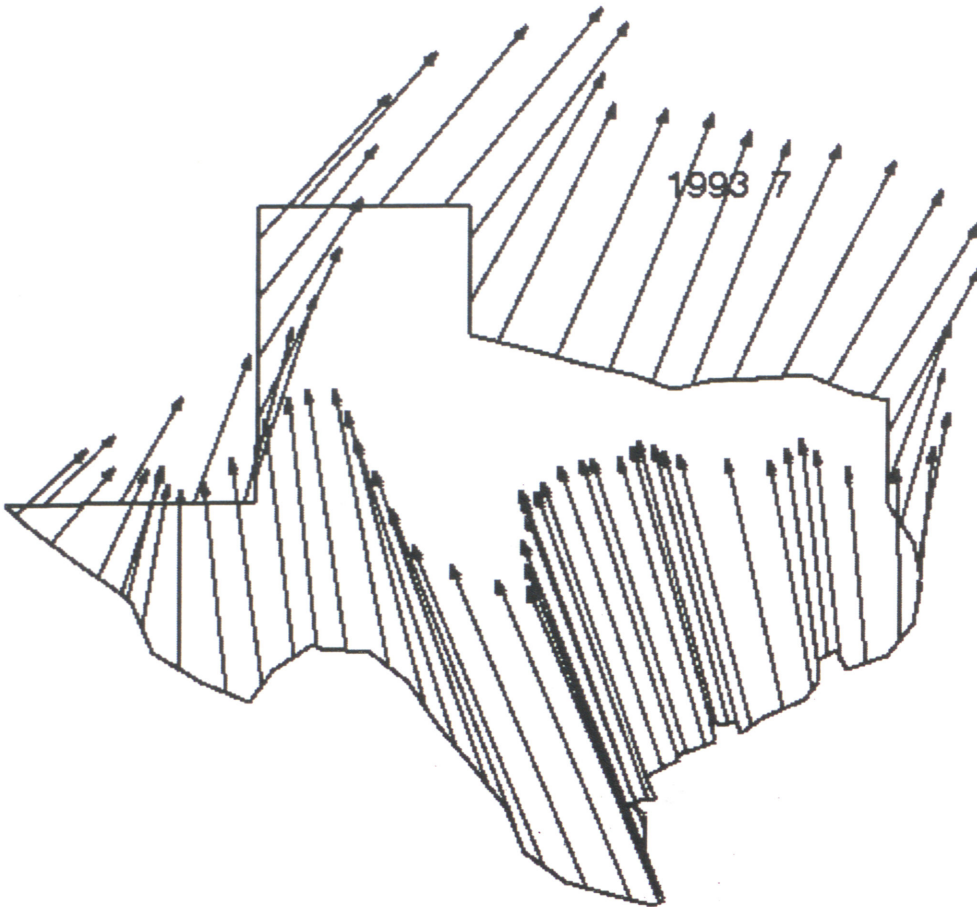


Figure 3-13: Moisture Flux Vectors in July, 1993

3.3.2 Sources of error

The sparseness of observation points, both horizontally and vertically, leaves room for significant error in the atmospheric flux calculations. Even if estimates at all the 2° grid points are accurate, this leaves only about 42 observations, after vertical integration, to describe the flux over an area of $690,000 \text{ km}^2$. In addition to problems with sparseness of measurements in the horizontal direction, Brubaker *et al.* note that the vertical resolution of atmospheric soundings, which typically include measurements at about 6 levels from 1000 to 300 mb (about 0 - 10 km), do not adequately resolve the atmospheric boundary layer (for which a typical depth is 1 km) where a large fraction of the atmospheric water vapor can be found.

Because of the large magnitudes of the numbers under consideration, a small error in the estimate of vapor flux across a single line segment may have a relatively large impact on the net

influx computation. For example, the flux across segment 1 (86 km) in Figure 3.11 is $9.180 \times 10^6 \text{ kg s}^{-1}$ which is equivalent to about $9810 \text{ m}^3 \text{ s}^{-1}$ or 36 mm month^{-1} when dividing by the area of the region being considered — this value is significant when compared with the netflux estimates given in Table 3.1 below. The fact that there are large volumes of water both entering and leaving the State means that calculating the net influx requires taking the difference between two large numbers of similar magnitude. As a result, a small percentage error in either the total influx or total outflux estimate can lead to a large percentage error in the result. Table 3.1 was constructed using data from 1977 to illustrate this point. The netflux is (outflux - influx) and the throughflux is (outflux + influx)/2.

Table 3-1: Comparison of Netflux and Throughflux in 1977

Month	Influx (mm)	Outflux (mm)	Netflux (mm)	Throughflux (mm)	Throughflux/Netflux
1977-1	665.0	668.7	3.8	666.9	178
1977-2	416.2	419.7	3.4	418.0	122
1977-3	928.3	867.2	-61.0	897.8	15
1977-4	624.2	540.2	-84.0	582.2	7
1977-5	926.1	786.4	-139.7	856.2	6
1977-6	738.4	618.9	-119.4	678.6	5.7
1977-7	715.0	594.6	-120.4	654.8	5.4
1977-8	819.5	577.7	-241.9	698.6	2.9
1977-9	603.4	480.1	-123.3	541.7	4.4
1977-10	603.0	545.6	-57.5	574.3	10.0
1977-11	500.3	471.9	-28.4	486.1	17.1
1977-12	732.3	737.4	5.0	734.8	145

If there is a 10% error in the influx estimate for January 1977, then the true influx might be 731.5 [mm month⁻¹], making the netflux -62.8 [mm month⁻¹] rather than 3.8 [mm month⁻¹] which is a 1750% difference. The absolute value of the throughflux to netflux ratio is given in the fourth column of Table 3.1. High values of this ratio indicate that the influx and outflux values are close to one another in magnitude, meaning that a small percentage error in an influx or outflux estimate, may lead to a large percentage error in the netflux result.

Another source of error relevant to the analysis using Bradley data is that mean monthly flux values were used, meaning that transient eddy flux terms were not considered. When time averaging is done on the product of two time-varying quantities – like velocity and specific humidity in this case – eddy flux terms arise because of random variations in velocity and in specific humidity at time scales less than the averaging period used for the analysis. These eddy

flux terms may have a significant influence on mass transport in certain situations. In their analysis of moisture flux into North and South America, Brubaker *et al.* decomposed the vertically integrated moisture flux into mean motion and transient eddy terms. They note that from a global perspective mean motion dominates Q_u while mean and transient eddy terms are of comparable magnitude in Q_v . From the results of their study, Brubaker *et al.* concluded that eddy flux terms contribute significantly to the north-south transport of water vapor, particularly along the Gulf of Mexico in the winter months. Thus, fluctuations on a few days time scale are important when considering the transport of water vapor, a conclusion also reached by Rasmusson, 1967.

3.3.3 Summary and Discussion

Two methods for computing the divergence of atmospheric moisture using rawinsonde data have been described – one using a finite difference approximation on a spherical grid and one by summing fluxes across boundary lines. The results of these computations were compared with output from a general circulation model. In general, computations based strictly on observed data yielded poor estimates of divergence, with the estimate of average annual divergence over Texas being 15 times greater than observed runoff. The divergence estimate from the general circulation model was about 5 times greater than observed runoff. Reasons for errors may include (1) the sparseness of observations, (2) errors associated with taking differences between large numbers, and (3) using monthly average flux values. With regard to the first reason for errors, improved observation networks and remote sensing may help to alleviate problems with data resolution in future studies. The United States National Meteorological Center is presently implementing a new mesoscale general circulation model over North America called the Eta model, using 40 km computational cells which will provide about 25 times greater horizontal resolution than the grid used in this study. The second problem may be difficult to overcome considering the large amounts of moisture that flow through the atmosphere relative to the amounts of precipitation, evaporation, and runoff. Statewide average estimates from this study indicate that the average annual throughflux (1973 - 1994) of atmospheric moisture is 7788 mm while the annual precipitation is 720 mm and average annual runoff is 78.4 mm (See Section 5), indicating that only 9% of the moisture passing over the State falls as precipitation and 11% of this precipitation becomes runoff. With regard to the third problem, data for making calculations

on shorter than monthly time steps are available, but were not used due to time and logistical constraints in this study.

When calculations made in this study were compared with the output of a National Meteorological Center GCM, the GCM results seemed more reasonable, but not entirely satisfactory. The GCM considers transient eddy behavior that is not captured by mean monthly observations because a much smaller time step is used. Simulation models also offer the advantage that equations of motion can be used to fill in areas with sparse observations. As products from higher resolution GCM simulations become available, simple operations in GIS can be used to estimate net fluxes into arbitrarily defined regions as done in this study.

Some additional information would have been useful to help assess the relative importance of different sources of error in this study. The use of 12 hourly data could have shed more light on problems associated with using monthly average values. It also would have been interesting to know the locations where rawinsonde observations were actually made. In addition, more water content computations could have been made to yield better evaporation estimates.

4. SOIL-WATER BALANCE

4.1 *Methodology*

4.1.1 Model Description

The soil-water balance model uses a simple accounting scheme to predict soil-water storage, evaporation, and water surplus. Surplus is precipitation which does not evaporate or remain in soil storage and includes both surface and sub-surface runoff. The conservation of mass equation for soil-water can be written as follows:

$$\frac{\partial w}{\partial t} = P - E - S \quad (4.1)$$

In Equation 4.1, S is surplus, P is precipitation, E is evaporation, w is soil moisture, and t is time. Horizontal motion of water on the land surface or in the soil is not considered by this model. Snow melt was also not considered in these computations, but this probably does not introduce significant error for a study in Texas. Willmott *et al*, 1985, describe a simple scheme that could be included to account for snow melt.

At first glance, it would seem that the most natural spatial unit to use in a soil-water balance would be a soil map unit, but these map units have very irregular shapes and a wide range of sizes. Because climate data also play an important role in the soil-water balance, the cells generated when climate data are interpolated onto regular grids are a judicious choice for use as the modeling units in the soil-water balance. Climate data interpolated onto 0.5° grid boxes are used in this study.

A major source of uncertainty in evaluating Equation 4.1 is estimating the evaporation. Estimation of evaporation is based upon knowledge of potential evapotranspiration, water-holding capacity of the soil, and a moisture extraction function. These concepts and a method for evaluating Equation 4.1 are described below. Special consideration of the potential evapotranspiration concept is provided in Section 4.2.

4.1.2 Description of input data

4.1.2.1 *Climate data*

Global data sets of mean monthly temperature and precipitation interpolated to a 0.5° grid were obtained from an anonymous File Transfer Protocol (ftp) server to the University of Delaware (climate.geog.udel.edu). These data are from the “Global Air Temperature and Precipitation Data Archive” compiled by D. Legates and C. Willmott. The precipitation estimates were previously corrected for gage bias. Data from 24,635 terrestrial stations and 2,223 oceanic grid points were used to estimate the precipitation field. The climatology is largely representative of the years 1920 to 1980 with more weight given to recent (“data-rich”) years (Legates and Willmott, 1990).

4.1.2.2 *Available water-holding capacity data*

Global estimates of “plant-extractable water capacity” have recently become available on a 0.5° grid (Dunne and Willmott, 1996). As used in this report, the term *plant-extractable water capacity* is equivalent to *available water-holding capacity*. One reason given for developing this global database was to eliminate the need for assuming spatially invariant plant-extractable water capacity in soil-water balance computations made over large areas. Information about sand, clay, organic content, plant rooting depth, and horizon thickness was used to estimate the plant-extractable water capacity. Figure 4.1 shows the distribution of this parameter throughout Texas. The global average for this parameter is 86 mm while the average in Texas is 143 mm.

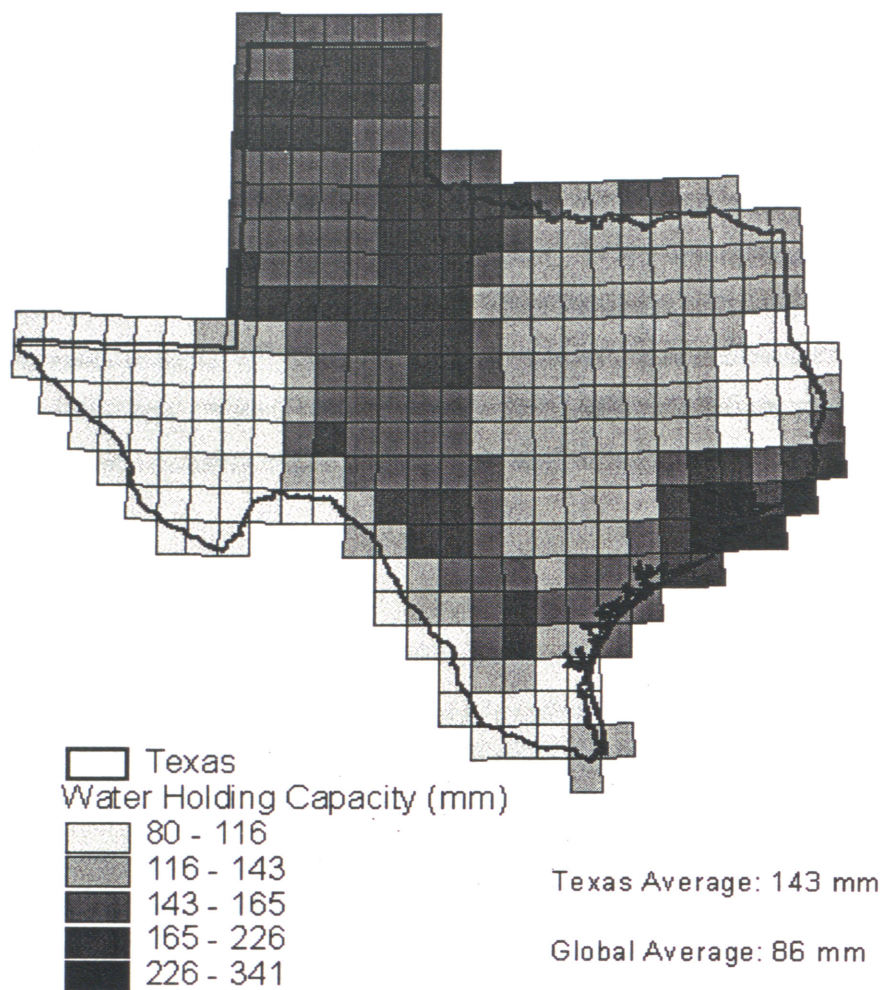
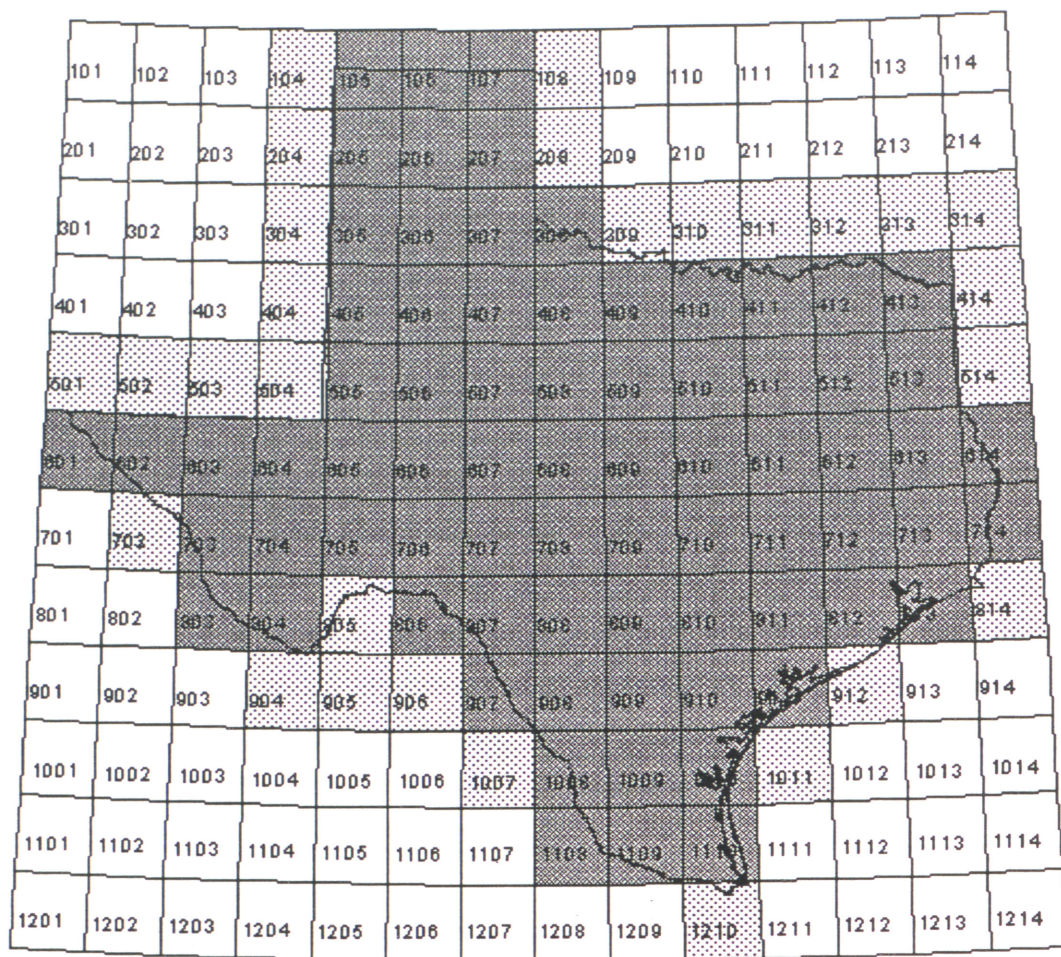


Figure 4-1: Available Soil-water Holding Capacity (mm)

4.1.2.3 *Open Water Evaporation Estimates*

Estimates of open water evaporation based upon pan evaporation measurements were provided by Alfredo Rodriguez at the Texas Water Development Board (TWDB, 1995). The data consist of monthly average gross reservoir evaporation estimates for one degree quadrangles in and around Texas. Monthly data for 1940 to 1990 are available in 75 quadrangles throughout Texas and monthly data for 1971-1990 in an additional 28 quadrangles at the border of Texas. Mean monthly values were computed from these data and used for estimates of potential evaporation in the soil-water balance calculations. Figure 4.2 shows the one degree quadrangle index map, shaded to indicate where data are available. Figure 4.3 shows mean annual reservoir evaporation. As an alternative, a global radiation data set described in the next section has recently become available that facilitates making potential evaporation estimates using the Priestley-Taylor equation. This method was also considered for use in the soil-water balance computations. An insightful comparison of these two methods for estimating potential evapotranspiration is described in Section 4.2.



Data Availability for Open Water Evaporation

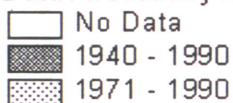


Figure 4-2: One Degree Quadrangle Index Map

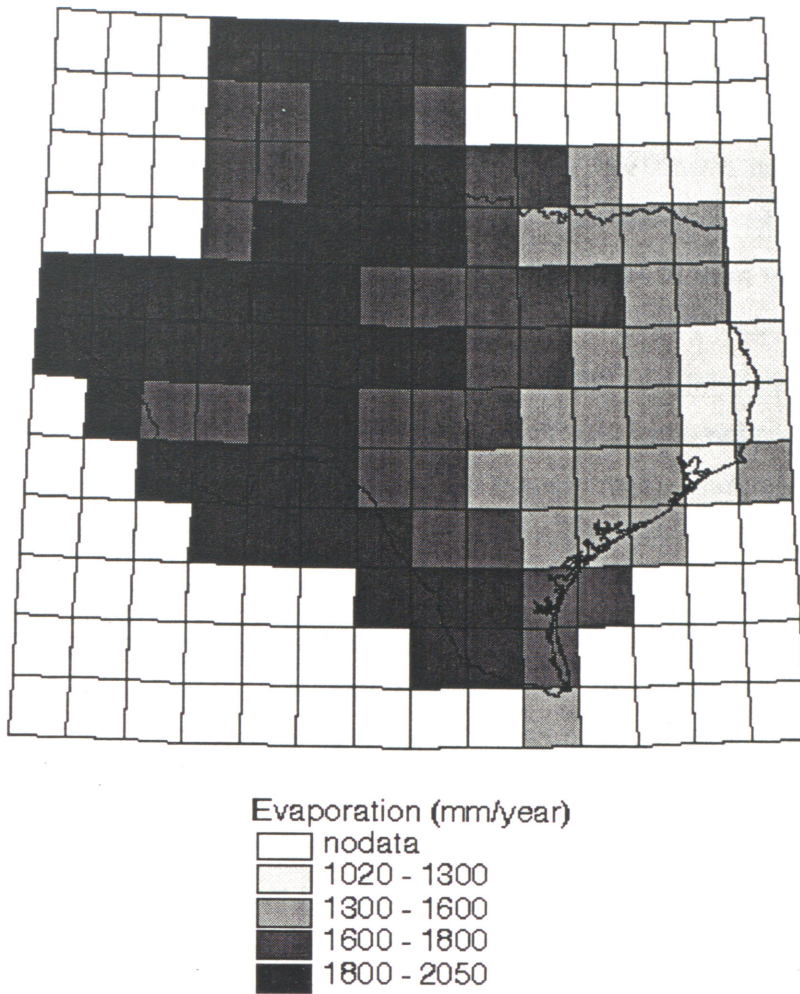


Figure 4-3: Mean Annual Open Water Evaporation (mm), TWDB, 1995

4.1.2.4 Radiation Data

A global radiation data set recently made available makes using the Priestley-Taylor method a feasible option for estimating potential evapotranspiration in large scale studies. These data are described by Darnell *et al.*, 1995, and were obtained by anonymous ftp to cloud.larc.nasa.gov. The data set includes longwave and shortwave radiation flux estimates for a 96 month period extending from July 1983 to June 1991. The data are given on the ISSCP equal-area grid which has a spatial resolution of 2.5° at the equator, although the data were interpolated to 0.5° cells in this study to be consistent with other data sets. Darnell *et al.*, 1992, describe advances in input data and flux estimation algorithms that improve the ability to assess the radiation budget on a global scale. Input data improvements have come from the International Satellite Cloud Climatology Project (ISCCP) and the Earth Radiation Budget Experiment (ERBE). Using this satellite data, the radiation budget components that cannot be measured directly are estimated independently using physical approaches that have been validated against surface observations. According to Darnell *et al.*, 1995, longwave flux estimates fall within $\pm 25 \text{ W/m}^2$ of surface measurements while Whitlock *et al.*, 1995, estimate the accuracy of shortwave estimates to be within $\pm 20 \text{ W/m}^2$ of surface measurements. For comparison, the energy required to evaporate 1 mm/day of water is about 30 W/m^2 . In this study, net radiation (equivalent to net shortwave + net longwave) is used.

4.1.3 Water-holding capacity of the soil

In order to calculate the soil-water budget, an estimate of the soil's ability to store water is required. Several terms are used by soil scientists to define the water storage capacity of soils under different conditions. The field capacity or drained upper limit is defined as the water content of a soil that has reached equilibrium with gravity after several days of drainage. The field capacity is a function of soil texture and organic content. The permanent wilting point or lower limit of available water is defined as the water content at which plants can no longer extract a health sustaining quantity of water from the soil and begin to wilt. Typical suction values associated with the field capacity and wilting point are -10 kPa (-0.1 bars) and -1500 kPa (-15 bars) respectively. Like water content, field capacity and permanent wilting point are defined on a volume of water per volume of soil basis. The water available for evapotranspiration after drainage (or the available water-holding capacity) is defined as the

field capacity minus the permanent wilting point. Table 4.1 gives some typical values for available water-holding capacity.

Table 4-1 : Typical Values for Soil-water Parameters by Texture*

Texture Class	Field Capacity	Wilting Point	Available Capacity
Sand	0.12	0.04	0.08
Loamy Sand	0.14	0.06	0.08
Sandy Loam	0.23	0.10	0.13
Loam	0.26	0.12	0.14
Silt Loam	0.30	0.15	0.15
Silt	0.32	0.15	0.17
Silty Clay Loam	0.34	0.19	0.15
Silty Clay	0.36	0.21	0.15
Clay	0.36	0.21	0.15

*Values obtained from ASCE, 1990, Table 2.6, p.21.

For budgeting calculations, it is useful to know the *total* available water-holding capacity in a soil profile. This value is typically expressed in mm and can be obtained by integrating the available water-holding capacity over the effective depth of the soil layer. A one meter soil layer with a uniform available water-holding capacity of 0.15 has a total available water-holding capacity of 150 mm. For the remainder of this paper, the term water-holding capacity means *total available* water-holding capacity in units of mm. The water-holding capacity is denoted with w^* and the current level of moisture storage in the soil is denoted by w [mm]. A large water-holding capacity implies a large annual evapotranspiration and small annual runoff relative to a small water-holding capacity under the same climatic conditions.

4.1.4 Estimating Actual Evapotranspiration

To estimate the actual evapotranspiration in the soil-water budget method many investigators have used a soil-moisture extraction function or coefficient of evapotranspiration, f , which relates the actual rate of evapotranspiration to the potential rate of evapotranspiration based on some function of the current soil moisture content and the water-holding capacity.

$$E = f * PE \quad (4.2)$$

Dyck, 1983, Table 1, (reprinted in Shuttleworth, 1993, Table 4.4.6) provides a summary of some moisture extraction functions used by different investigators. Mintz and Walker, 1993, Figure 5, also illustrates several moisture extraction functions. Many researchers agree that soils show the general pattern of behavior that moisture is extracted from the soil at the potential rate until some critical moisture content is reached when evapotranspiration is no longer controlled by meteorological conditions. Below this critical point, there is a decline in soil moisture extraction until the wilting point is reached. This type of behavior is illustrated by Shuttleworth, 1993, Figure 4.4.3, p. 4.46 and Dingman, 1994, Figure 7-21. Shuttleworth, 1993, notes that the critical moisture content divided by the field capacity is typically between 0.5 and 0.8. The type of moisture extraction function just described is commonly applied to situations when daily climate data are used. A function in which the ratio of evapotranspiration to potential evapotranspiration is proportional to the current moisture level, $f = w/w^*$, has been applied when budgeting with monthly climate values and this function is used here. This function predicts lower evapotranspiration rates than a function with a breakpoint which may offset (to some degree) the low rainfall intensities resulting from the use of monthly averaged rainfall.

There are drawbacks to using simple soil moisture extraction functions. Indices based on a function of soil moisture alone, do not account for the effects of vegetation. Mintz and Walker, 1993, cite field studies that show f may vary with potential evapotranspiration for a given soil wetness and f may also vary with leaf-area index. In addition, the spatial variation of water-holding capacity is difficult to determine. A new and possibly better approach to determine the relationship between plant transpiration and potential evapotranspiration is to correlate f with satellite-derived indices of vegetation activity so that f will reflect plant growth stage and the spatial vegetation patterns. Gutman and Rukhovetz (1996) investigate this possibility. Using their approach still requires an estimate of potential evapotranspiration to get actual evapotranspiration.

4.1.5 Budgeting soil moisture to yield surplus

Soil-water budget calculations are commonly made using monthly or daily rainfall totals because of the way data are recorded. Computing the water balance on a monthly basis involves the unrealistic assumption that rain falls at constant low intensity throughout the month, and consequently surplus estimates made using monthly values are typically lower than those made using daily values. In dry locations, the mean potential evaporation for a given month may be higher than the mean precipitation and budgeting with monthly values may yield zero surplus, even though there is some observed runoff. For this reason, the use of daily values is preferred over monthly values when feasible, yet daily budgeting still does not adequately describe storm runoff that occurs when the precipitation rate exceeds the infiltration capacity of the soil. One drawback to using daily data is that it is difficult to interpolate daily rainfall over space. For the statewide study undertaken here, the use of daily data was deemed too cumbersome.

Equation 4.3 describes how soil moisture storage is computed.

$$\begin{aligned}
 w_i &= w_{i-1} + P - f_{i-1}PE && \text{if } w_i < w^* \\
 S_i &= w_i - w^* \text{ and set } w_i = w^* && \text{if } w_i > w^* \quad (4.3)
 \end{aligned}$$

In Equation 4.3, w_i is the current soil moisture, w_{i-1} is the soil moisture in the previous time step, P is precipitation, PE is potential evapotranspiration, S_i is the surplus in a given day, f is the soil-moisture extraction function and w^* is the water-holding capacity. With monthly data, computations are made on a quasi-daily basis by assuming that precipitation and potential evapotranspiration for a given day are equal to their respective monthly values divided by the number of days in the current month. When evaluating Equation 4.3, if w_i drops below zero, then w_i is set equal to 0.01; if $w_i > w^*$, then the surplus for that day is $w_i - w^*$ and w_i is set equal to w^* . The soil-moisture extraction function $f = w/w^*$ was used for this study.

4.1.6 **Balancing Soil Moisture**

If the initial soil moisture is unknown, which is typically the case, a balancing routine is used to force the net change in soil moisture from the beginning to the end of a specified balancing period (N time steps) to zero. To do this, the initial soil moisture is set to the water-holding capacity and budget calculations are made up to the time period ($N+1$). The initial soil moisture at time 1 (w_1) is then set equal to the soil moisture at time $N+1$ (w_{N+1}) and the budget is re-computed until the difference ($w_1 - w_{N+1}$) is less than a specified tolerance.

4.2 *Potential Evapotranspiration*

One aspect of the soil-water budget that involves significant uncertainty and ambiguity is estimating potential evapotranspiration. Just the concept of potential evapotranspiration is ambiguous by itself, as discussed in the next section. Two potential evapotranspiration estimates were considered for this study, gross reservoir evaporation estimates from pan coefficients and estimates made using the Priestley-Taylor equation. As discussed later, the gross reservoir evaporation estimates are considered to be better than the Priestley-Taylor estimates for use in the soil-water budget calculations.

4.2.1 **Potential evaporation vs. potential evapotranspiration**

Thornthwaite, 1948, first used the concept of potential evapotranspiration as a meaningful measure of moisture demand to replace two common surrogates for moisture demand, temperature and pan evaporation. Potential evapotranspiration refers to the maximum rate of evapotranspiration from a large area completely and uniformly covered with growing vegetation and with an unlimited moisture supply. There is a distinction between the term potential evapotranspiration and potential evaporation from a free water surface because factors such as stomatal impedance and plant growth stage influence evapotranspiration but do not influence potential evaporation from free water surfaces.

Brutsaert, 1982, notes on pp. 214 and 221 the remarkable similarity in the literature among observations of water losses from short vegetated surfaces and free water surfaces. He poses a

possible explanation that the stomatal impedance to water vapor diffusion in plants may be counterbalanced by larger roughness values. Significant differences have been observed between potential evapotranspiration from tall vegetation and potential evaporation from free water surfaces. The commonly used α value of 1.26 in the Priestley-Taylor equation was derived using observations over both open water and saturated land surfaces. For the most part, the term potential evapotranspiration will be used in this paper and, as used, includes water loss directly from the soil and/or through plant transpiration.

An additional ambiguity in using the potential evapotranspiration concept is that potential evapotranspiration is often computed based on meteorological data obtained under non-potential conditions (Brutsaert, p. 214). In this study, temperature and net radiation measurements used for calculating potential evapotranspiration in dry areas and for dry periods will be different than the values that would have been observed under potential conditions. The fact that the Priestley-Taylor method exhibits weak performance at arid sites is related to this ambiguity because the assumptions under which the expressions were derived break down. This is particularly relevant to West Texas and is the main reason why evaporation estimates derived from pan coefficients are considered more applicable for the type of computations being made in this study. A comparison of the two methods is described in Section 4.2.3.3.

Although not used directly in this study, a brief review of the widely used Penman equation serves as a good starting point for discussing the estimation of potential evapotranspiration.

4.2.2 Penman combination method

Two requirements for evaporation to occur are an energy input and a mechanism for the transport of water vapor away from the saturated surface. In light of this, two traditional approaches to modeling evaporation are an energy budget approach and an aerodynamic approach. With the energy budget approach, the net radiation available at the surface (shortwave radiation absorbed less longwave radiation emitted) must be partitioned between latent heat flux and sensible heat flux, assuming that ground heat flux is negligible. This partitioning is typically achieved using the Bowen ratio which is the ratio of sensible heat flux to latent heat flux. Approximating the Bowen ratio typically requires measurements of temperature and humidity at two heights. The aerodynamic approach involves a vapor transport coefficient times the vapor

pressure gradient between the saturated surface and an arbitrary measurement height. Determination of the vapor transport coefficient requires measurements of wind speed, humidity, and temperature. Brutsaert, Chow *et al.*, and Dingman, present equations for calculating the Bowen ratio and vapor transport coefficients. Without simplifying assumptions, energy budget and the aerodynamic methods require meteorological measurements at two levels.

In 1948, Penman combined the energy budget and aerodynamic approaches. Penman's derivation eliminates the need for measuring water surface temperature; only the air temperature is required. The resulting equation is as follows:

$$E = \frac{\Delta}{\Delta + \gamma} E_r + \frac{\gamma}{\Delta + \gamma} E_a \quad (4.4)$$

where $E_r = \frac{R_n}{l_v \rho_w}$ and $E_a = K(u)(e_s - e)$. R_n is net radiation [W m^{-2}], l_v is latent heat of vaporization [J kg^{-1}], ρ_w is density of water [kg m^{-3}], $K(u)$ is a mass transfer coefficient, e_s is saturated vapor pressure at air temperature, and e is the actual vapor pressure.

The Penman equation is a weighted average of the rates of evaporation due to net radiation (E_r) and turbulent mass transfer (E_a). Provided that model assumptions are met and adequate input data are available, various forms of the Penman equation yield the most accurate estimates of evaporation from saturated surfaces. The "Evapotranspiration and Irrigation Water Requirements Manual," ASCE, 1990, offers a performance comparison of twenty popular methods for estimating potential evaporation. The top six rated methods in ASCE, 1990, are forms of the Penman equation (p.249).

4.2.3 Simpler Methods

Two simpler methods that are much easier to apply than forms of the Penman equation were considered in this study, a pan coefficient approach and the Priestley-Taylor method.

4.2.3.1 Pan coefficients

Evaporation pans are commonly used to estimate open water evaporation from nearby lakes and reservoirs. The rate of evaporation is estimated by measuring the change in water level with

time. Lake evaporation is estimated by multiplying the pan evaporation by a pan coefficient. Typical values of the pan coefficient range from 0.67 to 0.78 in Texas, so the measured evaporation from the pan is higher than that from the lake surface. Pan coefficients vary with location and season. The development of gross reservoir evaporation estimates used in this study is described by TWDB, 1995. As discussed in Section 4.2.1, open water evaporation and potential evapotranspiration are often of similar magnitude, justifying the use of open water evaporation estimates in soil-water budget calculations.

4.2.3.2 Priestley-Taylor Method

In 1972, C.B. Priestley and R.J. Taylor showed that, under certain conditions, knowledge of net radiation and ground dryness may be sufficient to determine vapor and sensible heat fluxes at the Earth's surface. When large land areas (on the order of hundreds of kilometers) become saturated, Priestley and Taylor reasoned that net radiation is the dominant constraint on evaporation and analyzed numerous data sets over land and ocean to show that the advection or mass-transfer term in the Penman combination equation tends toward a constant fraction of the radiation term under "equilibrium" conditions. According to Brutsaert, 1982, Slatyer and McIlroy, 1961, first defined the concept of equilibrium evaporation as a state that is reached when a moving air mass has been in contact with a saturated surface over a long fetch and approaches vapor saturation – thus causing the advection (aerodynamic) term in the Penman equation to go to zero. Both the Slatyer-McIlroy and the Priestley-Taylor definitions consider the radiation term in the Penman equation to be a lower limit for the evaporation from a moist surface. The form of the evaporation equation developed by Priestley and Taylor is as follows, a constant (α) times Penman's radiation term.

$$E = \alpha \frac{\Delta}{\Delta + \gamma} E_r \quad (4.5)$$

Equating this expression to the combination equation reveals that the advection term must be a constant fraction of the radiation term if α is a constant.

$$\alpha \frac{\Delta}{\Delta + \gamma} E_r = \frac{\Delta}{\Delta + \gamma} E_r + \frac{\gamma}{\Delta + \gamma} E_a \quad (4.6)$$

$$\alpha = 1 + \frac{\frac{\gamma}{\gamma + \Delta} E_a}{\frac{\Delta}{\Delta + \gamma} E_r} \quad (4.7)$$

Using micro-meteorological observations over ocean surfaces and over saturated land-surfaces following rainfall, Priestley and Taylor came up with a best-estimate of 1.26 for the parameter α . The fact that α is greater than one indicates that true advection-free conditions do not exist. Since 1972, several other researchers have confirmed that α values in the range 1.26-1.28 are consistent with observations under similar conditions. Some researchers have found significantly lower values for the α coefficient, but these coefficients were found for different types of surfaces (i.e. tall vegetation or bare soil as opposed to grass and open water). There have also been indications that the α coefficient may exhibit significant seasonal variation (Brutsaert, p. 221).

Priestley-Taylor estimates have shown good agreement with lysimeter measurements for both peak and seasonal evapotranspiration in humid climates; however, the Priestley-Taylor equation substantially underestimates both peak and seasonal evapotranspiration in arid climates. The advection of dry air to irrigated crops is likely to be greater in arid climates because large saturated areas are rare, resulting in a more dominant role of the advection term. A higher α coefficient may be required in arid climates (ASCE, 1990). Based on arid sites studied in ASCE, 1990, a value of $\alpha=1.7-1.75$ seems more appropriate for arid regions. Shuttleworth, 1993, states that the Priestley-Taylor method is the “preferred radiation-based method for estimating reference crop evapotranspiration.” Shuttleworth, 1993, notes that errors using the Priestley-Taylor method are on the order of 15% or 0.75 mm/day, whichever is greater, and that estimates should only be made for periods of ten days or longer.

4.2.3.3 Comparison of Pan and Priestley-Taylor Methods

Figure 4.4, Figure 4.5, and Figure 4.6 are maps of mean annual temperature, mean annual net radiation distribution, and mean annual potential evapotranspiration made using the Priestley-Taylor method. A comparison between Figure 4.4 which shows the mean annual Priestley-Taylor potential evapotranspiration and Figure 4.3 which shows the gross reservoir evaporation

is quite revealing. It is clear that the highest values of reservoir evaporation are in West Texas with a decreasing trend moving eastward. The converse is true for the Priestley-Taylor estimates where the lowest values occur in West Texas with an increasing trend towards East Texas. The reason for the non-intuitive, low potential evapotranspiration estimates from the Priestley-Taylor method in West Texas is that radiation and temperature data that were measured under non-potential conditions have been used. The Priestley-Taylor estimates are proportional to the net radiation (Figure 4.5) at the earth's surface. In wetter areas of East Texas, there is more water on the land surface and in the atmosphere to absorb incoming solar radiation and this results in higher net radiation values. In addition, greater cloud cover and water vapor in the atmosphere trap a larger percentage of the longwave radiation emitted from the earth. Spatial variation of surface albedo (fraction of incident shortwave radiation reflected) also contributes to this trend because drier, less vegetated areas in West Texas tend to have higher albedos. In addition to spatial trends caused by moisture variation, net radiation values increase from north to south because of the earth's shape and its tilt relative to the sun. The spatial patterns in Priestley-Taylor potential evaporation shown in Figure 4.6 reflect the spatial patterns of temperature and net radiation in Figures 4.4 and 4.5.

Because the net radiation at the earth's surface is directly related to the wetness of the area, it may be a better surrogate for actual evapotranspiration than potential evapotranspiration. In Figure 5.23 a map of Bowen ratios for Texas is presented. As discussed in Section 5.3.3, use of net radiation and temperature data, along with a map of Bowen ratios may be an alternative approach to estimating evaporation that eliminates the use of the difficult potential evapotranspiration concept.



Figure 4-4: Mean Annual Temperature in Texas from Legates and Willmott Climatology

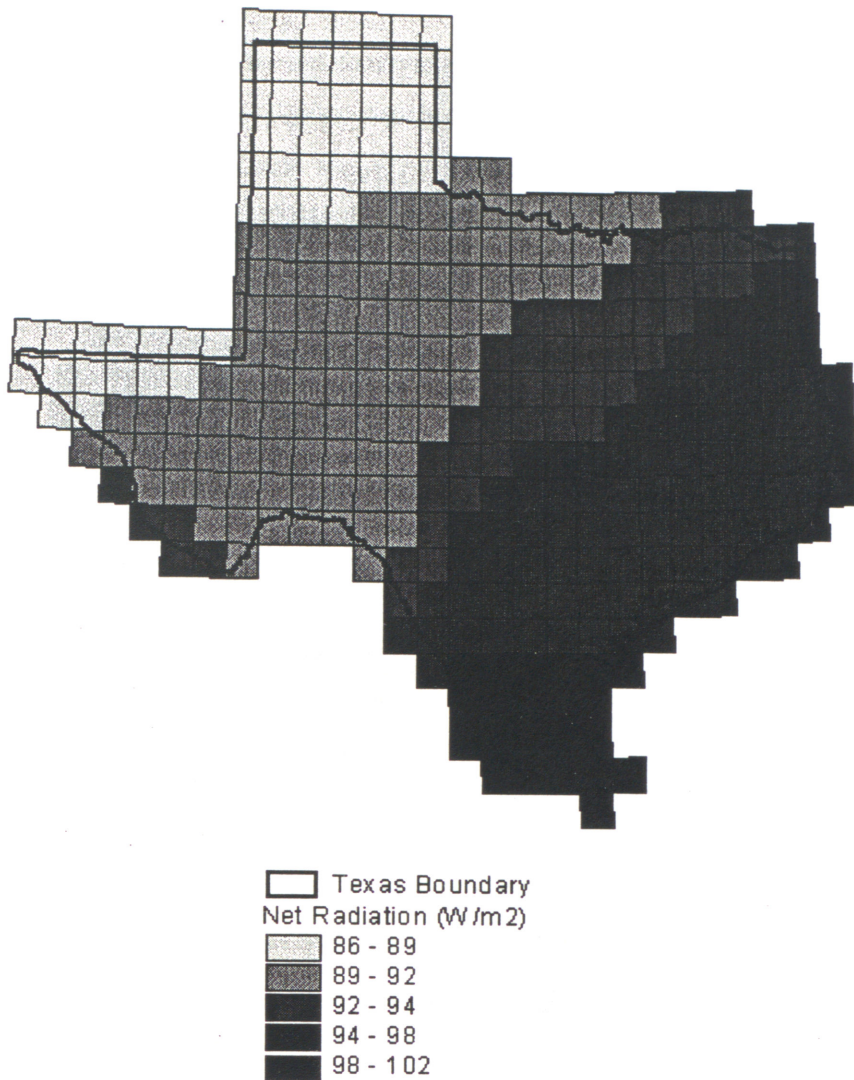


Figure 4-5: Mean Annual Net Radiation Estimates from the ERBE Program

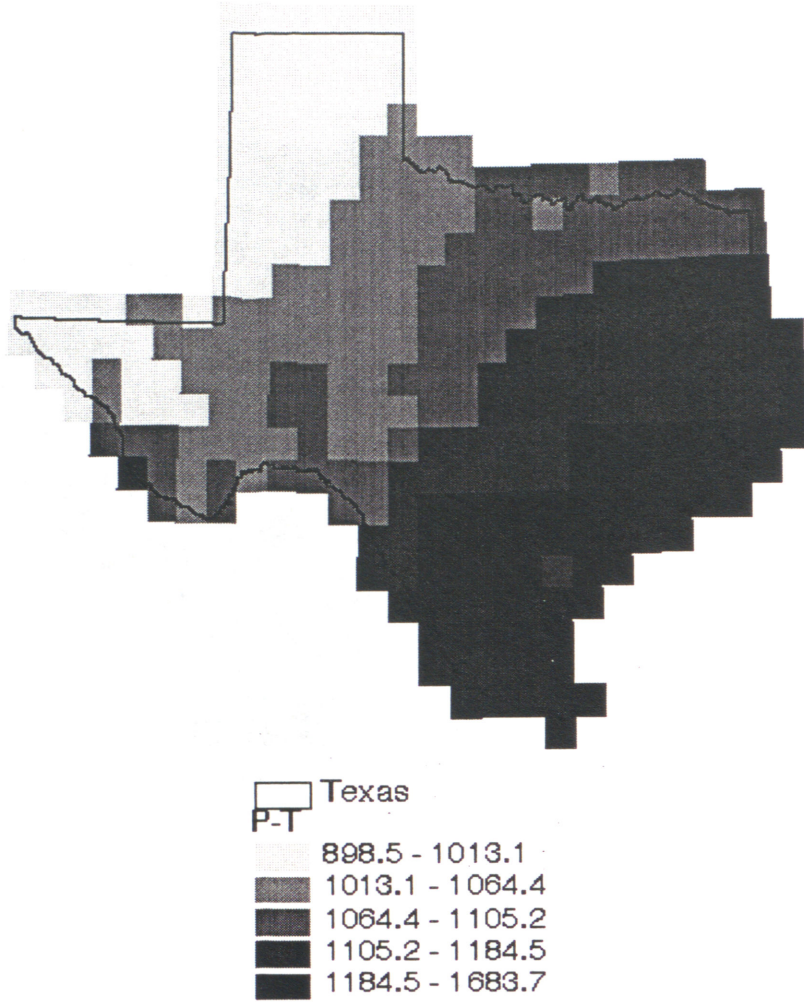


Figure 4-6: Priestley-Taylor Potential Evaporation (mm/year)

In terms of absolute magnitude, the statewide average reservoir evaporation is much higher $1690 \text{ mm year}^{-1}$ than the Priestley-Taylor estimate $1120 \text{ mm year}^{-1}$; however, the values in East Texas are more comparable because the lowest reservoir evaporation estimates and highest Priestley-Taylor estimates both occur here. Looking at the results of the next section, differences in the spatial and temporal distribution between the two potential evaporation estimates make a big difference in the resulting surplus.

4.3 *Results*

The results from the soil water balance are monthly estimates of evaporation, surplus, and soil moisture in each 0.5° grid cell covering the State. Figure 4.7 shows the mean annual surplus estimated from two separate calculations, the first using the Priestley-Taylor potential evapotranspiration method and the second using the reservoir evaporation as potential evapotranspiration. Using the Priestley-Taylor potential evapotranspiration method yields an average of 85 mm year^{-1} of surplus across the State while the use of the reservoir evaporation method yields 42 mm year^{-1} and the observed runoff ($78.4 \text{ mm year}^{-1}$ from Section 5) is somewhere between these two estimates. A major problem is that this soil-water balance model predicts zero runoff for much of the State even though it is known that some runoff occurs in these areas. The time distribution of precipitation, actual evaporation, soil moisture, and surplus for two cells are shown in Figure 4.8. In the cell on the left, the water-holding capacity (162.5 mm) is never reached, but for the cell on the right the water-holding capacity (91 mm) is exceeded during seven months out of the year and surplus is generated.

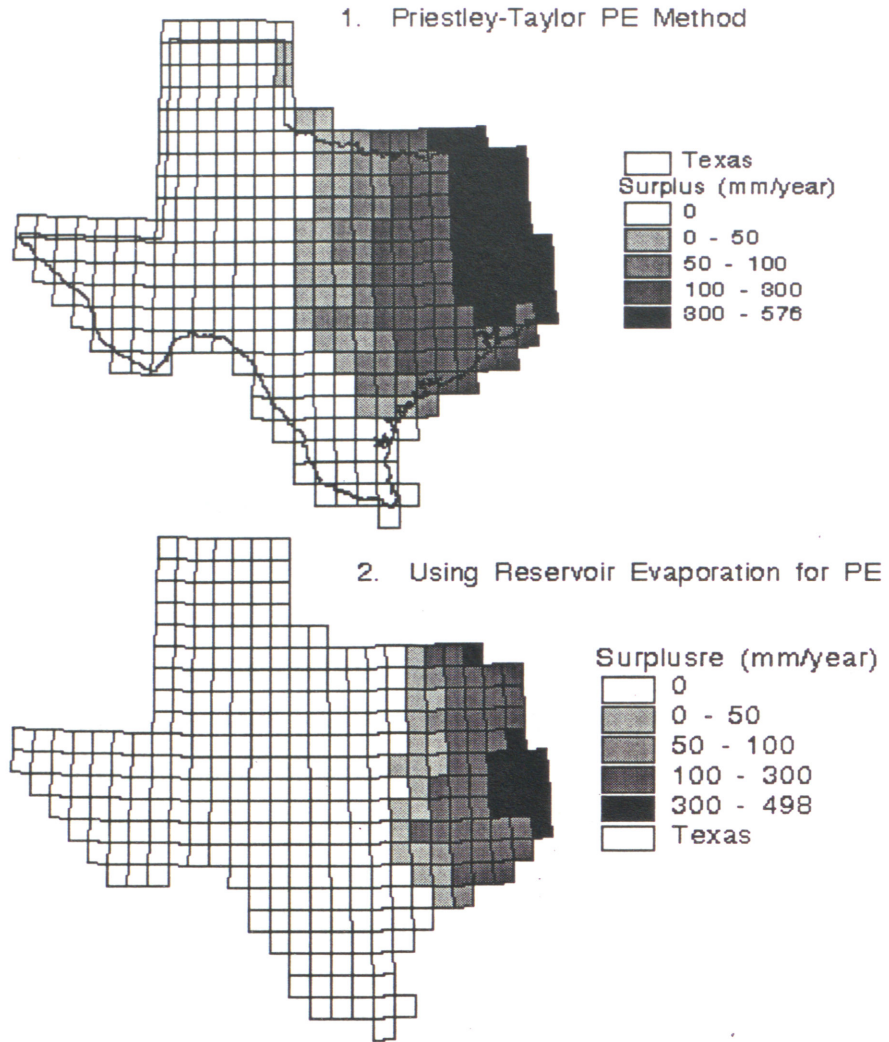


Figure 4-7: Annual Surplus from Soil-water Balance

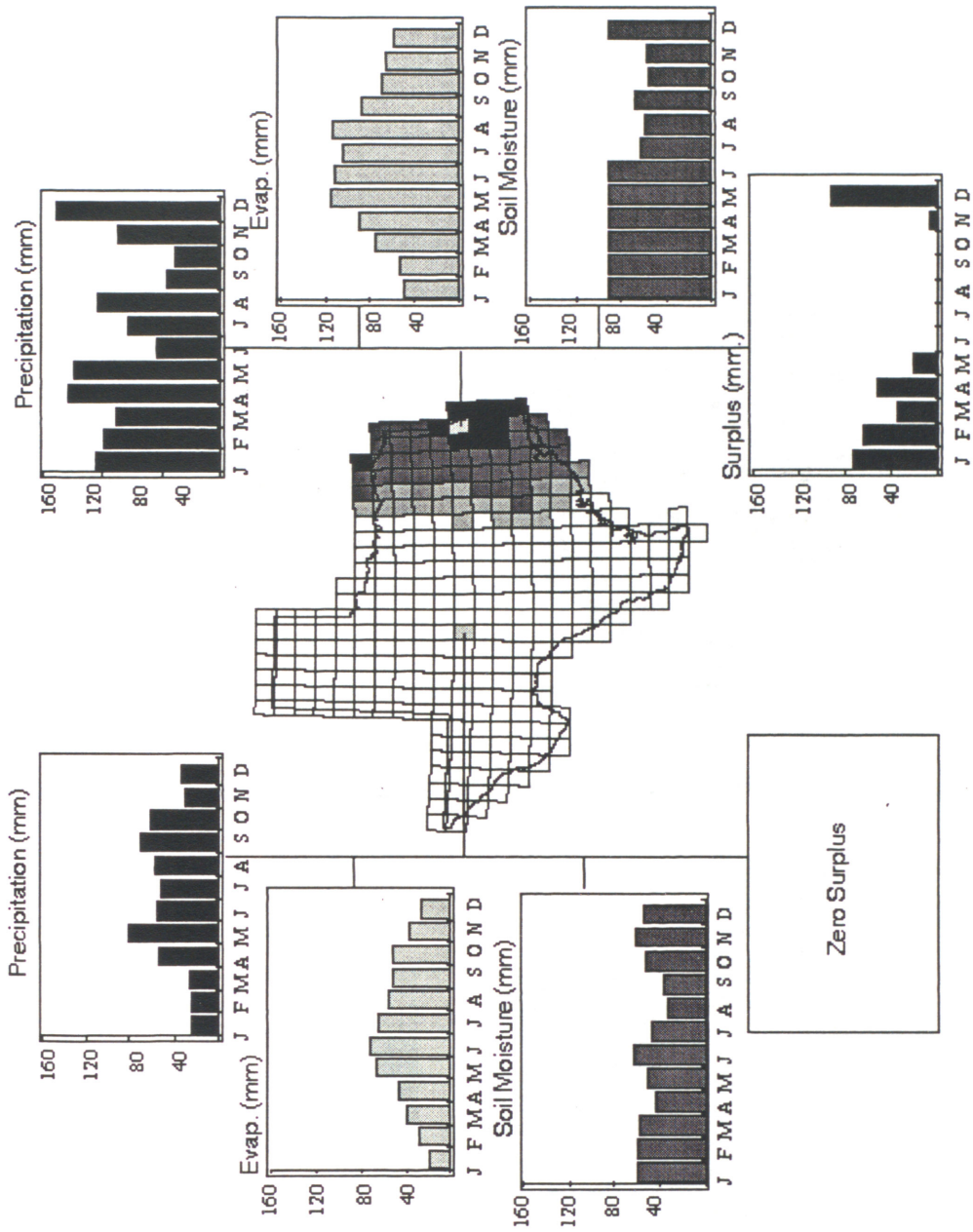


Figure 4-8: Soil-water Balance Monthly Results for Two Cells

The effects of that the water-holding capacity estimate has on soil-water budget can be seen in Figures 4.9 and 4.10. Figure 4.9 shows the mean annual soil moisture [mm] and Figure 4.10 shows the mean annual soil moisture divided by the water holding capacity. The differences in Figure 4.9 and 4.10 occur where the soil water-holding capacity has a limiting effect on evaporation relative to surrounding cells.

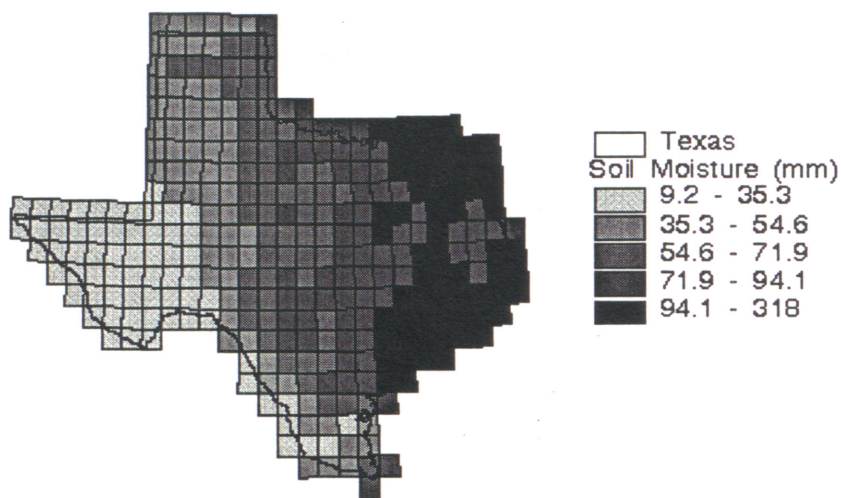


Figure 4-9: Mean Annual Soil Moisture (mm)

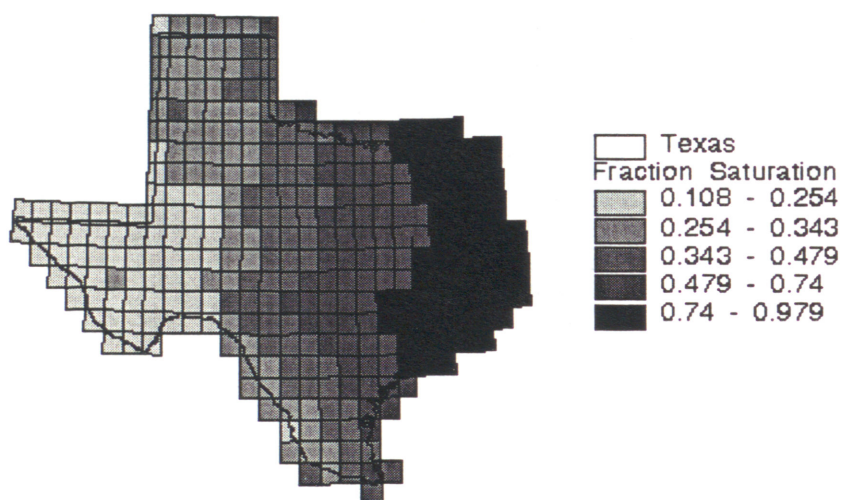


Figure 4-10: Mean Annual Saturated Fraction of Soil-water Holding Capacity

4.4 *Summary*

The rudimentary soil-water balance approach used in this study provides a qualitative sense of how precipitation is partitioned between runoff, evaporation, and soil moisture storage. The surplus and soil moisture values computed with this model are interpreted better as indexes of relative wetness rather than absolute estimates because none are calibrated against measured values. Use of a monthly time step, a simplified representation of soil and plant hydrology, the ambiguity in applying the potential evapotranspiration concept to dry areas, and the errors in estimating potential evapotranspiration are major limitations of this model. The model time step cannot account for storm runoff, an important mechanism for runoff generation. The soil-water balance model is an incomplete hydrology model because it is very difficult to calibrate against observed values. Coupling a soil-water balance model with measured runoff is the only realistic way to derive accurate runoff estimates. A simplified coupling of the soil-water balance model to a surface runoff model was achieved in a recent study to develop a GIS-based water planning tool for the Niger River Basin in West Africa (*Maidment et al.*, 1996; <http://www.ce.utexas.edu/prof/maidment/GISHydro/africa/africa.htm>). This model was calibrated for monthly flows but not validated. A more detailed approach to this type of study could be taken by implementing a continuous stream flow simulation model with daily time stepping (or less); however, implementing this type of model on a region the size of Texas is a formidable task.

5. SURFACE WATER BALANCE

5.1 *Overview*

A 5 km precipitation grid, a 500 m digital elevation model (DEM), gaged streamflow data, and other data sets were used to generate spatially distributed maps of mean annual runoff and evaporation for the state of Texas. In the process of creating these maps, 166 gaged watersheds were delineated and a set of hydrologic attributes was compiled for each watershed including net measured inflow, precipitation, reservoir evaporation, recharge, urban landuse fraction, and springflow. To estimate the runoff in ungaged locations, a curve of “expected” annual runoff as a function of rainfall was developed. The term “expected” refers to runoff that occurs under normal or natural conditions. In other words, watersheds with unique hydrogeology that exhibit unusually large recharge or springflows were removed from consideration, as well as watersheds with a *large* amount of urban development, and watersheds with *significant* reservoir evaporation. The terms *large* and *significant* are described by a set of criteria developed using GIS data layers.

An equation fitted to the expected rainfall-runoff curve was applied to each cell in the precipitation grid to generate an expected runoff grid. For gaged watersheds, the difference between the actual runoff per unit area and the expected runoff per unit area was computed, and these values (one per watershed) were used to create an adjustment grid. The adjustment grid has a 500 m cell resolution so that watersheds delineated at this threshold and 5 km cell information could be combined. Adding the adjustment grid to the expected runoff grid results in a grid of actual runoff. This method forces the sum of cells in the actual runoff grid within each watershed to equal the net measured inflow for that watershed. In ungaged areas, the actual runoff was assumed to be equal to the expected runoff. By applying a flow accumulation function to the runoff maps, the expected and actual flows were calculated at each 500 m DEM cell in Texas and flow maps were created.

Using the assumption that the change in annual watershed storage is zero, a grid of losses was created by subtracting the runoff grid from the precipitation grid. This grid can be interpreted as a grid of evaporation except in locations where there is significant inter-watershed

transfer (Edward's Aquifer flowing to Comal Springs for example). Inter-watershed transfer, of course, depends on which watersheds are delineated.

In this study, rainfall and streamflow data were averaged over the time period 1961-1990. The reason for choosing this time period was that 2.5 minute grids of mean annual and mean monthly rainfall representative of the 1961-1990 period are available for the entire United States. These grids were created at Oregon State University using the PRISM model for interpolation (Daly *et al.*, 1994).

5.2 Methodology

Accomplishing the tasks described above involved a large amount of data processing using ArcView GIS with Avenue, Arc/Info GIS, and FORTRAN. Major steps in the analysis included (1) DEM processing, (2) selecting a set of flow gages spanning the appropriate period of record, (3) delineating watersheds from selected gages, (4) determining the average annual precipitation in each watershed, (5) determining the net measured inflow to each watershed, (6) compiling a set of watershed attributes including percent urbanization, reservoir evaporation, recharge, and springflow, (7) plotting runoff per unit area versus rainfall per unit area and deriving an "expected" runoff function, and (8) creating grids of expected runoff, actual runoff, and evaporation.

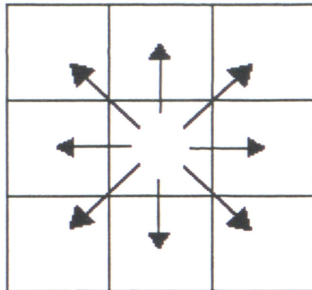
5.2.1 Digital Elevation Model Processing

Two digital elevation models (DEMs) were used for defining watersheds in this study. The portion of the 15" USGS DEM covering the conterminous United States that either falls within or drains to Texas was clipped for use in this study. To approximate the Rio Grande drainage contribution from Mexico, a piece of the 30" USGS DEM of North America was merged with the 15" DEM. A 15" DEM corresponds to approximately 500 m on the earth's surface and a 30" DEM corresponds to approximately 1 km. To cover all areas draining to Texas a grid of approximately 10 million cells was processed, although only about 2.7 million of these cells actually fall within Texas.

The eight direction pour point model is the basic model that underlies watershed and drainage network delineation with grid processing. As illustrated in Figure 5.1, the assumption is

that water in a given cell will flow towards only one of its neighboring cells, whichever cell lies in the direction of steepest descent. A Flowdirection function applied to an elevation grid (Figure 5.1b) yields a grid of flow directions (Figure 5.1c). From this grid of flow directions, a drainage network is derived (Figure 5.1d). The flow accumulation is the number of cells upstream of any given cell in the drainage network.

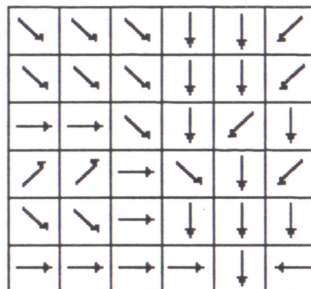
(a) Eight-direction Pour Point Model



(b) Grid of Terrain Elevations

78	72	69	71	58	49
74	67	56	49	46	50
69	53	44	37	38	48
64	58	55	22	31	24
68	61	47	21	16	19
74	53	34	12	11	12

(c) Grid of Flow Directions



(d) Drainage Network Showing Flowaccumulation

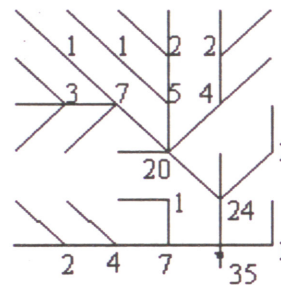


Figure 5-1: Drainage Network Delineation

Before defining the drainage network using the eight direction pour point model, several processing steps were taken in order to create a "hydrologic" DEM from the raw DEM. First, the data from the two DEMs (Texas and Mexico) were merged into one grid. Next, the combined DEM was filled to remove pits. A pit is a cell or group of cells that is lower than all of its neighboring cells. Pits are removed so that there will be no discontinuities in the drainage network derived from the DEM; no internal drainage is allowed by this model. The DEM was also modified so that streams delineated from the DEM are consistent with digitized streams in EPA's River Reach File 1 (RF1). This process of DEM modification is referred to as "burning in

the streams." The simplest stream burn-in procedure involves (1) creating a gridded representation of the digitized stream network (RF1) and identifying cells as being either stream cells or land surface cells, (2) raising the elevation of land surface cells relative to stream cells, and (3) deriving the drainage network based upon flow direction values defined by the burned DEM. Because many arcs in RF1 are not connected to the major river systems, burning in these arcs creates inland drainage basins or pits. Some of these disconnected arcs may represent real inland drainage basins or playas; however, information as to where inland drainage occurs was not readily available, so the DEM was filled a second time to eliminate pits created by the burning procedure. One drawback of the DEM analysis used here is that non-contributing drainage areas are considered as contributing to downstream runoff. This may cause the runoff per unit area estimates in some watersheds to be too low; however, the runoff total at watershed outlets is still consistent with measured flows. Figure 5.2 is a map showing the processed DEM and Figure 5.3 is a map showing RF1 streams.

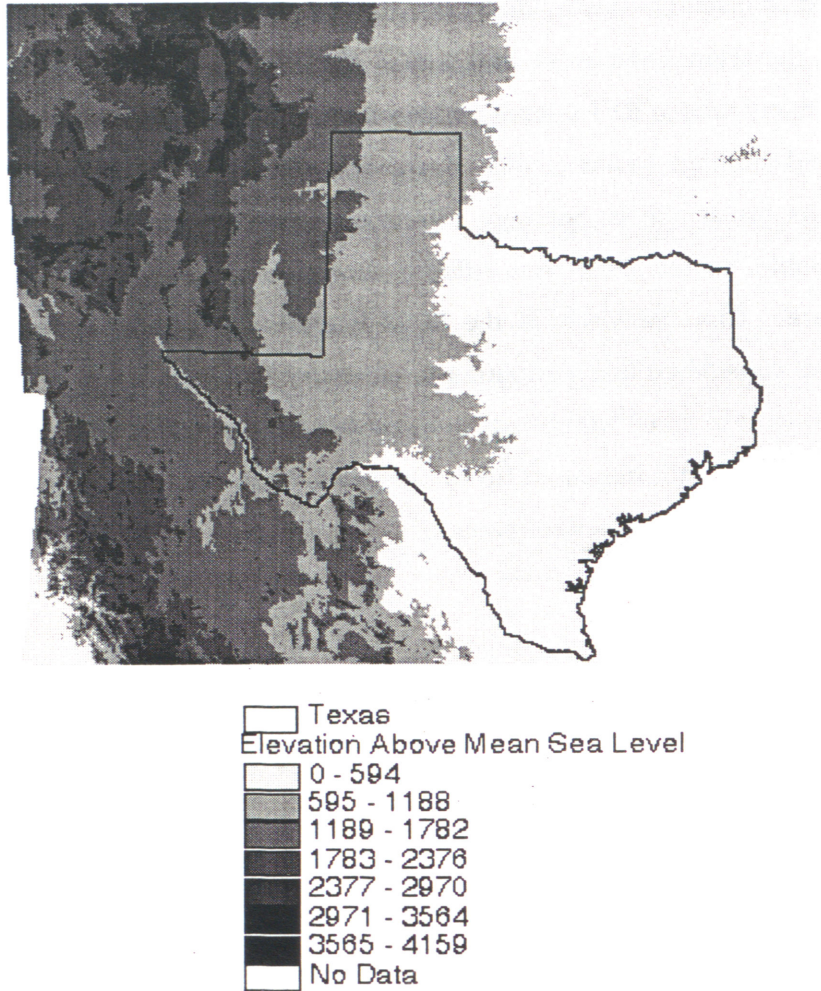


Figure 5-2: Processed Digital Elevation Model



Figure 5-3: EPA River Reach File 1 Streams

The flow direction and flow accumulation grids derived from the burned DEM were used to delineate watersheds and streams. A grid of stream cells contains those cells with a flow accumulation greater than 1000 cells or 250 km². Cells on this stream network are candidates for selection as watershed outlet cells. A 1000 cell threshold was chosen because watersheds delineated with fewer than 1000 cells tend to be poorly defined. A grid of stream links was also created using the stream network and flow direction grids. In the stream link grid, each stream reach is assigned a unique value. This is useful because each outlet cell used to delineate watersheds needs to have a unique value and outlet cells selected directly from the stream link grid satisfy the criterion as long as there are not two gages along the same reach. In this study, outlet cells were selected based upon the location of USGS gaging stations. The manner in which stations were selected for analysis is described in the next section.

5.2.2 Selecting Gaging Stations for Analysis

All monthly and daily flow records for the water years 1961 - 1990 and for all USGS gaging stations in Texas were extracted from the Hydrosphere CD-ROM "USGS Daily Values : West 2." The Hydrosphere software was used to write the flow records for all Texas stations to a dBase file. This dBase file also includes latitude, longitude, and other station information. Because this dBase file is very large, with up to 360 records for each of 693 stations, an Avenue script was used to extract summary information for each station. The result is a dBase file that contains only one record for each station. Key attributes available for each station record are latitude, longitude, starting year, ending year, 30-year mean monthly flows, and 30-year mean annual flows.

From the list of 693 stations, stations operating during the entire 1961-1990 period were selected, yielding a set of 164 stations. Even with all 164 stations, there is almost no coverage of the Rio Grande basin and sparse coverage of the western part of the Red River basin; therefore, an additional 21 gages were selected to cover these areas. Figure 5.4 is a map of station locations. Although these gages have incomplete records for the 1961-1990 averaging period, the 30-year mean flows were approximated by using an adjustment based on a nearby gage with a complete record for this period. The following equation was used for making flow adjustments:

$$Q_{b,30} = Q_{a,30} \times \frac{Q_{b,x}}{Q_{a,x}} \quad (5.1)$$

In Equation 5.1, station b is a station with incomplete records covering x years ($x < 30$) of the period from 1961 - 1990 and station a is a nearby station with complete records for this period.

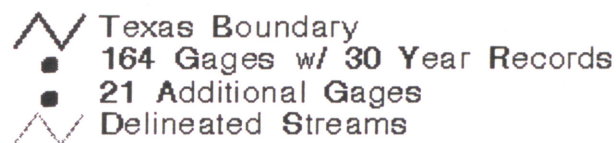
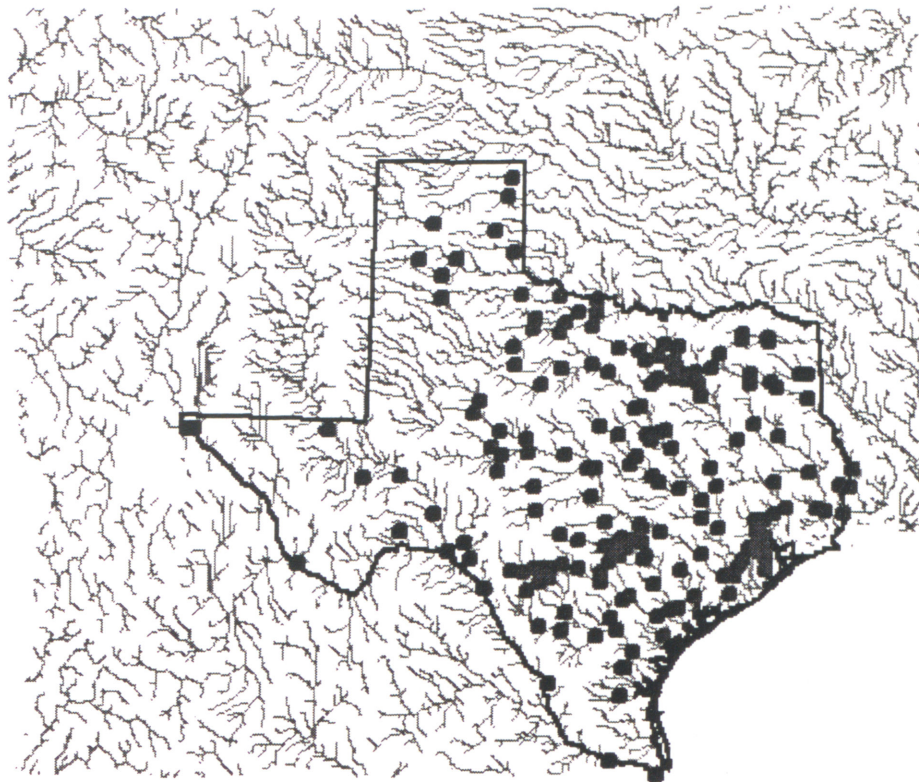


Figure 5-4: USGS Flow Gaging Stations

5.2.3 Watershed Delineation

Watershed delineation requires a grid of flow directions and a grid of outlet cells. Deriving a grid of flow directions was described in the above section on "DEM Processing." Because the latitude and longitude coordinates of the USGS gaging stations do not fall precisely on the gridded stream network, some mechanism for choosing outlet cells is required. An AML script that runs in Arc/Info Grid was used to select outlet cells. This script takes a point coverage of gaging stations and a grid of stream links as input. The script is interactive and works in the following way: The program loops through the point coverage and the vicinity of the current

point (approximately ten cells in each direction) is displayed. The user is then prompted to select an outlet cell and after selection, the coordinates of the selected cell are written to a text file. Using the output text file, a point coverage of outlets can be created and this point coverage converted to a grid of outlets. With this grid of outlets and the flow direction grid, watersheds are delineated. The reason for interactive selection of outlets is that some user discretion may be required. In this study, watersheds with a drainage area less than 250 km² were not delineated, resulting in the delineation of 166 watersheds.

After studying the watershed delineation, two correctable errors in the delineation were found. The first error was that part of the Red River Basin drained southward into the Rio Grande Basin. This error was caused by the burn-in procedure – the proximity of two tributaries in RF1 that drain towards different basins resulted in the creation of a ditch that crossed a ridge line. This error was corrected by manually editing two cell values in the burned DEM. The second error involves the delineation of the Mexico portion of the Rio Grande. Although no counterpart to the RF1 line work was available for Mexico, a comparison of the delineated Rio Grande basin with a published map revealed an extraneous area in Mexico (southwest of El Paso) draining towards the Rio Grande. This problem appears to be caused because the fill procedure filled an area that may actually be an inland drainage basin or basins. The problem was corrected by editing a string of cells in the burned DEM; however, this correction is only an approximate visual correction and the accuracy of the resulting delineation in defining the drainage area of the Rio Conchos tributary of the Rio Grande is questionable. After these DEM edits were made, the flow direction grid was re-calculated and the watershed re-delineated. Figure 5.5 shows the delineated watersheds. For reference, the fifteen major river basins in Texas were also delineated using a similar procedure to that used for delineating all 166 watersheds.

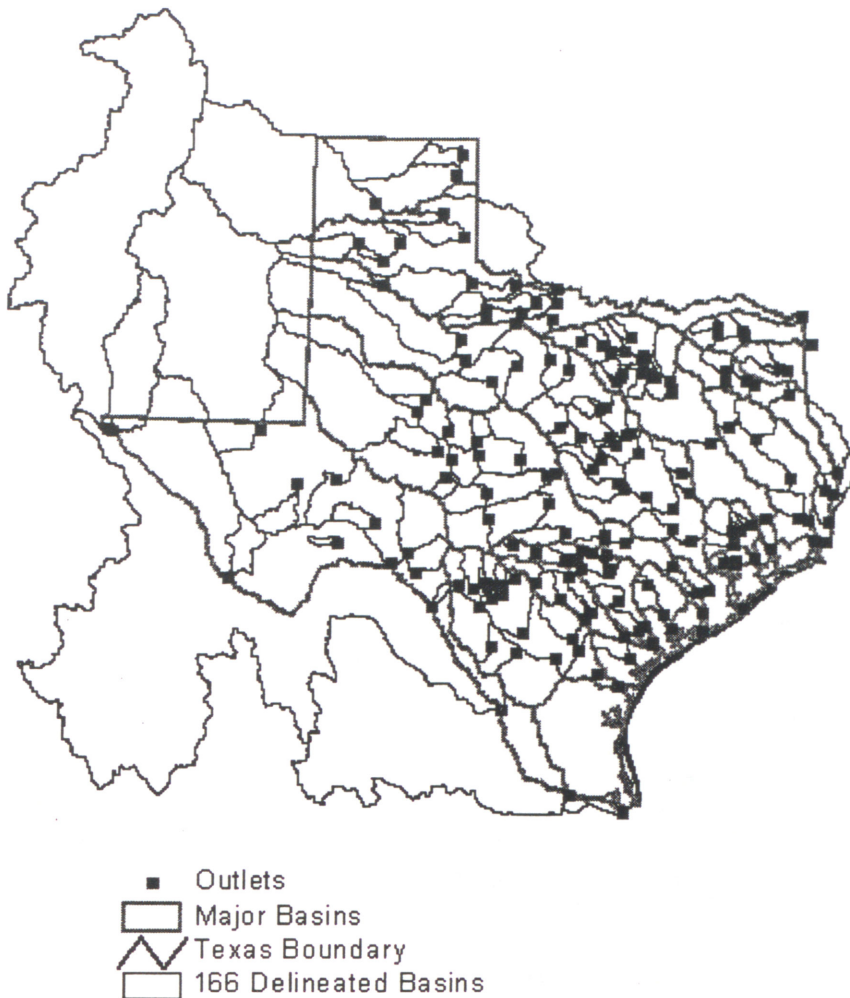


Figure 5-5: 166 Delineated Watersheds

A comparison was made between the drainage areas defined by the DEM and those reported by the USGS for each gage. Since the USGS reports total upstream drainage area, the USGS incremental drainage areas were computed for non-source watersheds. For all but 16 of the delineated watersheds, the DEM area is within 15% of the area reported by the USGS. This comparison is shown in Figure 5.6. The 16 watersheds with incorrect areas were not used in the analysis. The reasons for some of the worst discrepancies are obvious, and some of the discrepancies are clearly problems with using the DEM while others point to errors in the USGS values. For example, one station on the Sabine River has a USGS reported drainage area of about 19,000 km² while an upstream station has a reported drainage area of 21,000 km² which can't be true. In another situation, the USGS gage measures flow in a government ditch rather than a natural stream and DEM analysis cannot identify a government ditch. The drainage area

of the Rio Grande from Mexico is suspect because of inaccuracies associated with using the 30" DEM. Despite these problems, the accuracy achieved using the 500 m DEM is satisfactory in most of the watersheds, especially since the total runoff predicted for each watershed (sum of the runoff in all cells) is forced to match that dictated by the gaging stations.

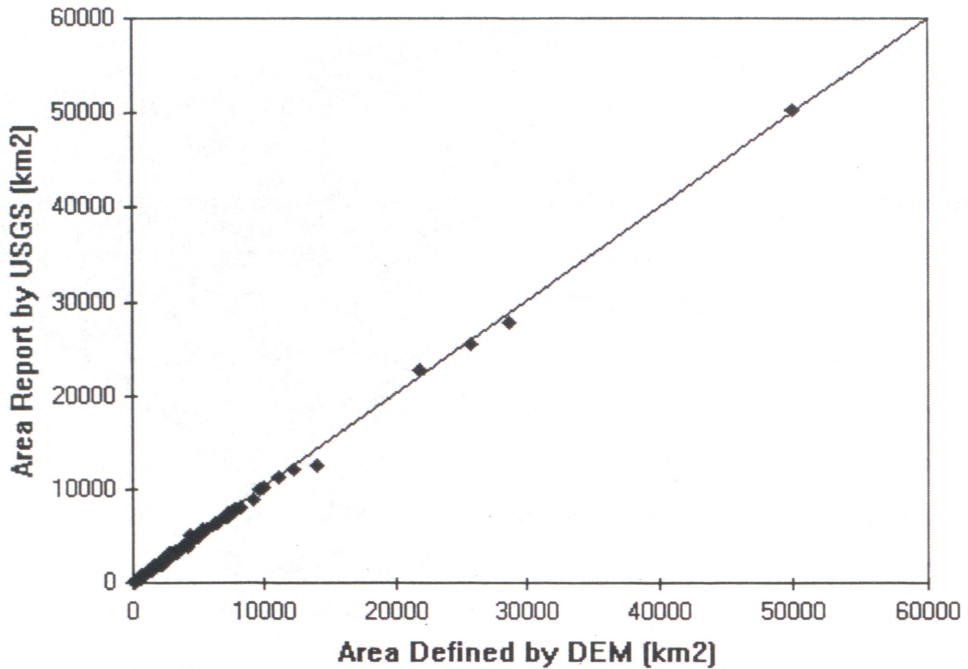


Figure 5-6: Watershed Areas Reported By USGS versus Areas Defined by DEM for All But 16 Watersheds

5.2.4 Compiling Watershed Attributes

5.2.4.1 Determining Mean Precipitation and Net Inflow

Given a grid of precipitation values and a grid of watersheds, a single Arc/Info Grid function (Zonalstats) creates a table of the mean precipitation in each watershed, provided the two grids are defined with the same cell size. Precipitation grids of the United States (2.5') with mean monthly and mean annual values (approximately 5 km in projected space) were used in this study. The precipitation grids were resampled to a 500 m cell size to match the resolution of the watershed boundaries and enable the computation of watershed averages. Since the Mexico portion of the Rio Grande is not covered by these 2.5' grids, a global 0.5° data set obtained from Cort Willmott at the University of Delaware was used to fill in this space. The values in the Willmott grids were adjusted by a ratio to reflect the same climatic averaging period as that used

to create the Oregon State grids. The combined grid of mean annual values is shown in Figure 5.7.

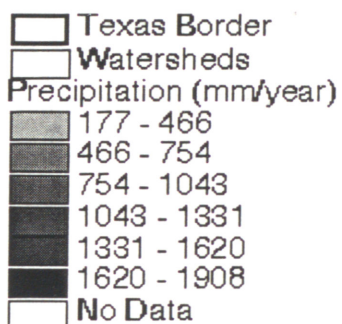


Figure 5-7: Grid of Mean Annual Precipitation

Based on computed 30 year mean flows for each station (see Section 5.2.2), the net measured inflow (outflow minus the sum of inflows) for each of the 166 watersheds was computed with the assistance of Avenue scripts described in the Appendix. To make a comparison of the runoff

characteristics among different size watersheds, the net measured inflow [cfs] was normalized by the watershed area and expressed in [mm year^{-1}].

5.2.4.2 *Reservoir Evaporation*

Mean annual evaporation due to reservoirs in each of the 166 watersheds was estimated. The data used to make these estimates, reservoir evaporation data and a reservoir area, were provided by the Texas Water Development Board (TWDB). A text file containing monthly average gross reservoir evaporation estimates for 1° quadrangles in Texas was provided by Alfredo Rodriguez, TWDB, (personal communication, 1996). This text file contains monthly data for 1940 to 1990 in 75 quadrangles and monthly data for 1971-1990 in 28 quadrangles. The gross monthly evaporation data were written to an INFO file and the average potential reservoir evaporation for each year was computed, as well as the average reservoir evaporation for our 30 year study period 1961 - 1990 (or 1971 - 1990 for those quadrangles lacking records back to the 1960's). An Arc/Info coverage of the quadrangles was created and several attributes were joined to this coverage: TWDB identification number, starting and ending years for available data, mean reservoir evaporation from 1961-1990, and mean reservoir evaporation from 1971-1990. As discussed in Section 4.1.2.3, Figures 4.2 and 4.3 show the quadrangle index map and mean annual evaporation respectively.

An Arc/Info coverage of reservoirs was obtained from the TWDB. This coverage includes both reservoirs that have already been built and proposed reservoirs. A spreadsheet was also provided which contains information about impoundment date; flood area, capacity, and elevation; conservation area, capacity, and elevation; and dead storage area, capacity, and elevation. These attributes were joined to the coverage of reservoirs. Since this study is being made based on mean flow and precipitation data from 1961 to 1990, the total reservoir evaporation from each watershed was estimated for two cases: reservoirs with pre-1960 impoundment dates and reservoirs with pre-1990 impoundment dates. Assuming that reservoir evaporation estimates are accurate, the estimates from these two cases should bound the actual reservoir evaporation that occurs in each watershed. The volume of reservoir evaporation was estimated by multiplying evaporation rate (depth/year) times reservoir conservation area. The total reservoir evaporation for each delineated watershed and each major basin in Texas were also computed by summing up the contributions from each reservoir within these areas. This

information was used as a selection criterion for determining which watersheds have a significant anthropogenic influence.

5.2.4.3 *Urban Land Use*

To identify watersheds where the runoff characteristics might be affected by large amounts of urbanization, the fraction of each watershed covered with "urban or built up land" according to the Anderson Level 1 land use codes was computed. A polygon coverage for the state of Texas with land use attributes was compiled by Smith (1995) using data obtained from the USGS. A few modifications were made to this coverage to simplify the calculations made in this study. This information was also used to identify watersheds where human influence may have altered natural runoff characteristics.

5.2.4.4 *Recharge*

A map of DRASTIC ratings for net recharge was obtained from Dr. Samuel Atkinson at the University of North Texas. DRASTIC is a method developed by the United States Environmental Protection Agency (EPA) to assess groundwater pollution potential. Lumped recharge estimates published in TWDB Report 238 based upon zones defined by river basin and county boundaries were used to create this DRASTIC map. A simple assumption was made in the DRASTIC study to distribute this recharge over aquifer outcrop and downdip areas (Atkinson *et al.*, 1992). Since the data obtained from Dr. Atkinson were actually DRASTIC ratings for recharge rather than explicit recharge values, these ratings were converted to recharge estimates in mm year^{-1} based upon Table R-2 in Atkinson *et al.*, 1992. There are only four unique recharge rating values in the DRASTIC grid of Texas. Figure 5.8 shows that most of Texas has less than 51 mm year^{-1} of recharge and the highest recharge values occur in the Edward's Aquifer. Based on this recharge map, the average recharge in each watershed was calculated. Watersheds with high recharge were not considered in the development of the expected runoff function.

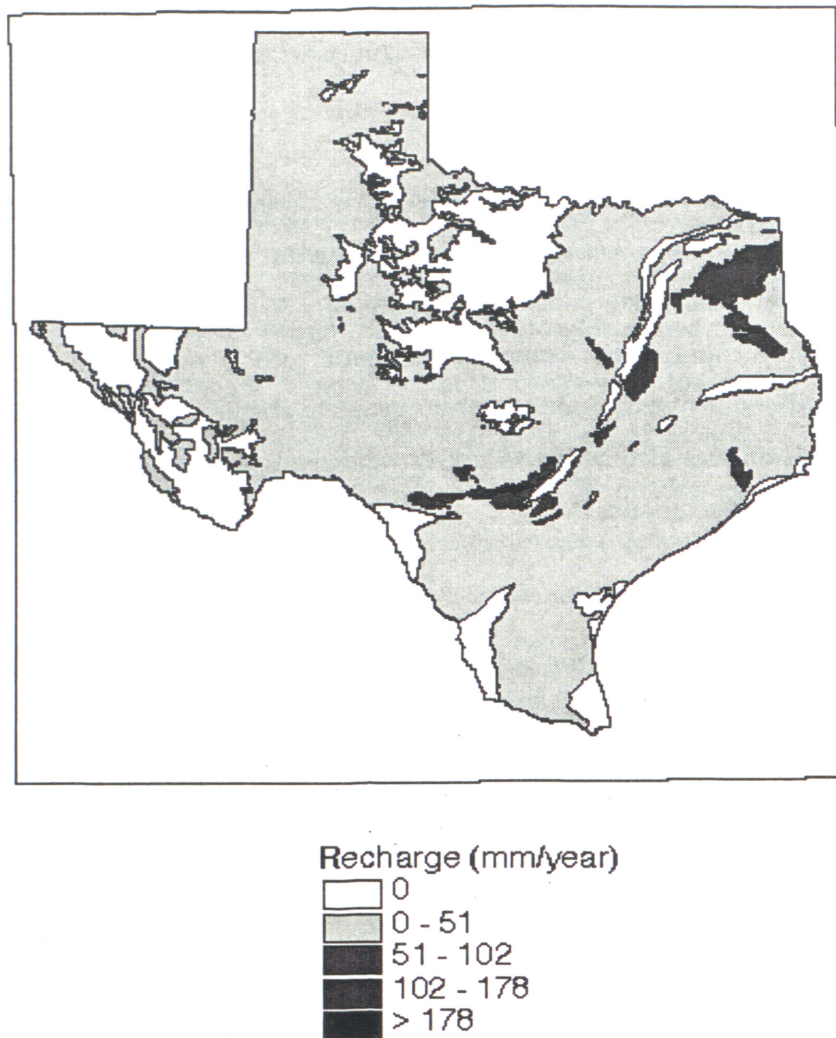


Figure 5-8: Average Annual Recharge (mm/year) Based Upon DRASTIC Ratings

5.2.4.5 Springs

When looking at the runoff data, it became clear that springflow can dominate the runoff characteristics of watersheds in certain locations (the watershed containing Comal Springs for example). For this reason, a point coverage of springs in Texas was created using information from TWDB Report 189, "Major and Historical Springs of Texas." Springs described in Report 189 with an observed flow of at least 2 cfs at any time in history are included in this point coverage. The coverage includes spring name, maximum observed flow, and year of maximum observed flow. The reason that maximum observed flows were used rather than mean flows is

that Report 189 contains limited observations for many of the springs. Maximum spring flows also serve as a conservative estimate if the question is whether or not a streamflow is significantly influenced by springflow. To try to quantify the influence of spring flow on watershed runoff characteristics, the sum of maximum spring flows within each watershed was computed, and this flow rate (cfs) was normalized by watershed area to get millimeters of springflow per year per watershed area. Use of the estimated spring flow values did not turn out to play a large role in the development of the expected runoff function because using a recharge rate criterion eliminated almost all watersheds with large spring flows from consideration.

5.3 Results and Discussion

5.3.1 Expected Runoff

A plot of the average runoff per unit area (mm) versus average rainfall (mm) for all delineated watersheds is shown in Figure 5.9. A trend of increasing runoff with rainfall is clear, but there are a number of outliers from the general trend. These are the points that merit further investigation. Most of the outlying points are from watersheds with significant anthropogenic influence in the form of urbanization, reservoirs, agriculture, or diversions for municipal use. A few of these outliers result from unusual hydrogeology. For example, karst formations in the Edwards Aquifer transfer significant quantities of water between watersheds delineated in this study. This results in lower than expected runoff in the watershed where recharge is occurring and higher than expected runoff in the spring fed stream of an adjacent watershed. Heavy recharge and re-emergence of this same water as springflow within a watershed may also limit evaporative losses and result in higher than expected runoff values. These observations regarding outlying points led to the hypothesis that a set of criteria could be used to define the runoff expected under conditions of minimal human influence and in the absence of large groundwater transmissions.

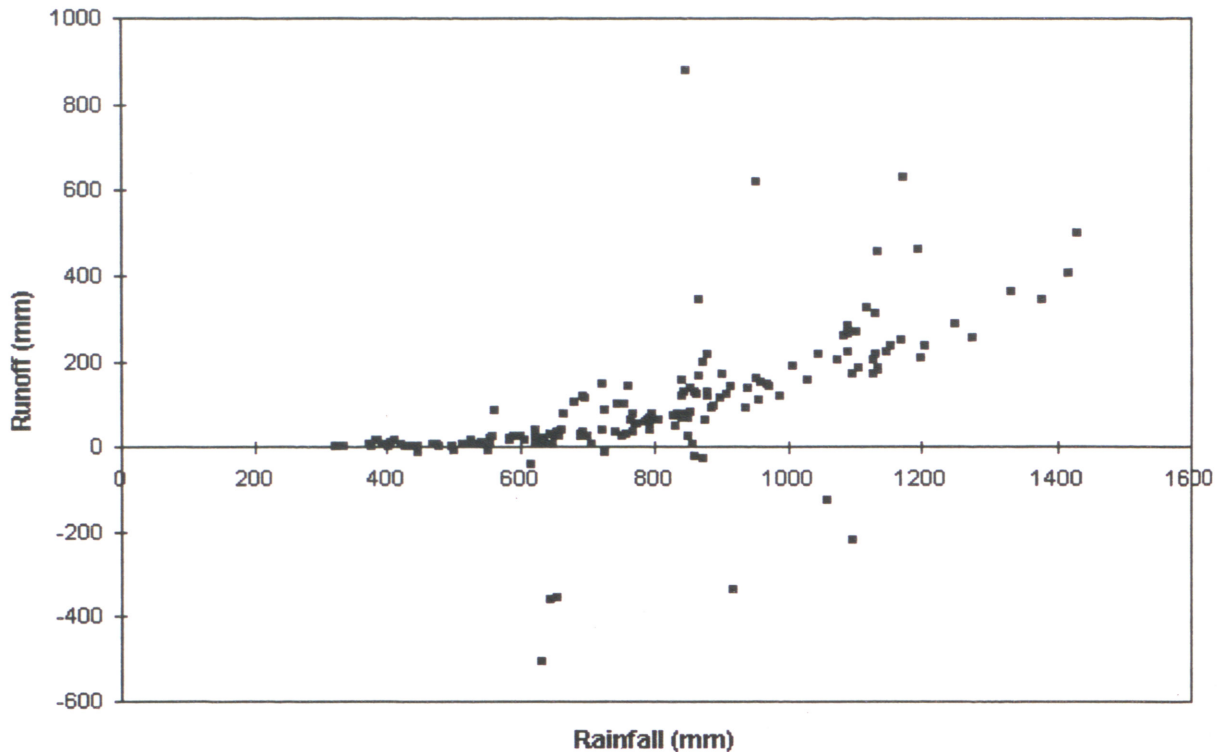


Figure 5-9: Runoff vs. Rainfall for All Watersheds

As described in the previous section, many attributes have been compiled for each watershed. Using this set of attributes, query tools in ArcView GIS facilitate expedient analysis of how different criteria affect the plot of rainfall versus runoff shown in Figure 5.9. After trying many sets of criteria, the following set was selected as a reasonable set that produces a subset of watersheds with a more definitive relationship between rainfall and runoff than that seen using all 166 watersheds:

- net measured inflow is greater than zero
- area delineated from the DEM is within 15% of the area reported by the USGS
- the fraction of the drainage area that is urbanized is less than 0.1
- annual recharge is less than 51 mm year^{-1} (note that most of the state has a recharge between 0 and 51 mm year^{-1})
- the reservoir evaporation [mm/watershed area] from reservoirs impounded before 1990 divided by the rainfall [mm] is less than 0.1

After these criteria are satisfied, two distinctive outliers from the general trend remain. One of these points represents data for a spring fed river in south Texas called Devil's River. Including another criterion that limits the maximum springflow [mm/watershed area] divided by rainfall [mm] to less than 0.03 eliminates this point. The last outlying point is for a section of the Sulfur River in northeast Texas. The increased runoff at this location may be due to channelization of this river by the U.S. Army Corps of Engineers, but this is only speculation. This point was not considered when deriving the expected runoff function.

A function that minimizes the sum of squared errors was fit to the remaining data points. Figure 5.10 shows this selected set of 90 watersheds and Figure 5.11 is a plot of the data points for these watersheds with the fitted function. The fitted function takes the following form

$$\begin{aligned} Q &= 0.00064P \exp(0.0061P) & P < P_0 & \quad (5.2) \\ Q &= 0.510P - 339.1 & P \geq P_0 & \end{aligned}$$

where Q is runoff (mm year^{-1}) and P is precipitation (mm year^{-1}). An exponential function was fit to the data in drier areas with mean annual rainfall less than $P_0 = 801 \text{ mm year}^{-1}$. It turns out that a linear function yields a better fit to the wetter watersheds with rainfall above P_0 . In theory, with increasing rainfall, one might expect the slope of the rainfall-runoff curve to keep increasing until a value of 1 is reached, indicating that the maximum amount of evaporation possible has been reached. At this point, the only difference between the precipitation and observed runoff would be the potential evaporation. The amount of annual rainfall needed to reach this theoretical slope of 1 is certainly beyond the range of rainfall values in this data set. Figure 5.12 is a plot of the annual runoff coefficient (runoff/rainfall) versus rainfall based on the function of Figure 5.11.

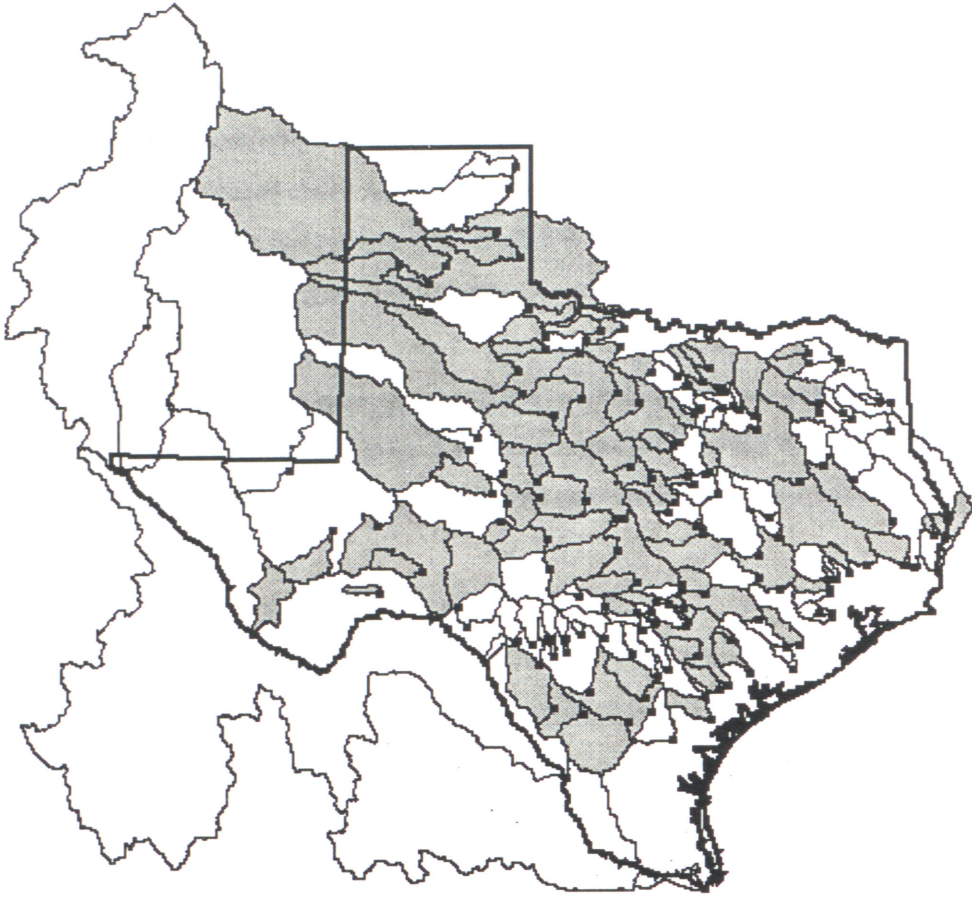


Figure 5-10: 90 Selected Watersheds

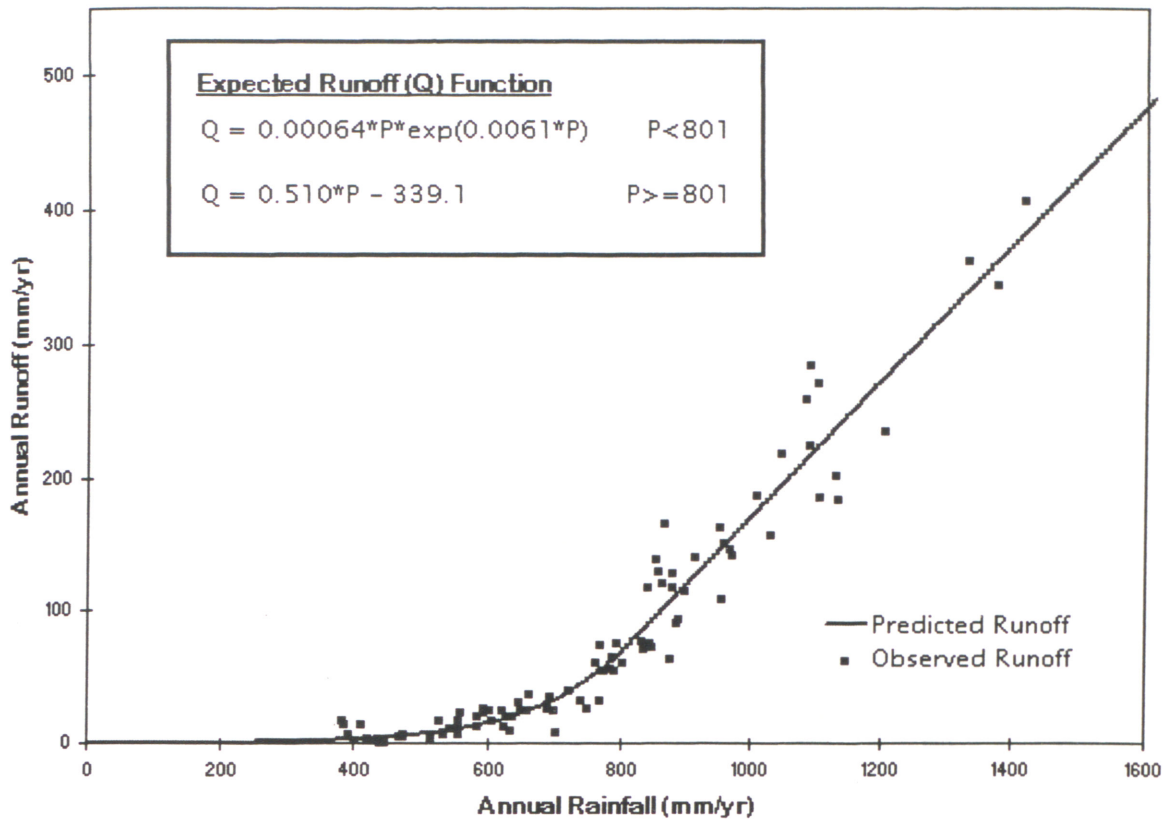


Figure 5-11: Runoff vs. Rainfall for Selected Watersheds

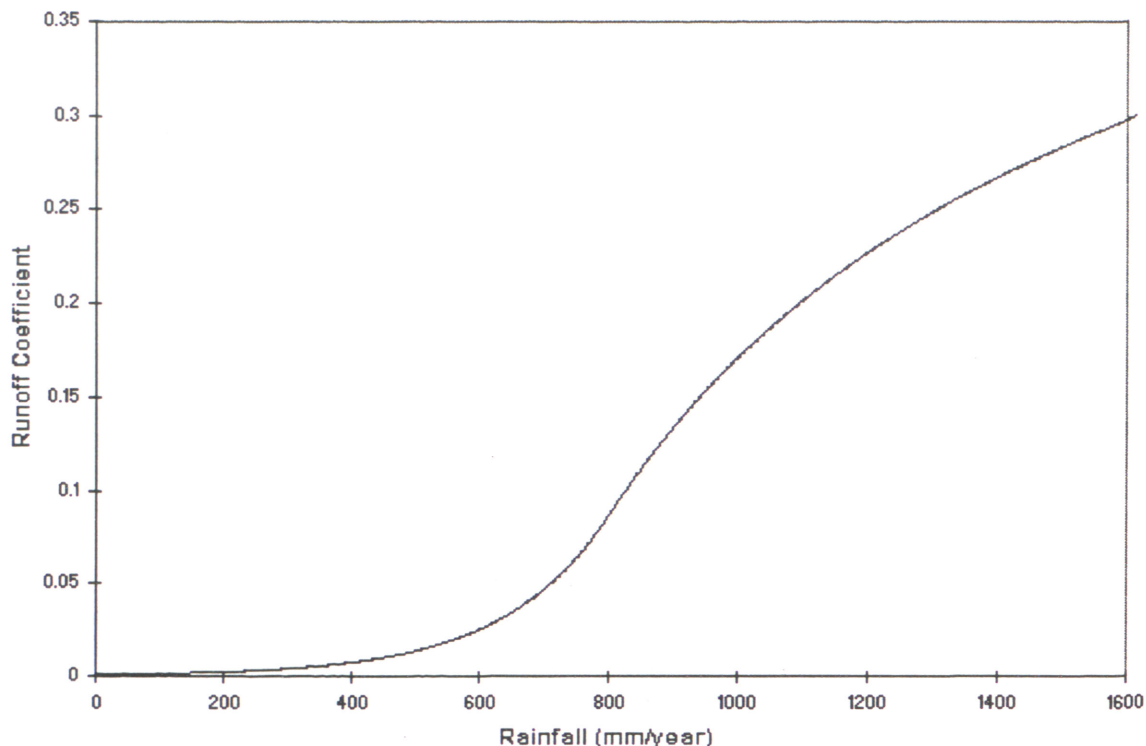


Figure 5-12: "Expected" Annual Runoff Coefficient

By choice of selection criteria, the notion is that the expected runoff function can be used to estimate natural runoff in all areas except major groundwater recharge and discharge zones. The map of recharge shows that 97% of the state has less than 51 mm of recharge annually, implying that estimates of natural runoff are valid over most of the state.

Criticisms of the expected runoff curve are easy to come by. The concept of expected runoff is artificial and the precise form of the curve is subjective. The criteria used in developing this curve were specifically chosen to eliminate data points that don't fit the trend, an approach that certainly will not please statisticians. In their defense, the criteria used to derive the expected runoff curve are based upon real, physical data that define the concept itself. In addition, information from the outlying points was not discarded; this information was used to create a map of actual runoff. The fact that data from watersheds ranging in size from 250 to 50,000 km² follow the same trend, implies that the behavior represented by the expected runoff curve is scale-independent, which is an interesting result. Using the inference of scale-independence, the expected runoff function was applied to the 5 km precipitation grid to create a spatially

distributed map of expected runoff. This runoff function is not suitable for application in urban areas because data from watersheds with considerable urbanization were not used in its development.

5.3.2 Mapping Actual Runoff and Evaporation

A grid of actual runoff was created on a 500 m grid by combining net runoff information at the watershed scale with expected runoff information at the 5 km grid scale. To create the actual runoff grid, an adjustment grid was created in which all cells in a given watershed were assigned the value of measured runoff per unit area less the watershed mean expected runoff, and this adjustment grid was added to the expected runoff grid (which had been resampled to a 500 m cell size). The expected runoff grid, the adjustment grid, and the actual runoff grid are shown in Figure 5.13, Figure 5.14, and Figure 5.15 respectively.¹ The expected runoff map reflects the precipitation variation across the state. Expected runoff values range from less than 10 mm year⁻¹ in West Texas to about 415 mm year⁻¹ in the wettest part of East Texas.

¹ The adjustment and actual runoff grids have been resampled to a 5 km grid size for display.

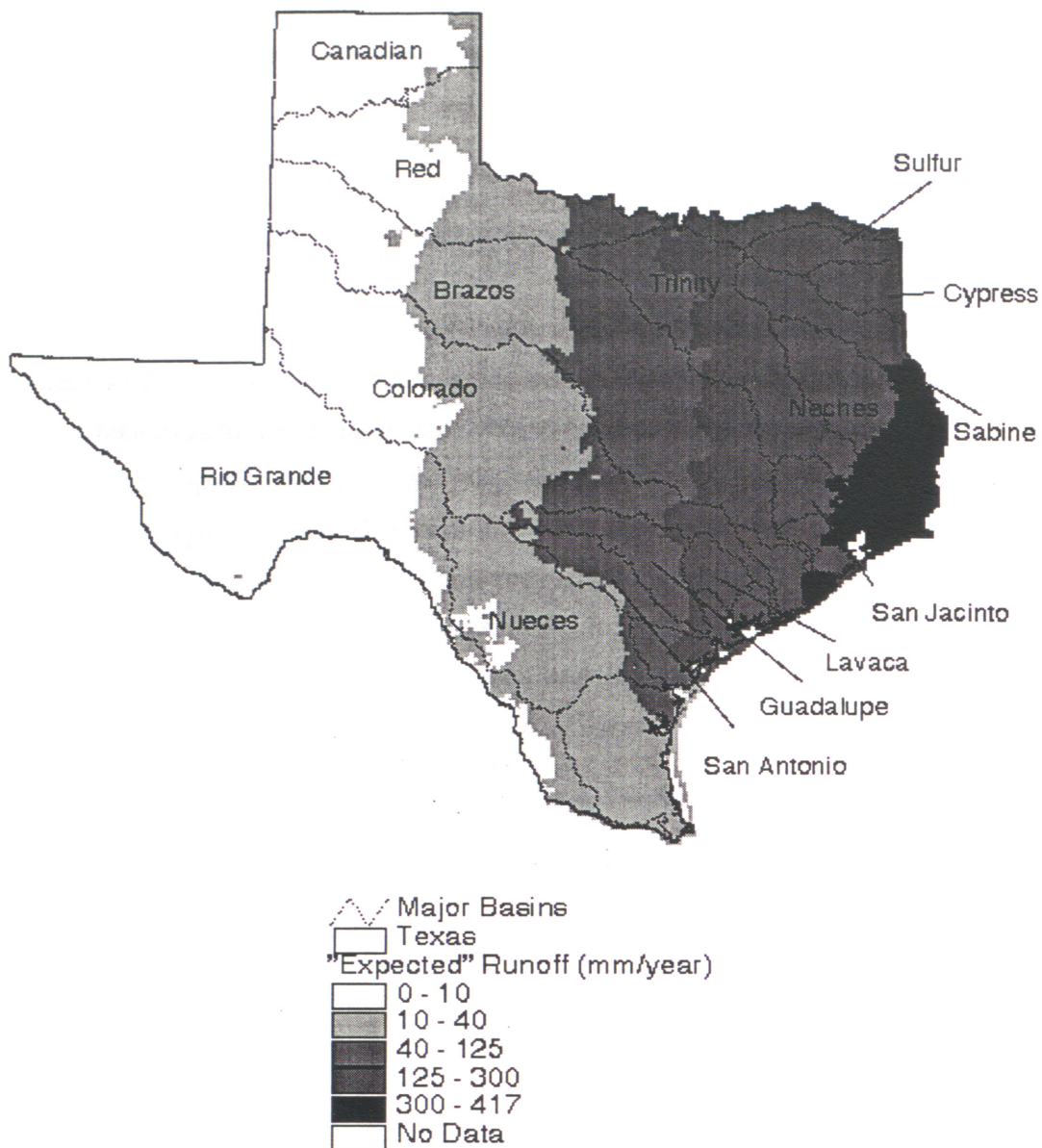


Figure 5-13: "Expected" Mean Annual Runoff

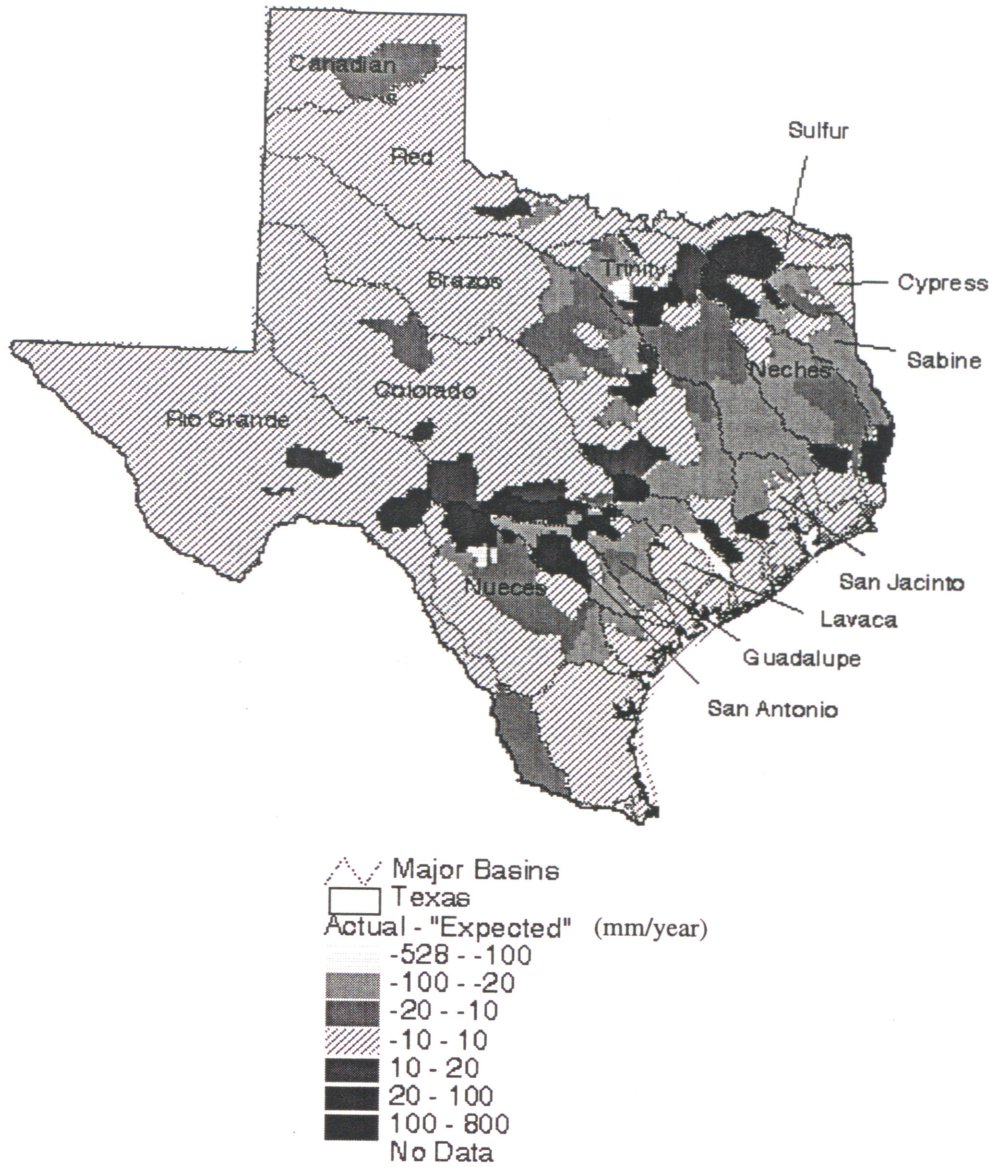


Figure 5-14: Actual - "Expected" Runoff

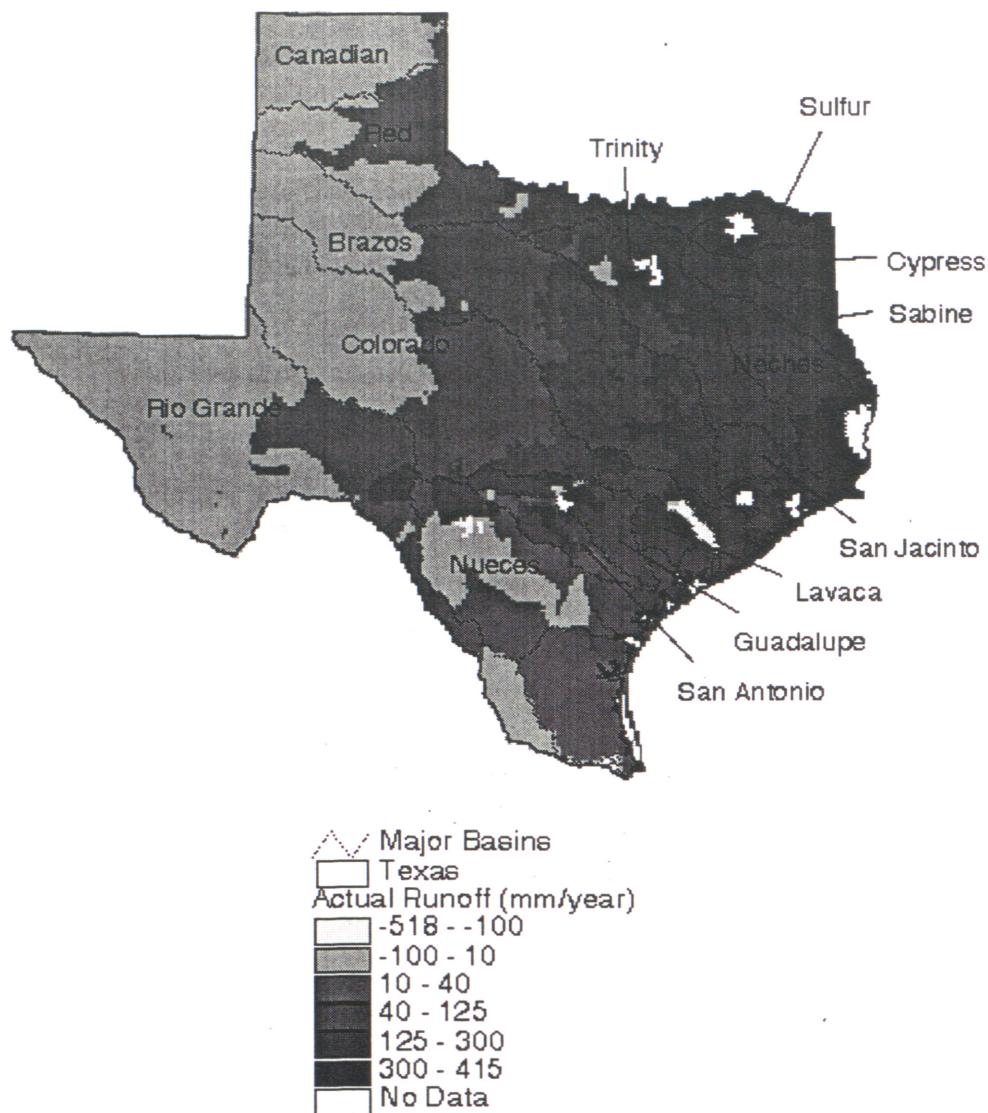


Figure 5-15: Actual Mean Annual Runoff

The adjustment map shown in Figure 5.14 highlights areas with unusually large (dark gray) or small measured runoff (light gray or white). Logical explanations exist for many of these "extreme" adjustment areas. For example, the white and lightly shaded areas in the lower reaches of the Rio Grande and Colorado basins are likely caused by large agricultural diversions in these areas. The white areas in the upper portion of the Nueces basin are likely due to large amounts of recharge to the Edward's Aquifer. Water that recharges the Edward's Aquifer at these locations flows to the northeast, crossing the boundaries of watersheds delineated in this study and emerges as springflow in other locations. The large darkest gray spot in the Guadalupe basin

is caused by the emergence of Comal Springs. One drawback with using this type of runoff map is that the effect of Comal Springs is averaged over the entire watershed in which it emerges so it appears that a large area is generating excess runoff when the excess runoff is primarily due to a point discharge from groundwater. The accumulated runoff maps described below may provide a more realistic representation for this type of flow phenomenon. Several areas with both higher than expected and lower than expected runoff can be seen in the upper part of the Trinity basin near Dallas. These anomalies are likely caused by inter-watershed transfer of water for municipal and industrial use. Another possible explanation for the excessively high runoff near Dallas, but not for excessively low runoff is that extensive urbanization has increased the runoff coefficient.

By applying a flow accumulation function to the runoff maps, the expected and actual flows were calculated at each 500 m DEM cell in Texas. Using this information, flow maps were created using line thickness and color to distinguish between minor creeks and major rivers. Figure 5.16, Figure 5.17, and Figure 5.18 are examples of these flow maps showing expected runoff, runoff adjustment, and actual runoff respectively. Flow maps of this type show statewide spatial trends such as the increased density of stream networks in East Texas, and also reveal localized phenomena attributable to large springflows and agricultural diversions. To demonstrate this further, more detailed maps for the Guadalupe and San Antonio basins are shown in Figure 5.19 and Figure 5.20. Figure 5.20 highlights the deviations from expected flow in these two basins. The influence of springs on the runoff is evident from this map. One use for the accumulated runoff grids derived from this study is to attribute stream reaches with mean flow estimates. An estimate of the flow is available at each 500 m DEM cell on the land surface.

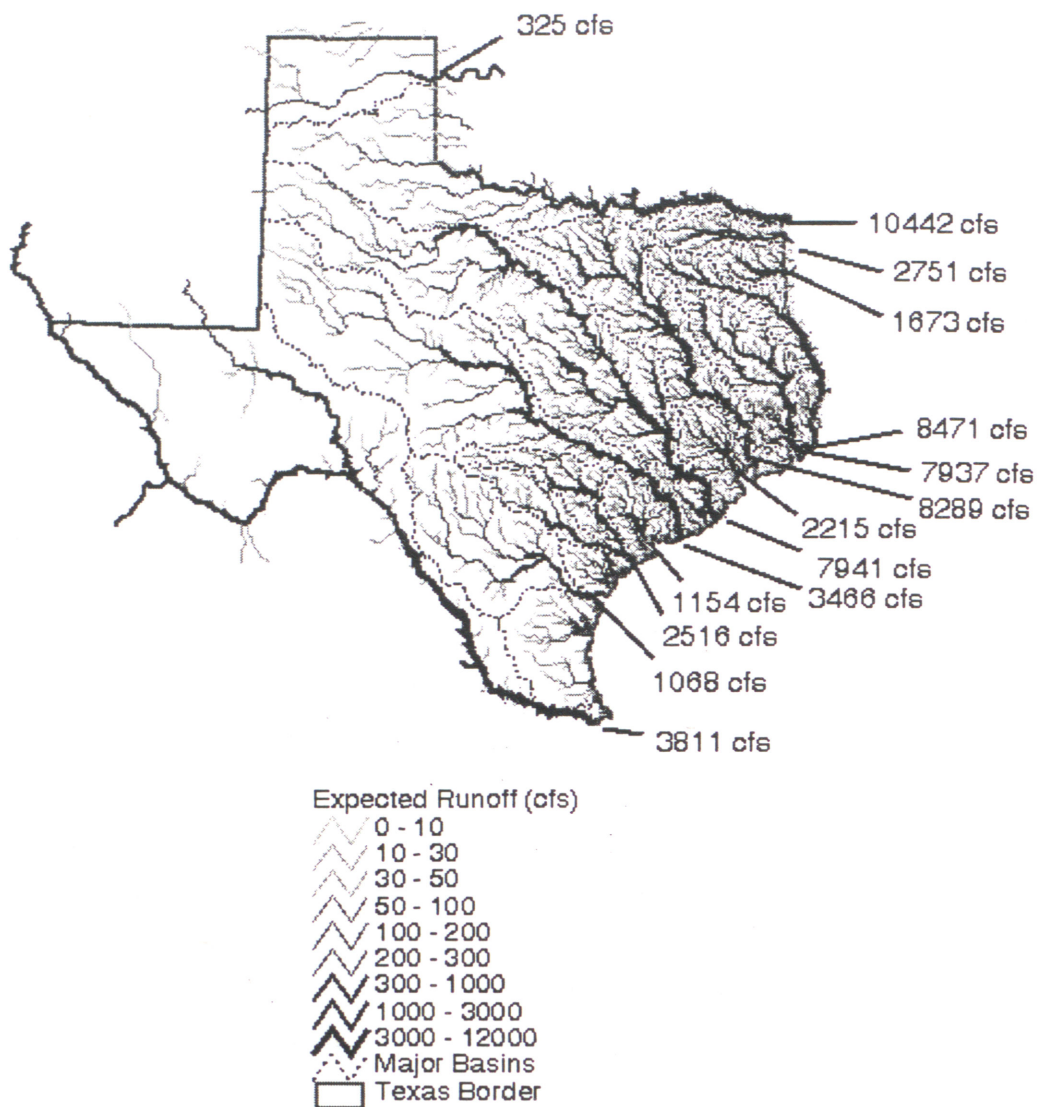


Figure 5-16: "Expected" Accumulated Runoff

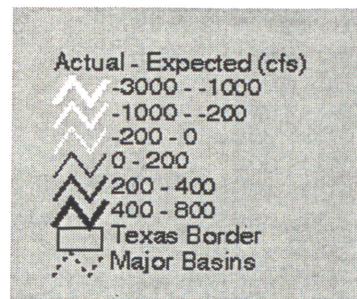
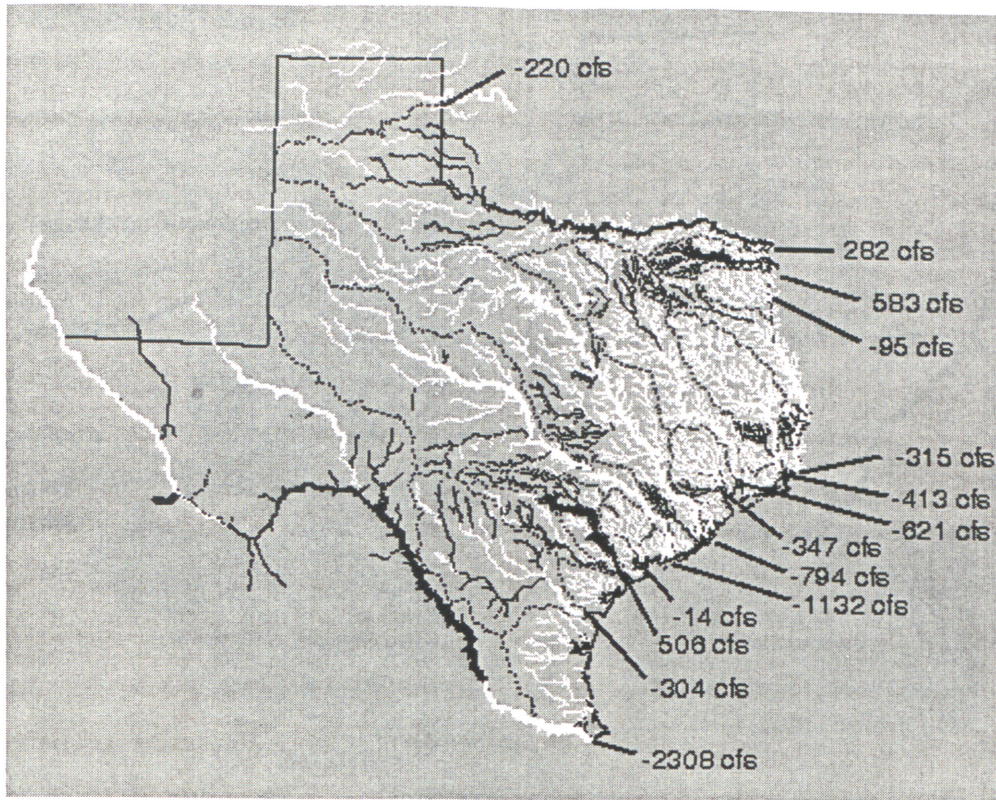


Figure 5-17: Actual - "Expected" Accumulated Runoff

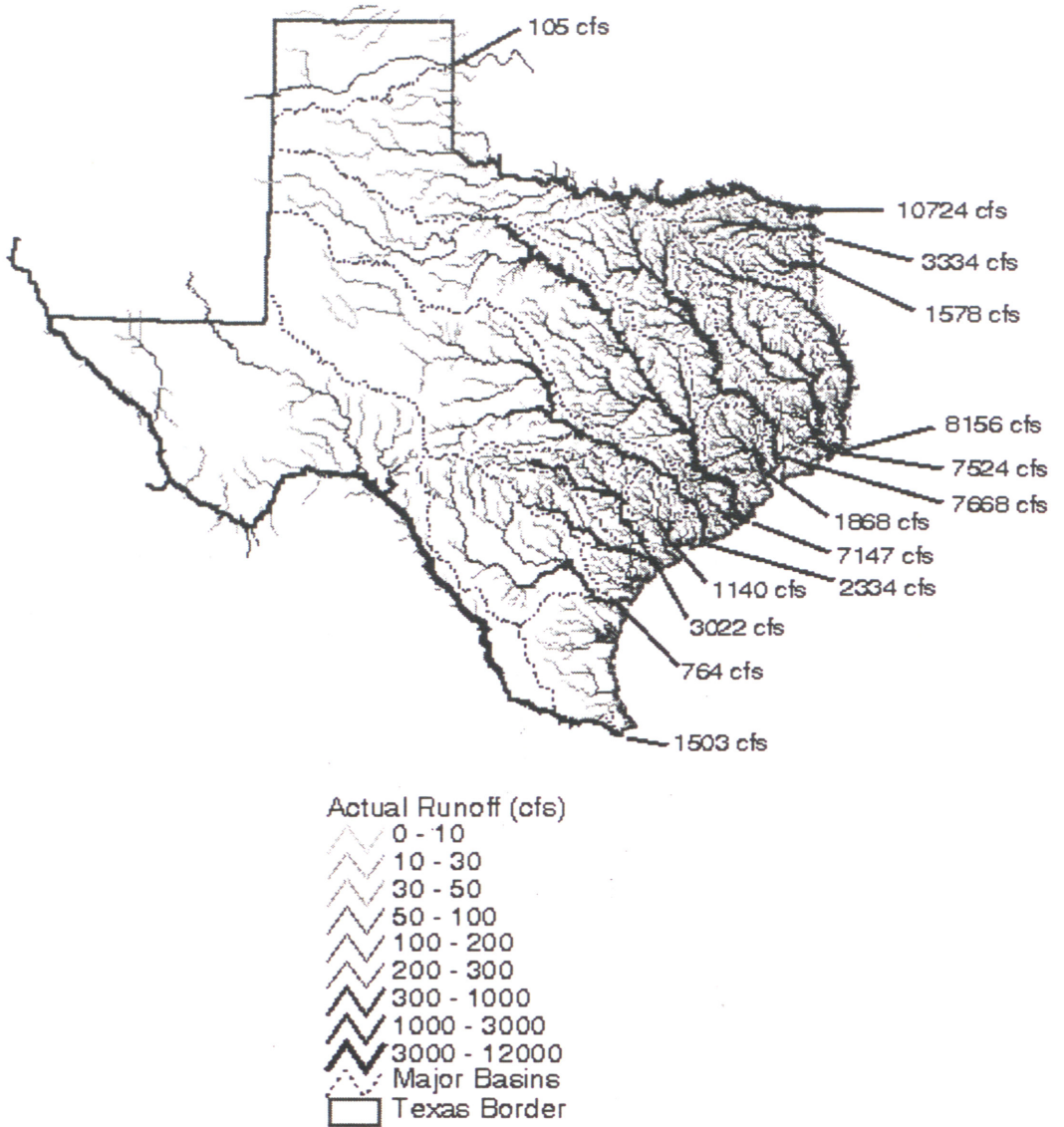
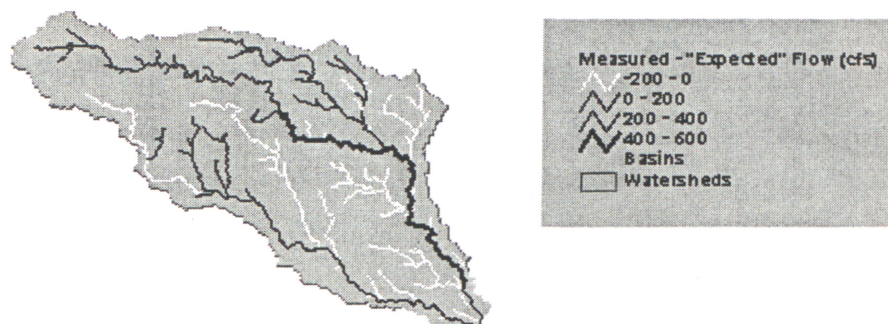


Figure 5-18: Actual Accumulated Runoff

A. "Expected" Runoff



B. Measured Runoff - "Expected" Runoff



C. Measured Runoff



Figure 5-19: Accumulated Runoff in the San Antonio and Guadalupe Basins

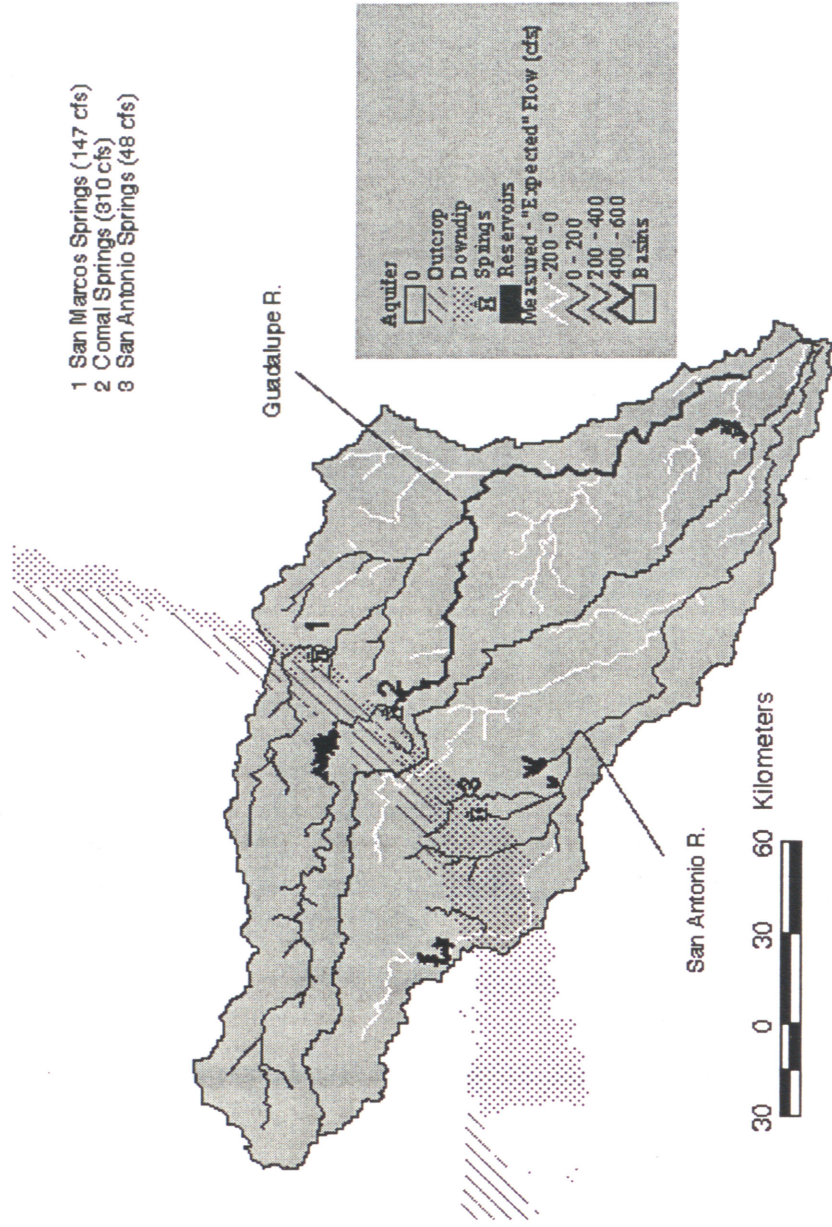


Figure 5-20: Deviations from "Expected" Accumulated Runoff in the Guadalupe and San Antonio Basins

A map of losses was created by subtracting the actual runoff map from the precipitation map. Creation of this map assumes that the annual change in water storage is zero. This map of losses, shown in Figure 5.21, is equivalent to a map of actual evaporation in locations where inter-watershed transfers are negligible.

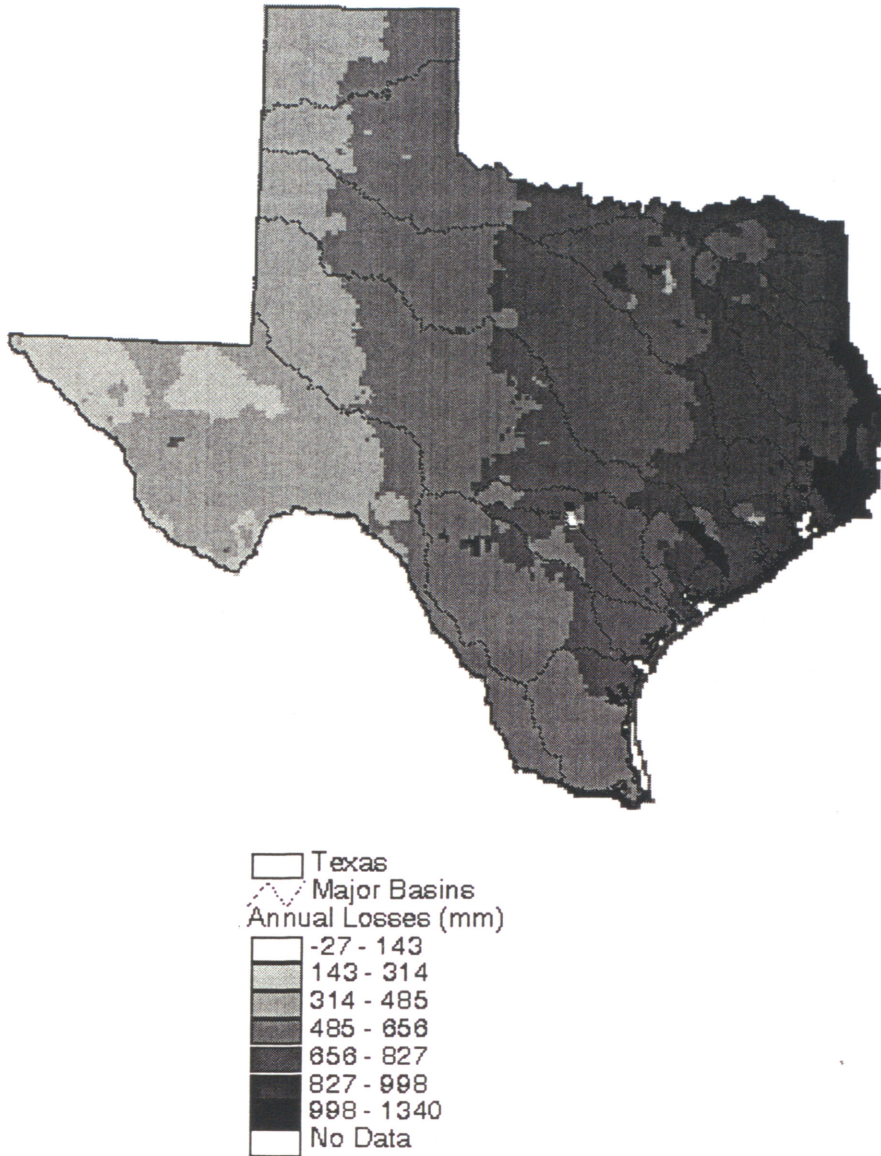


Figure 5-21: Annual Losses: Rainfall - Runoff

5.3.3 Mapping the Bowen Ratio

Using maps of net radiation, temperature, and expected evaporation, a map of mean annual Bowen ratios for the State can be computed. The Bowen ratio (β) is the ratio of sensible heat flux (H) to vapor heat flux (E).

$$\beta = \frac{H}{E} \quad (5.3)$$

These flux units can be expressed in units of equivalent depth of liquid water [$L T^{-1}$]. If the ground heat flux is assumed to be zero, then the net radiation can be approximated as

$$E_r = H + E \quad (5.4)$$

where E_r [$L T^{-1}$] is $\frac{R_n}{l_v \rho_w}$ and R_n is net radiation [$W m^{-2}$], l_v is latent heat of vaporization [$J kg^{-1}$], and ρ_w is density of water [$kg m^{-3}$]. Both l_v and ρ_w are functions of temperature and were estimated using a mean annual temperature map in this case. Combining Equations 5.3 and 5.4, the Bowen ratios were estimated using

$$\beta = \frac{E_r}{E} - 1 \quad (5.5)$$

with E taken as expected evaporation [$mm year^{-1}$] and E_r converted to the same units. Maps of mean annual net radiation and temperature required to estimate E_r were presented in Figures 4.5 and 4.4 respectively. A map of annual expected evaporation (precipitation - expected runoff) is shown in Figure 5.22. The map of Bowen ratios computed from Equation 5.5 is shown in Figure 5.23.

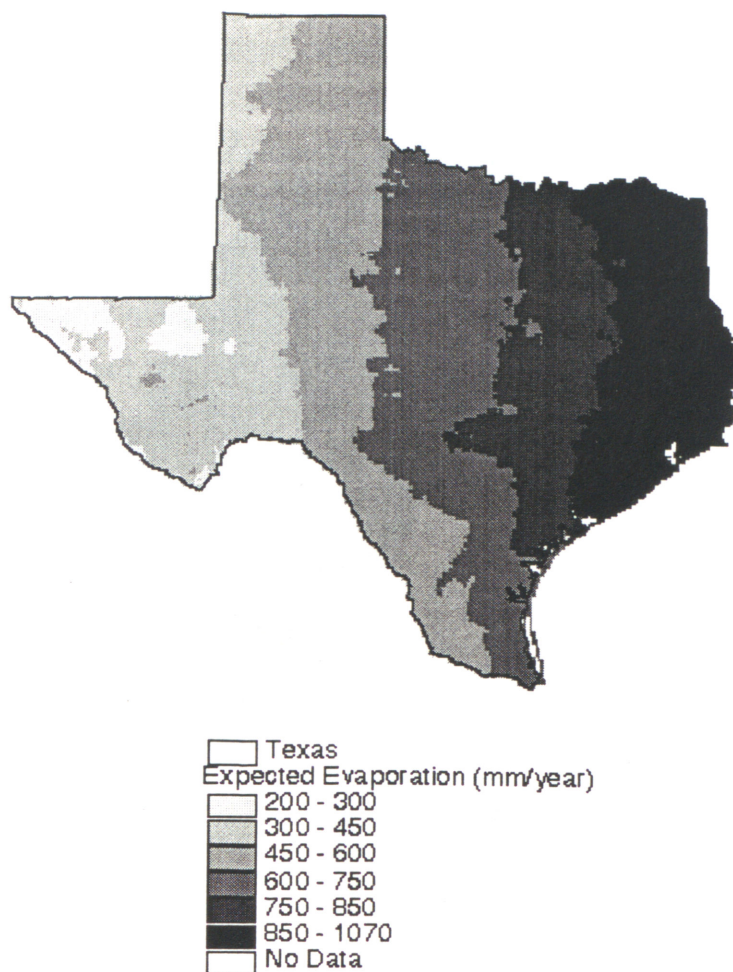


Figure 5-22: Expected Annual Evaporation Computed as Precipitation Minus Expected Runoff

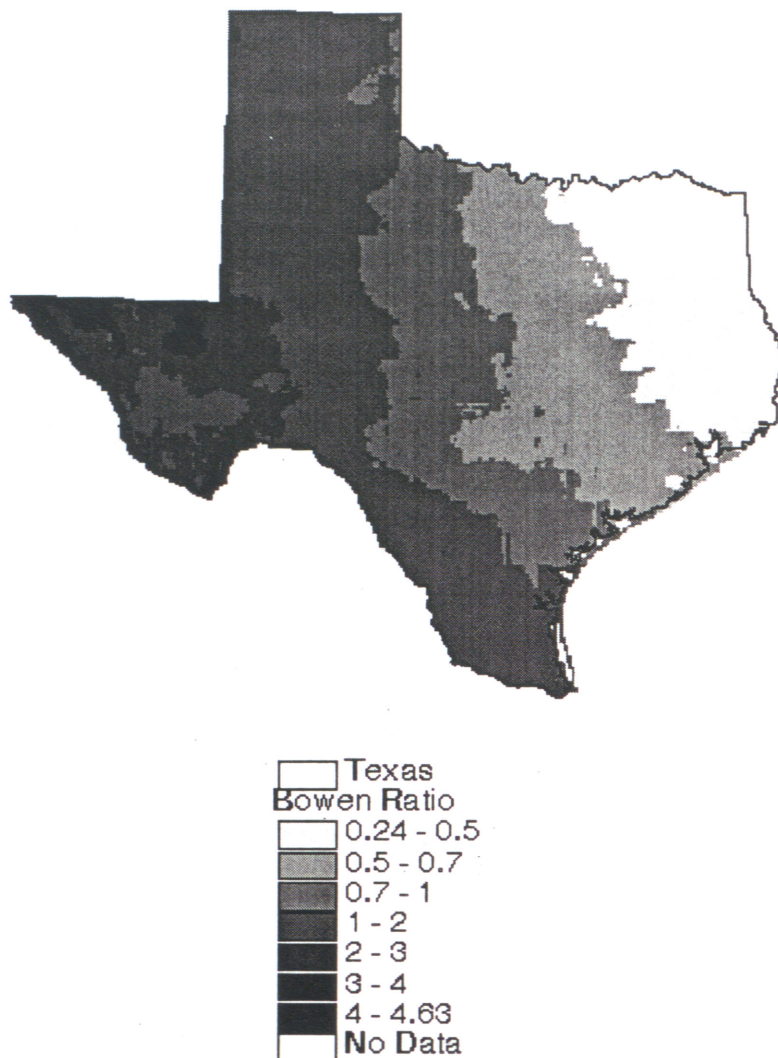


Figure 5-23: Map of Bowen Ratios Computed from Equation 5.5

By combining the information in this Bowen ratio map with information about mean annual saturated soil moisture fraction shown in Figure 4.10, a relationship between the Bowen ratio and soil moisture fraction could be derived. This information could be used in the soil-water balance method to eliminate the need for using the potential evapotranspiration concept. At each time step, the soil moisture level is known, so the Bowen ratio could be estimated from this relationship. In addition, the net radiation and temperature are known so that Equation 5.5 could be used to solve for E . This approach to estimating evaporation is attractive because it is simple and eliminates the use of the ambiguous potential evapotranspiration concept, but it needs further investigation.

5.3.4 Summary Tables

Table 5.1 summarizes the annual precipitation, evaporation, and recharge in Texas by major river basin. By virtue of the method used to estimate evaporation, runoff equals precipitation minus evaporation in this table. The recharge estimates in Table 5.1 are based on an independent study made by Atkinson *et al.* (See Section 5.2.5.4). It is difficult to relate recharge to runoff because recharged water may have a number of fates – it may be used to replenish groundwater storage, it may re-emerge as springflow in a different location from where the recharge occurred, or it may be pumped out of the ground and used consumptively by humans.

Table 5-1: Summary of Annual Hydrologic Cycle Fluxes by River Basin

ID	Name	Area (km ²)	Precip. (mm)	Evap. (mm)	Runoff (mm)	Recharge (mm)
1	Canadian	33262.0	472.5	471.4	1.1	24.8
2	Red	63641.0	637.9	594.3	43.6	18.2
3	Brazos	109130.3	735.4	677.1	58.3	19.5
4	Sulfur	9359.0	1153.3	849.2	304.1	19.8
5	Trinity	45721.3	983.1	833.3	149.8	21.4
6	Colorado	103268.5	609.1	589.0	20.1	21.4
7	Sabine	19538.5	1212.3	941.9	270.4	31.9
8	Cypress	7576.2	1177.4	927.8	249.6	56.8
9	Neches	25624.8	1208.4	946.2	262.2	28.5
10	Rio Grande	128967.7	396.7	391.3	5.4	16.7
11	San Jacinto	7558.2	1179.0	958.4	220.6	25.6
12	Guadalupe	15561.7	856.9	735.7	121.2	25.9
13	Nueces	43799.2	630.7	615.1	15.6	24.9
14	San Antonio	10946.2	787.6	713.4	74.2	55.1
15	Lavaca	5975.8	1003.5	833.4	170.1	25.4
16	Coastal	50778.5	1096.0	864.6	231.4	--
Texas		680709.0	720.0	641.6	78.4	22.0

Table 5.2 was constructed to see whether or not the differences between expected runoff and actual runoff are comparable to the excess evaporation caused by reservoirs. The actual and expected runoff values in Table 5.2 represent 30 year mean values for 1961-1990. Since a number of reservoirs were impounded in Texas between 1961 and 1990, the average influence of reservoirs on runoff during this period is difficult to estimate; however, if reservoirs were the only cause of differences between expected runoff and actual runoff, then one might expect the values in Column 4 of Table 5.2 to be bounded by the estimates in Columns 5 and 6. Although

this condition is met for some basins, it is not true for all basins. There are several reasons why this condition may not be met. First, the reservoir evaporation estimates are rough estimates based on the assumption that the average reservoir surface area is equal to its conservation area and these estimates involve all the assumptions used to estimating open water evaporation using pan coefficients. Second, other factors such as agricultural diversions may have a significant influence on the actual runoff in some locations. Third, gross lake surface evaporation estimates were used to compute the numbers given in Table 5.2, but it would have made more sense to use net evaporation estimates for this comparison. Despite these problems, there is a general trend that basins with higher differences between expected and actual runoff are basins with a larger amount of estimated reservoir evaporation. Two major exceptions to this trend are the Red River basin and Sulfur River basin. In the Red River basin, there is a large lake, Lake Texoma, downstream of the last flow gaging station used to create runoff maps; therefore, the actual runoff estimate might be too high. In the Sulfur River basin, the last flow gaging station used in the creation of runoff maps is upstream of the only major reservoir in this basin, potentially causing the “observed” flow map value to be too high. A channel modification project undertaken by the U.S. Army Corps of Engineers could be another reason for unusually high runoff observed in the Sulfur River basin.

Table 5-2: Examining the Influence of Reservoirs on Runoff

Basin	Observed Flow (cfs)	Expected Flow (cfs)	"Exp." - Obs (cfs)	Estimated Evaporation (cfs) from Reservoirs Impounded :	
				Before 1960	Before 1990
Canadian	105	325	220	4	147
Red*	10724	10442	-282	277	554
Sulfur**	3334	2751	-583	204	215
Cypress	1578	1673	95	291	386
Sabine	8156	8471	315	297	1585
Neches	7524	7937	413	102	990
Trinity	7668	8289	621	734	2678
San Jacinto	1868	2215	347	73	206
Brazos	7147	7841	794	546	1257
Colorado	2334	3466	1132	619	1237
Lavaca	1140	1154	14	0	75
Guadalupe	2112	1715	-397	10	91
San Antonio	910	801	-109	40	75
Nueces	764	1068	304	143	332
Rio Grande	1503	3811	2308	916	1462
Coastal	13158	12754	-404	336	418

* There is a large reservoir, Lake Texoma, downstream of the last gage. Thus, the observed flow might be too high for this reason.

** The last flow gage station is way above the reservoir in this watershed. Also, channel modification by the U.S. Army Corps of Engineers could be affecting runoff in this basin.

5.3.5 Summary and Discussion

A technique for mapping mean annual runoff has been developed and applied in the state of Texas. The procedure involved extensive data collection and manipulation of hydrologic and geographic data. The basic approach was to first develop an "expected" rainfall-runoff function by plotting mean annual runoff per unit area versus mean annual rainfall for different watersheds. The watersheds used in the analysis were delineated from a 500 m digital elevation model. A detailed screening process was used to identify watersheds with limited anthropogenic influence and no large groundwater transmissions – the resulting set of 90 watersheds was used to develop the expected runoff function. Applying the expected runoff function to each cell in a gridded rainfall map yielded a grid of expected runoff. To map the observed runoff, rather than the runoff estimated from this empirical relationship, an adjustment grid was created in which all cells in each watershed were assigned the value of the difference between the observed runoff per unit area and the expected runoff [mm]. By adding this adjustment grid to the expected

runoff grid, the sum of the runoff from all cells in delineated watersheds is forced to equal the observed flow at gaged outlets.

In addition to runoff maps, maps of mean annual losses were also computed by assuming that losses equal precipitation minus runoff. A map of mean annual Bowen ratios for the state was created in Section 5.3.3. A simple method for estimating annual evaporation across the State using the Bowen ratio map is proposed, but the soundness of the approach needs further investigation.

Many short computer programs, written mostly in Arc/Info's script language (AML) for grid processing and ArcView's script language (Avenue) for processing time-series data and performing spatial analysis on vector coverages, were used in this study. This means that making modifications to the procedure or applying a similar procedure to another region would not be too difficult; however, any potential user must be familiar with AML and Avenue to modify these programs for other uses.

There are several potential uses for the runoff maps developed in this study. A grid of actual runoff could be useful in determining non-point source pollutant loadings in a manner similar to that described by Saunders and Maidment, 1996. Another application would be to apply the expected runoff concept in the determination of water rights; however, use of the specific function developed in this study is not necessarily recommended. Water rights determination requires an estimate of what the runoff at any location might be in the absence of human influence. The accumulated expected runoff grid defines how much flow is expected at each 500 m DEM cell in Texas. The expected runoff function used in this study serves as a useful baseline for runoff mapping and for estimating runoff in ungaged areas; however, it is difficult to know whether or not the watersheds used for developing the expected runoff function are truly free from anthropogenic influence. The effects of reservoirs and urbanization were roughly accounted for, but other factors such as landuse changes due to farming or groundwater pumping and surface water diversions for agriculture, municipal, or industrial use were not explicitly accounted for in developing the expected runoff function. The maps of observed runoff do, however, inherently account for these other factors. Maps of accumulated observed runoff like that shown in Figure 5.18 could be used to attribute vector coverages of river networks such as EPA's River Reach File 3 with mean annual flows.

In this study, the decision was made to analyze one time period (1961-1990) and plot data for many different spatial locations. This was primarily a data driven decision – a detailed study had been made at Oregon State University to create a precipitation grid for this time period. An alternative approach to developing an annual runoff curve would be to use fewer spatial divisions and more time divisions. For example, plotting mean runoff versus rainfall for a few watersheds over several different years.

6. CONCLUSIONS

Three water balance methods – an atmospheric water balance, a soil-water balance, and a surface water balance – have been used in an attempt to gain an improved understanding of the stocks of water in different components of the hydrologic cycle and the fluxes between these components. Long term average values indicate that the air flowing over Texas carries 7800 mm year⁻¹ of moisture, of which 720 mm year⁻¹ becomes precipitation, from which 78 mm year⁻¹ becomes surface runoff, all of these quantities being spatially averaged over the State. The runoff estimate of 78 mm year⁻¹ comes from the surface water balance which has the least uncertainty and highest spatial resolution of the three methods. Comparing mean annual runoff estimates from the other two methods to this figure is one way to assess the accuracy of these methods.

Given adequate data, the atmospheric water balance is a promising method for estimating regional evaporation, runoff, and changes in basin storage; however, data used in this study were not at a high enough resolution to make accurate calculations for Texas. Estimates of mean annual divergence over the State were made using both observed rawinsonde data and the output data from a general circulation model. Both methods show that there is significant uncertainty associated with atmospheric water balance calculations at the scale of Texas, yielding runoff estimates of 1206 mm year⁻¹ and 379 mm year⁻¹ which are about 15 times and 5 times greater than the observed runoff, respectively. A review of literature indicates that the magnitude of the errors found in these calculations are not unheard of, although results for some regions have proven much more accurate, particularly when the water balance is assessed over larger areas. Assuming that monthly changes in atmospheric storage are negligible, estimates of monthly evaporation were made for 1992 using the relation ($E = \nabla \cdot \bar{Q} + P$). The 1992 evaporation estimates based on the observed data are not physically realistic while the estimates generated using the general circulation model output show reasonable monthly trends except in January, February, and March. Several sources of error were identified including the sparseness of observations, errors associated with taking the difference between two large numbers, and using monthly average flux values when a significant amount of mass transport can occur at smaller time scales. The contributions of the first and third sources of error mentioned here may be reduced as better data sets become available and if more detailed calculations are made.

The soil-water balance is a climatological approach which is instructive, but also contains substantial uncertainties. The main reasons for the uncertainties in the soil-water balance are a simplified representation of land surface hydrology, the use of monthly average rainfall data, and the fact that there is no calibration with observed data of either soil moisture or runoff. Because of these assumptions, the soil-water balance model predicts zero runoff over large areas of the State where surface runoff actually does occur. The soil-water balance does provide qualitative information about the space and time variability of soil moisture and evapotranspiration that are not revealed by the annual surface water balance, but a way to confirm these results has not been worked out.

Use of the soil-water balance requires an estimate of potential evapotranspiration. One approach taken to estimating potential evapotranspiration was to use the Priestley-Taylor method because a net radiation data set described by Darnell *et al.*, 1995, was available. The other approach was to use gross reservoir evaporation estimates (TWDB, 1995) derived using pan coefficients. As expected, the Priestley-Taylor method was not appropriate for arid areas in West Texas and it is seen that net radiation may be a better surrogate for actual evapotranspiration rather than potential evapotranspiration.

To facilitate the surface water balance, 166 USGS gaging stations were selected for analysis, and a 500 m digital elevation model was used to delineate the drainage areas for each gage. A 5 km grid of mean annual precipitation and mean annual runoff values compiled for each gage (both time averaged from 1961-1990) were used to derive a relationship between mean annual precipitation (mm) and the mean annual surface runoff (mm). This relationship is given in Equation 5.2 and applies in areas without unusually large groundwater recharge, springflow, urbanization, or reservoir impoundment. Applying this relationship to the precipitation grid, a grid of expected runoff was derived. While the precipitation in Texas ranges from about 200 mm year⁻¹ in West Texas to 1483 mm year⁻¹ in East Texas, the expected runoff varies from near 0 in West Texas to 417 mm year⁻¹ in the wettest parts of East Texas.

In locations where information about observed flows was used, the differences between expected runoff and observed runoff could be determined, and Figure 5.14 is a map showing where deviations from expected runoff occur. On this map, areas where observed runoff is much higher than the expected runoff correspond to watersheds where inter-watershed transfers are

received or urbanization has caused high runoff coefficients, while the areas where observed runoff is much lower than expected correspond to watersheds from which recharge is transferred to other watersheds or the impacts of agriculture are significant. Adding the grid of deviations from expected runoff to the grid of expected runoff yielded a grid of actual runoff for the State (Figure 5.15). Accumulated flow maps were also created, using these runoff maps and a 500 m digital elevation model to define the drainage network. Using various line colors and line thicknesses to represent accumulated flow, these maps reveal statewide spatial trends such as the increased density of stream networks in East Texas, while also capturing localized phenomena such as large springflows. The runoff grids developed in this study have several potential uses. The grid of observed runoff may be useful in estimating non-point source pollution loads in a manner similar to that described by Saunders and Maidment, 1996. Use of the expected runoff grid or a similar grid may be helpful in assessing the amount of water available for human use. Accumulated flow maps may be useful in attributing digitized stream networks with flow data.

A grid of mean annual expected evaporation was estimated by subtracting the grid of expected runoff from the precipitation grid. The values of expected evaporation range from 200 mm year⁻¹ in West Texas to 1066 mm year⁻¹ in East Texas. Using the evaporation grid, the net radiation grid, and a temperature grid, a map of mean annual Bowen ratios for the State was created. These Bowen ratio values vary from 4.6 in West Texas (sensible heating of air dominates evaporation in a dry area) to 0.24 in East Texas (latent heat absorbed by evaporation dominates over sensible heating of air in a wet area).

As spatial data sets from remote sensing continue to improve along with tools like a GIS for manipulating spatial data, hydrologists can think in terms of water maps both in the atmosphere and on the land surface rather than thinking just in terms of point measurements. Working with a GIS allows for the computation of water balances on arbitrary control volumes and simplifies the use of complex spatial data. A large amount of data for the state of Texas has been compiled during this study, and this data will be useful to others in the future. A CD-ROM is available from the Center for Research in Water Resources (CRWR), University of Texas at Austin, that contains the data and programs used to make the computations described in this report. A description of the contents of this CD-ROM is provided in the Appendix to this report. Data used to plot the figures presented in this report are included on this CD-ROM and these data files are indexed in Part C of the Appendix.

7. ACKNOWLEDGEMENT

This research was sponsored by the Texas Water Resources Institute and the U.S. Geological Survey under Project 5903. The authors wish to acknowledge the advice and assistance of Allen Bradley of the Iowa Institute for Hydraulic Research, Alfredo Rodriguez of the Texas Water Development Board, Cort Willmott of the University of Delaware, and Sam Atkinson of the University of North Texas.

8. REFERENCES

1. Alley, W.M., "On The Treatment Of Evapotranspiration, Soil Moisture Accounting, and Aquifer Recharge in Monthly Water Balance Models," *Water Resources Research*, 20,1137-1149,1984
2. Arnell, N.W., "Grid Mapping of River Discharge," *Journal of Hydrology*, 167, 39-56, 1995.
3. ASCE, *Evapotranspiration and Irrigation Water Requirements*, Jensen, M.E., R.D. Burman, and R.G. Allen (editors), ASCE Manuals and Reports on Engineering Practice No. 70, 1990.
4. Atkinson, S.F., J.R. Thomlinson, B.A. Hunter, J.M. Coffey, and K.L. Dickson, "The DRASTIC Groundwater Pollution Potential of Texas," prepared by The Center for Remote Sensing and Landuse Analyses Institute of Applied Sciences, University of North Texas, Denton, Texas, September, 1992.
5. Atkinson, S.F., J.R. Thomlinson, "An Examination of Ground Water Pollution Potential Through GIS Modeling," ASPRS/ACSM Annual Convention and Exposition : Technical Papers, Reno, Nevada, 1994.
6. Brubaker, K.L., D. Entekhabi, and P.S. Eagleson, "Atmospheric Water Vapor Transport and Continental Hydrology over the Americas," *Journal of Hydrology*, 155, 407-428, 1994.
7. Brutsaert, W., *Evaporation into the Atmosphere: Theory, History, and Applications*, D. Reidel Publishing Company, Dordrecht, Holland, 1982.
8. Chow, V.T., D.R. Maidment, and L.W. Mays, *Applied Hydrology*, McGraw-Hill, Inc., New York, NY, 1988.
9. Church, M. R., G.D. Bishop, and D.L. Cassell, "Maps of Regional Evapotranspiration and Runoff/Precipitation Ratios in the Northeast United States," *Journal of Hydrology*, 168, 283-298, 1995.
10. Daly, C., R. Neilson, and D. Phillips, "A Statistical-Topographic Model for Mapping Climatological Precipitation over Mountainous Terrain," *Journal of Applied Meteorology*, 33, 2, February 1994.
11. Darnell, W.L., W.F. Staylor, S.K. Gupta, N.A. Ritchey, and A.C. Wilber, "Seasonal Variation of Surface Radiation Budget Derived from ISCCP-C1 Data," *J. Geophysical. Res.*, 97, 15741-15760, 1992.
12. Darnell, W.L., W.F. Staylor, S.K. Gupta, N.A. Ritchey, and A.C. Wilber, "A Global Long-term Data Set of Shortwave and Longwave Surface Radiation Budget," *GEWEX News*, 5, No.3, August 1995.
13. Dingman, S.L., *Physical Hydrology*, Prentice Hall, Inc., Englewood Cliffs, NJ, 1994.

14. Dugas, W.A., and C.G. Ainsworth, *Agroclimatic Atlas of Texas*, Part 6: Potential Evapotranspiration, Report MP 1543, Texas Agricultural Experiment Station, College Station, December, 1983.
15. Dyck, S., "Overview on the Present Status of the Concepts of Water Balance Models," *New Approaches in Water Balance Computations* (Proceedings of the Hamburg Workshop), IAHS Publ. No. 148, 1983.
16. Dunne, K.A., and C.J. Willmott, "Global Distribution of Plant-extractable Water Capacity of Soil," *International Journal of Climatology*, 16, 841-859, 1996.
17. Gutman, G., and L. Rukhovetz, "Towards Satellite-Derived Global Estimation of Monthly Evapotranspiration Over Land Surfaces," *Adv. Space Res.*, 18, No. 7, 67-71, 1996.
18. Hydrodata CD-ROM, "NCDC Summary of the Day - West 2," Hydrosphere, Boulder, CO, 1994.
19. Hydrodata CD-ROM, "USGS Daily Values - West 2," Hydrosphere, Boulder, CO, 1994.
20. Kreyszig, E., *Advanced Engineering Mathematics*, 7th Edition, John Wiley and Sons, Inc., 1993.
21. Legates, D.R., and Willmott, C.J., "Mean Seasonal and Spatial Variability in Gauge-Corrected, Global Precipitation," *International Journal of Climatology*, 10, 111-127, 1990.
22. Lullwitz, T. and A. Helbig, "Grid Related Estimates of Streamflow within the Weser River Basin, Germany," *Modeling and Management of Sustainable Basin-scale Water Resource Systems*, Symposium Proceedings, Boulder, Colorado, IAHS Publ. No. 231, 1995.
23. Maidment, D.R., "GIS and Hydrologic Modeling - an Assessment of Progress," <http://www.ce.utexas.edu/prof/maidment/GISHydro/meetings/santafe/santafe.html>.
24. Maidment, D.R., F. Olivera, Z. Ye, S. Reed, and D.C. McKinney, "Water Balance of the Niger Basin," accepted for publication in the Proceedings of the ASCE North American Water and Environment Congress '96, Anaheim, CA, 1996.
25. Manabe, Syukuro, "Climate and the Ocean Circulation: I. The Atmospheric Circulation and the Hydrology of the Earth's Surface," *Monthly Weather Review*, 97, No. 11, Nov. 1969.
26. Mather, J.R., *The Climatic Water Budget*, Lexington Books, 1972.
27. Mintz, Y., and Serafini, Y.V., "A Global Monthly Climatology of Soil Moisture and Water Balance," *Climate Dynamics*, 8, 13-27, 1992.
28. Mintz, Y., and G.K. Walker, "Global Fields of Soil Moisture and Land Surface Evapotranspiration Derived from Observed Precipitation and Surface Air Temperature," *J. Applied. Meteor.*, 32, 1305-1334, 1993.

29. Oki, T., K. Musiake, H. Matsuyama, K. Masuda, "Global Atmospheric Water Balance and Runoff from Large River Basins," *Scale Issues in Hydrological Modeling*, Chapter 24, 411-434, 1994.
30. Patoux, Jerome, "Atmospheric Water Balance of Texas," Departmental Report, Environmental and Water Resources Engineering, University of Texas at Austin, December 1994.
31. Penman, H.L., "Natural Evaporation from Open Water, Bare Soil and Grass," *Proc. R. Soc. London, Ser. A*, 193, 120-145, 1948.
32. Priestley, C.H.B., and R.J. Taylor, "On the Assessment of Surface Heat Flux and Evaporation Using Large-Scale Parameters," *Monthly Weather Review*, 100, No. 2, 81-92, February 1972.
33. Rasmusson, E.M., "Atmospheric Water Vapor Transport and the Water Balance of North America: Part 1. Characteristics of the Water Vapor Flux Field," *Monthly Weather Review*, 95, 7, pp. 403-426, July 1967.
34. Saunders, W.K., and D.R. Maidment, "A GIS Assessment of Nonpoint Source Pollution in the San Antonio-Nueces Coastal Basin," Online Report 96-1, Center for Research in Water Resources, University of Texas at Austin.
35. Shuttleworth, J.W., "Evaporation," Handbook of Hydrology, D.R. Maidment Editor, McGraw-Hill, Inc., 1993.
36. Shiklomanov, A., and A.A. Sokolov, "Methodological Basis of World Water Balance Investigation and Computation," *New Approaches in Water Balance Computations* (Proceedings of the Hamburg Workshop), IAHS Publ. No. 148, 1983.
37. Smith, P.H., "Hydrologic Data Development System," Master's Thesis, University of Texas at Austin, August, 1995.
38. Snyder, J.P., "Map Projections – a Working Manual," Professional Paper 1395, U.S. Geological Survey, Washington, D.C., 1987.
39. Thornthwaite, C.W., "An Approach Toward a Rational Classification of Climate," *Geographical Review*, 38, 55-94, 1948.
40. TBWE Bulletin 6001, "Surface Runoff from Texas Watersheds and Basins," by Lockwood, Andrews, and Newman Consulting Engineers for the Texas Board of Water Engineers, February, 1960.
41. TDWR Report LP-192, "Climatic Atlas of Texas," Larkin, T.J. and G.W. Bomar, December 1983.
42. TWDB Report 64, "Monthly Reservoir Evaporation Rates for Texas 1940 through 1965," Kane, J.W., October, 1967.

43. TWDB Report 189, "Major and Historical Springs of Texas," Brune, G., March, 1975.
44. TWDB Report 238, "Groundwater Availability in Texas : Estimates and Projections through 2030," Muller, D.A., and Price, R.D. 1979.
45. TWDB, "Water for Texas Today and Tomorrow," 1990.
46. TWDB, "Monthly Reservoir Evaporation Rates for Texas Using GIS THEVAP Model," August, Rodriguez, A., 1995.
47. Ward, G.H., "A Water Budget for the State of Texas with Climatological Forcing," *Texas Journal of Science*, 45, No. 3, 249-264, 1993.
48. Whitlock *et al.*, "First Global WCRP Shortwave Surface Radiation Budget Data Set," *Bull. Amer. Meteor. Soc.*, 76, 6, 905-922, 1995.
49. Willmott, C.J., C.M. Rowe, and Y. Mintz, "Climatology of the Terrestrial Seasonal Water Cycle," *Journal of Climatology*, 5, 589-606, 1985.
50. Willmott, C.J., "WATBUG: A FORTRAN IV Algorithm for Calculating the Climatic Water Budget," *Publications in Climatology*, 30, 2, 1977.
51. Wilm, H.G., C.W. Thornthwaite, E.A. Colman, N.W. Cummings, A.R. Croft, H.T. Gisborne, S.T. Harding, A.H. Hendrickson, M.D. Hoover, I.E. Houk, J. Kittredge, C.H. Lee, C.G. Rossby, T. Saville, and C.A. Taylor, "Report of the Committee on Transpiration and Evaporation, 1943-44," *Transactions, American Geophysical Union*, 25, 683, 1944.

9. APPENDIX

A. General Information

- The data and programs used in this study are available on a CD-ROM from the Center for Research in Water Resources (CRWR), University of Texas at Austin. This appendix contains general information about the CD-ROM contents, an overview of the directory structure, a listing of figures and the data files used to create them, and a description of all data files and programs.
- As this research project has progressed, programs developed at different times vary significantly in the quality of comments and flexibility of application. Many of the programs will require some changes if they are to operate on data sets other than those for which they were originally written. Programmers may find entire programs or sections of programs useful, but only a few of the programs are written for the casual user to simply copy and run.
- The main directory on the CD-ROM is TEXAS. This directory contains a "readme" file that provides a brief description of all data files and programs, including sub-directories. Most sub-directories also contain a file called "whatidid" which explains procedures used to develop data sets and make calculations. There also may be files called "whatidi2," "whatidi3," etc. which are more succinct versions of "whatidid."
- The map projection used in this study was an Albers projection with the parameters for the Texas State Mapping System. When possible, data sources were transformed to NAD83; however, errors associated with choice of datum are negligible when considering the scale of the data used in this study. Here are the projection parameters used in this study:

```
projection albers
units meters
datum nad83
parameters
27 25 00
34 55 00
-100 00 00
31 10 00
1000000.0
1000000.0
end
```

A few coverages used in the atmospheric water balance are in an Albers projection with parameters typically used for national maps of the United States. This is sometimes referred to as the "national" Albers projection in file descriptions below. The projection description for these coverages is as follows:

```
projection albers
units meters
datum nad83
```

parameters
 29 30 00
 45 30 00
 -96 00 00
 23 00 00
 0.0
 0.0

B. Key Sub-directories

Here is a brief description of key subdirectories. The complete contents of these directories are listed in Appendix D.

ATMOBAL: files used to make atmospheric water balance calculations.

AVEFILES: Avenue scripts.

BASINS: data and programs involved in the process of watershed and stream delineation; delineated watersheds (txmshdc3) with attributes used to derive expected runoff function (Section 5.3.1).

EVAP: raw data of gross and net pan evaporation for Texas 1 degree quadrangles obtained from TWDB; a coverage of 1 degree quads attributed with annual average gross evaporation (see Figures 4.2, 4.3); a reservoirs coverage with several attributes including impoundment data, flood capacity, conservation area, etc.; estimated mean annual evaporation from each reservoir and each watershed.

LANDUSE: directory in which a coverage of areas described as "urban or built up" by the Anderson Level 1 landuse codes was created.

PRECIP: grids of the mean annual and mean monthly precipitation grid from Oregon St. PRISM study; grids which combine the data from Oregon St. with Willmott data to provide coverage of the Mexico portion of the Rio Grande; expected, difference, and actual runoff grids and files used to create accumulated flow maps (data shown in Figures 5.13 through 5.20); evaporation grid (Figure 5.21).

RECHARGE: grid of recharge estimates converted from ERDAS file obtained from the University of North Texas and associated files.

REFERENC: coverages of major basins, USGS HUICS, Texas boundary, county boundaries, and cities used for spatial reference.

REPORT: contains a copy of this report in Microsoft Word 7.0 format.

RF1: contains portion of EPA's River Reach File 1 that covers Texas (includes associated INFO files.)

SBUDGET: programs and data files used in computing the soil-water balance (Chapter 4).

SPRINGS: a coverage of major springs in Texas was created based on information taken from TWDB Report 189 by Gunnar Brune. A set of attributes including name, maximum observed flow, and the year that this maximum flow was observed has been compiled for each spring.

STFLOW: streamflow data extracted from a Hydrosphere CD-ROM; point coverages of stream gage locations with relevant information such as mean monthly and mean annual flows; a number of Avenue scripts including scripts to manage data extracted from the Hydrosphere CD-ROM, to make unit conversions, and to assist in computing net potential inflow and net measured inflow to each basin.

C. Listing of data used to create figures presented in this report

The following table gives the data files that were used to create figures in this report. The ~ symbol indicates the path to the "texas" directory which varies with system and is dependent on the identity of the CD-ROM drive. Figures that were not created using GIS data may not be listed. The name of the project file used to create the figures is also given. Note that the pathnames in the project file must be changed in order to successfully open these projects on a system different than that on which they were developed. As saved on the CD-ROM, all of these projects reference pathnames that begin with "/home/seann/texas."

Figure #	Project File	Data Source Files
1.1	~/rung2.apr	~/precip/prectxs, ~/referenc/txbndp
3.1	~/atmobal/diverge.apr	~/atmobal/bradley/bradpnt, ~/atmobal/txbndpp
3.3	~/atmobal/diverge.apr	~/atmobal/bradley/gpoints, ~/basins/txmskgeo
3.4	~/atmobal/diverge.apr	~/atmobal/bradley/atmtexb
3.6		plysurp.dbf
3.7		plysurp.dbf
3.8		plysurp.abf, Patoux, 1994
3.9		plysurp.abf, Patoux, 1994
3.10		plysurp.abf, Patoux, 1994
3.11	~/atmobal/atmobal.apr	~/atmobal/bradley/qvfile.txt, ~/atmobal/bradley/qvfile.txt
3.12	~/atmobal/atmobal.apr	~/atmobal/bradley/qvfile.txt, ~/atmobal/bradley/qvfile.txt
3.13	~/atmobal/atmobal.apr	~/atmobal/bradley/qvfile.txt, ~/atmobal/bradley/qvfile.txt
4.1	~/sbudget/sbudget.apr	~/sbudget/wholditx, ~/basins/txmsk3c
4.2	~/evap/txevap.apr	~/evap/quadsp, ~/referenc/txbndp
4.3	~/evap/txevap.apr	~/evap/quadsp, ~/referenc/txbndp
4.4		~/sbudget/txclimt, ~/basins/txmsk3c
4.5	~/sbudget/bowen.apr	~/sbudget/txradpg, ~/basins/txmsh3c
4.6	~/sbudget/sbudget.apr	~/sbudget/txpevtr.dbf, ~/sbudget/shpfiles/txrun.shp, ~/basins/txmsh3c
4.7	~/sbudget/sbudget.apr	~/sbudget/surprtr.dbf, ~/sbudget/shpfiles/txrun2.shp, ~/sbudget/surp0tr.dbf, ~/basins/txmsh3c
4.8	~/sbudget/sbudget.apr	~/sbudget/prec_tr.txt, ~/sbudget/evapre.dbf, ~/sbudget/stre.dbf, ~/sbudget/surpre.dbf
4.9	~/sbudget/sbudget.apr	~/sbudget/stretr.dbf
4.10	~/sbudget/sbudget.apr	~/sbudget/shpfiles/txrun2.shp – field "satur"
5.2	~/dem.apr	~/basins/demres, ~/basins/txmsk3c
5.3		~/rf1/rl1txp

5.4	~/results4.apr	~/basins/txst1c, ~/stflow/30plus, ~/stflow/30year, ~/referenc/txbndp
5.5	~/results4.apr	~/basins/txmshdc3, ~/referenc/majbtxc2, ~/stflow/out2n
5.6		~/areachk.txt
5.7	~/precip.apr	~/precip/allann, ~/basins/txmshdc3, ~/basins/txmsk3c
5.8	~/figures.apr	~/recharge/rechpc
5.9		~/all.txt
5.10	~/results4.apr	~/basins/txmshdc3, ~/stflow/out2n, ~/referenc/txbndp
5.11		~/90f.txt
5.13	~/rung2.apr	~/precip/runtxs, ~/referenc/txbndp2, ~/referenc/majbtxc2
5.14	~/rung2.apr	~/precip/drunxp, ~/referenc/txbndp2, ~/referenc/majbtxc2
5.15	~/rung2.apr	~/precip/aruntxs, ~/referenc/txbndp2, ~/referenc/majbtxc2
5.16	~/stflow1.apr	~/precip/run_txc, ~/basins/txmsk2c, ~/referenc/majbtxc2
5.17	~/stflow1.apr	~/precip/drun_txc, ~/basins/txmsk2c, ~/referenc/majbtxc2
5.18	~/stflow1.apr	~/precip/stf_tx2, ~/basins/txmsk2c, ~/referenc/majbtxc2
5.19	~/interp.apr	~/precip/run_txc, ~/precip/drun_txc, ~/precip/stf_txc
5.20	~/interp.apr	~/precip/drun_txc, ~/springs/springsp, ~/referenc/majbtxc2
5.21	rung2.apr	~/precip/aevaptxs, ~/referenc/majbtxc2, ~/referenc/txbndp2
5.22	bowen.apr	~/precip/evaptxs, ~/basins/txmsk3c
5.23	bowen.apr	~/sbudget/bowen, ~/basins/txmsk3c

D. Description of files by directory

TEXAS (MAIN DIRECTORY)

PROJECT FILES (*.apr):

NOTE: almost all project files assume that the pathname for files starts with "/home/seann/texas/." Most of these project files could be opened using data from the CD-ROM if the project paths are re-written to reflect the path on which the CD-ROM is mounted.

dem.apr : contains layout for Figure 5.3 (RF1 Streams) of final report.

figures.apr : contains recharge figure for report and other figures used in presentations but not in report.

interp.apr : contain layouts of accumulated expected and actual runoff in the San Antonio and Guadalupe basins.

precip.apr: contains layout for Figure 1.1.

results*3.apr, results4.apr : several versions of a project which loads much of the spatial data associated with Texas. These projects also load several useful scripts. Results4.apr is the most recent version. Using this project, queries on watersheds were made to evaluate criteria for the expected runoff function. See section 5.3.1.

rung.apr : project file used to map grids of results; displays the results of the runoff and evaporation grids that have been resampled and converted to polygon coverages for display; Used to create figures 5.13, 5.14, 5.15, and 5.21 in final report.

stflow1.apr : project file used to display maps of accumulated runoff. This project file contain layouts used to create Figures 5.15, 5.16, and 5.17 in the final report.

tab51.apr: project used to create Table 5.1 in the final report.

TEXT OR DBASE FILES:

90f.txt : list of watershed grid-codes, mean rainfall, and mean runoff selected to created expected runoff function.

all.txt : list of all 166 watershed grid-codes, mean rainfall, and mean runoff values.

areachk.txt : file used to check the consistency between areas reported by the USGS and areas delineated from the 500 m DEM.

areaf.txt : contains grid-code, DEM area, fraction error between DEM and USGS areas.

checkfl.txt : created by checkfl.ave to compare flow at outlet points in actual runoff grid with observed flow at USGS gaging stations to make sure that runoff mapping method worked.

readme : general description of the data on this ROM.

texas.prj : projection used to transform coordinates from geographic space to coordinates in the Albers projection with the parameters of the Texas State Mapping System.

ATMOBAL

PROGRAMS:

arrow.ave : draw arrow graphics proportional in length to the moisture flux across a boundary segment; program called by plotflux.ave.

atmobal.ave : computes the atmospheric water balance for a region; required inputs are qufile.txt and qvfile.txt which are created using refq.f and header.ave.

./bradley/refq.f : reformat raw data files of moisture flux at the boundary points into a format that can be read into ArcView as Text files.

./bradley/refqg.f : reformat raw data files of moisture flux at 2 degree grid points into a format that can be read into ArcView as Text files.

./bradley/thiess.aml : used to generate map of 2 degree polygon boundaries in projected space.

calclen.ave : estimates the actual lengths of the x and y components of the Texas boundary segments given the latitude and longitude of segment endpoints (based on the Clarke 1866 ellipsoid).

convert.utl : convert time series table of divergence values for cells into a time series of divergence values for the state; input table is divbrad.txt and output table is plysurp.dbf.

diverge.ave : calculate divergence based on coordinates in point coverage gpoints and data in files qvgrid.txt and qugrid.txt; evaluates Equation 3.7; output file is divbrad.txt.

header.ave : creates a header for qufile.txt and qvfile.txt used by the atmobal.ave program.

plotflux.ave : plot flux vectors along the boundary of Texas; calls arrow.ave; an exercise using earlier versions of atmobal.ave, plotflux.ave, and arrow.ave is described at <http://www.ce.utexas.edu/prof/maidment/ce394k/atmobj/atmobj.htm>.

PROJECT FILES:

atmobj.apr : project used to make flux integration calculations; accesses files in and below the directory /home/seann/texas/atmobj.

diverge.apr : project used to make divergence calculations; accesses files in and below the directory /home/seann/texas/atmobj.

OTHER TEXT OR DBASE FILES:

./bradley/mqu00.bnd : monthly qu flux for Texas boundary points at 0 UTC

./bradley/mqv00.bnd : monthly qv flux for Texas boundary points at 0 UTC

./bradley/mqu12.bnd : monthly qu flux for Texas boundary points at 12 UTC

./bradley/mqv12.bnd : monthly qv flux for Texas boundary points at 12 UTC

./bradley/mqu00.grd : monthly qu flux for 2x2 degree grid at 0 UTC

./bradley/mqv00.grd : monthly qv flux for 2x2 degree grid at 0 UTC

./bradley/mqu12.grd : monthly qu flux for 2x2 degree grid at 12 UTC

./bradley/mqv12.grd : monthly qv flux for 2x2 degree grid at 12 UTC

./bradley/inters.ctl : control file for the script convert.utl; specifies input and output file names, key fields, etc.

./bradley/qufile.txt, ./bradley/qvfile.txt : files created by the program refq.f; contain mean monthly flux estimates for each boundary segment in kg/m/s.

./bradley/qugrid.txt, ./bradley/qvgrid.txt : files created by the program refqg.f; contain mean monthly flux estimates at each 2 degree grid point in kg/m/s.

./bradley/read.me : file describing data provided by Allen Bradley at the University of Iowa.

./bradley/texflux3.dbf : results of flux integration calculation across the border of Texas; Fields: year, month, influx (mm/month), outflux (mm/month), netflux (mm/month), and throughflux (mm/month), C1, C2, . . .etc (mm/month)

divbrad.txt : output file from diverge.ave; fields are cell ID #'s and records are months; units are $\text{kg}/\text{m}^2/\text{s}$; this file input to the program convert.utl.

plysurp.dbf : contains mean monthly divergence results for Texas; the field in plysurp.dbf, labeled "tx0" contains average divergence estimates in units of $\text{kg}/\text{m}^2/\text{s}$. If the values in this field are multiplied by the number of seconds in the month, the divergence in mm/month is obtained.

COVERAGES:

./boundary/txcntgeo : point coverage of the midpoints of the boundary segments in txlgeo.lin.

./boundary/txlgeo : coverage containing line and node topology of Texas boundary segments in geographic coordinates -- used for flux integration calculations. Attributes include "lx", "ly", and "l" which are the corresponding length of these segments on the Clarke 1866 ellipsoid in meters; the point coverage of segment endpoints is attributed with lat/lon coordinates which are used by the program calclen.ave.

./boundary/txrgline : generalized border of Texas in an Albers projection with parameters used for national maps.

./bradley/atmtexb : polygon coverage -- intersection of generalized Texas border (txrgline) and 2 degree cells (bradptt).

./bradley/bradptt : polygon coverage of 2 degree cells as shown in Figure 3.1 of the report; projection is Albers with parameters used for national maps.

./bradley/gpoints : point coverage of 2 degree by 2 degree grid points used for divergence calculations (Equation 3.7).

./bradley/gpointsp : projected version of gpoints.

txbndpp : polygon coverage of Texas boundary; projection is Albers with parameters used for national maps.

AVEFILES

PROGRAMS:

dr_area.ave : script used to determine the incremental drainage area of each basin delineated according to the USGS.

addfields.ave : add fields to the attribute table of the delineated watershed coverage ~/texas/basins/txmshdc3 and compute values for these fields.

checkfl.ave : compare flow at outlet points in actual runoff grid with flow at gaging stations to make sure that the runoff mapping method worked. Output file is checkfl.txt.

checkneg.ave : script used to check problems with negative reported flow values in the point coverage 30plus.

convuni2.ave : create new fields in txmshdc3 with different units for flow, average rain, or drainage area, etc.

plotxy.ave : plot x,y charts on selected columns in an INFO table. User is prompted to enter fields for plotting.

query.ave : make a query on delineated basins in results*.apr. Simplifies making slight changes in a complicated query.

wrttext.ave : write a text file for specified fields in an attribute table.

BASINS

PROGRAMS:

demproc.aml : describes DEM processing, including 30 second data from Mexico DEM cells.

burndes.aml : description of stream burn_in procedure for Texas only -- prior to including the Mexico data -- many of the output grids are obsolete and these have been deleted.

calcflux.aml : adds up all of the values in the fluxgrid created by netflux3.aml.

getcoord.ave : script used to write a file containing the points of coordinates clicked by the user; used to help identify the outlets of major basins.

inflow.ave : script used to get information about net inflow for selected points and write the results to an INFO file; linked to a button and used interactively.

majbas.aml : AML used to delineate major basins.

makeout.aml : AML used to generate outlet grid from text file for 166 basins.

netflux3.aml : program used to calculate the net flux of runoff across the border of Texas given a flowaccumulation grid, a flowdirection grid, and a grid of the Texas border.

out2n.txt : file with coordinates of outlets used to delineate 166 watersheds; created with selout.aml

outflow.ave : script used to write the outflow from selected points to a table; linked to a button and used interactively.

plotcoef.ave : script used to plot measured flow vs. potential flow.

selout.aml, seloutm.aml : AMLs that allow the user to interactively select watershed outlets given a point coverage and a link grid.

OTHER TEXT OR DBASE FILES:

keyatt.txt : text file describing the key attributes of the final coverage of 166 delineated watersheds.

COVERAGES :

arcbasn2 : major watersheds in Texas; taken from a CD-ROM created by Smith, 1995, and possibly re-projected.

majbasn : coverages of major basins derived from 15" data (not clipped with the State boundary).

majout3 : point coverage of outlets to the major basins

outpotc2 : coverage of 166 outlets with potential flow as attributes

rf1clip : EPA's River Reach File 1 (RF1) coverage with coastal polygons eliminated; TSMS projection; line topology not built (6/9/96).

rf1clipn : EPA's River Reach File 1 (RF1) coverage with coastal polygons eliminated; national projection.

rf1gulfc, rf1gulfc2 : polygon coverages used to eliminate coastal polygons from the RF1 coverage prior to stream burn-in.

txmsk2c, txmsk3c : polygon coverages of mask of Texas border for which all elevation values are greater than 0; txmsk3c has many islands clipped out.

txmskgeo : mask of Texas border in geographic coordinates; from the same data source as txmsk2c.

txsh2geo : delineated watershed boundaries in geographic coordinates.

txst1c : delineated streams at a 1000 cell threshold.

txst3c2 : delineated streams at a 3000 cell threshold.

txst3cut : delineated streams at a 3000 cell threshold clipped by the border of Texas.

txmshdc3 : basins delineated from txfdmod and out2ng, the attributes of this coverage are used to select basins for the "expected" runoff curve; attributes of this coverage are described in the text file keyatt.txt.

txsh2geo : txmshdc3 in geographic coordinates

GRIDS:

demnat : portion of the U.S. 500 m DEM that covers Texas and areas draining to Texas, in national Albers projection; obtained from usdem2; starting point for delineation (see burndes.aml).

demf2 : filled and projected 500 m DEM for Texas (see burndes.aml for creation details).

demf2mf0 : filled version of the combined Mexico and Texas DEM.

demres : demf2mf0 resampled to a larger cell size to make it faster to display in ArcView3.

ditchgmf : zeros in the streams and raised grid on the landscape including the Mexico terrain (filled twice see demproc.aml for reasoning). A few cells in ditchgmf were edited with Gridtools to make sure that two problematic areas drained in the correct direction (see Section 5.2.3 for problem description and the whatidid file in this directory for solution details).

majoutg : 13 major basins delineated based on user selected outlet points.

majout2 : grid of outlet points for major basins.

mexnd0 : selected portion of the North American 30 second dem in geographic coordinates, water is assigned the value NODATA.

out2n.txt, out2n, out2ng : text file, coverage, and grid of 166 outlet points.

streamg : gridded version of rf1clip with a cell size and mapextent consistent with the DEM (see burndesc.aml for creation details).

txst1m : gridded streams for Texas and Mexico with a 1000 cell threshold.

txst3m : gridded streams for Texas and Mexico with 3000 cell threshold.

txst9m : gridded streams at 900 cell threshold.

txlnkm : stream links from txst1m and txmfd.

txmfdmod : flowdirection from modified version of ditchgmf.

txfamod : flowaccumulation grid from txmfdmod.

txmshd2 : basins delineated from out2ng using txmfdmod.

EVAP

PROGRAMS:

alfredo2.ave : script used to reformat gross reservoir evaporation data; creates INFO file ldeggevp.

basevap.ave : determine the approximate evaporation from each major basin in Texas.

evapavg.ave : adds fields of "ann_mean" and "ann71" to the INFO file "evyears". "Ann_mean" is the average PE over 1961-1990 and "ann71" is the average annual PE from 1971 - 1990. ** THE UNITS ARE ACTUALLY MM/MONTH SO FOR ANNUAL TOTAL, multiply by 12.** These two values are the same for those quads that only have the 71-90 period of record.

evrate2.ave : estimate annual gross evaporation from each reservoir in reserb90 and add a field ("ev_rate") containing this information to the reservoirs coverage.

fixquad.aml : repair problems with polygon ID's in first column of 1 degree quads.

getalfr.f : reformats gross evap estimates so that they can be loaded into ArcView. Input: grs-4090. Output: evapalf.txt

monavg.ave : create an INFO table (monavg.dat) that contains monthly average gross evaporation from each quadrangle.

plotres.ave : script that can be used to plot time series data.

quad.f : FORTRAN program used to write generate file (quads.gen) for 1 degree quads.

shdevap.ave : determine the approximate reservoir evaporation from each delineated watershed.

shiftid.f : FORTRAN program used to create a file with the correct quadrangle index IDs to match Alfredo's data; input: joinid.txt; output: joinidn.txt. ** Arc/Info won't assign correct user IDs so I manually changed them (I've seen this error before when generating square cells) and added a column called tquad-id; needed very short FORTRAN program shiftid.f--this program reads joinid.txt and creates joinidn.txt).

year.ave : add the field called year to the reservoir coverage; this is the year the reservoir was impounded -- simplifies the "imp_date" field in daminf2.dat.

yevapavg.ave : computes the weighted average evaporation in each year and adds a new field called "annual" to the INFO table evapalf.

OTHER TEXT OR DBASE FILES:

1deggevp.dbf : dBase file containing gross reservoir evaporation estimates on a 1 degree grid.

all_4090.dnl : raw data file with net reservoir evaporation from Alfredo.

damin2.dbf : table containing reservoir attributes corresponding to the reservoirs in the coverage reserp; these attributes have been joined to reserp and reserb90.

evapalf.txt : text file containing quad ID, year, and 12 monthly gross evaporation estimates (mm).

evcb60.txt, evcb90.txt, evpb60.txt, evpb90.txt : text files containing estimates of average reservoir evaporation by watershed based on either conservation or polygon area for reservoirs

impounded before 1960 or before 1990. For example, evcb60.txt contains evaporation estimates for reservoirs impounded before 1960 based on conservation area.

grs-4090 : gross evaporation estimates for quadrangles covering Texas obtained from Alfredo Rodriquez (TWDB) (units are inches/month). Some quads contain monthly estimates from 1940 to 1990 while others contain data from 1971 to 1990.

joinid.txt, joinidn.txt : text files with used to match quadrangle index numbers in the coverage of 1 degree quadrangles.

quadpt.gen : generate file for a point coverage at the center of each 1 degree quadrangle.

quadsn.gen : generate file for 1 degree quad polygons.

INFO FILES:

evyears : contains quad-id, styear and endyear, annual mean evaporation / 12 (1961-1990) -- "ann_mean," and annual mean evaporation / 12 (1971-1990); this information is joined to quads and quadsp.

evapalf : INFO table that contains reformatted gross reservoir evaporation data.

daminf2.dat : INFO file containing dam attributes.

monevap.dat : 30 year monthly averages of gross evaporation: 12 values for each quad.

COVERAGES:

quads : 1 degree quads in geographic space attributed with quadrangle index number and x,y coordinates of center point.

quadsp : 1 degree quads in TSMS Albers with these attributes:

styear = start year when estimates are available

endyear = end year when estimates are available

ann_mean = 30 year mean (mm/month)

ann71 = 20 year mean (mm/month)

anntot = annual 30 year (or 20 year when 30 year not available) mean evaporation (mm/year)

quadptp : projected point coverage of the centers of 1 degree quads.

reserp : polygon coverage of reservoirs in Albers projection with TSMS parameters.

reserb90 : coverage of reservoirs built before 1990; field "poly_evap" contains evaporation estimate (m³/year) based on polygon area; field "cons_evap" contains evaporation estimate (m³/year) based on conservation area.

LANDUSE

txlus : landuse coverage from Smith, 1995, CD-ROM.

lu_urb : polygons in txlus with 'Li' = 1 (urban landuse types).

urb_disp : lu_urb was dissolved to make a smaller coverage (see whatidid file) and projected.

urbshds : intersect urb_disp ~/texas/basins/txmshdc3 urbshds poly.

perclu.aml : determine the fraction of area in each delineated watershed that is classified as urban landuse.

PRECIP

PROGRAMS:

arun2.aml : determine the actual runoff and accumulated runoff using the expected runoff grid computed with runoff2.aml.

combpot.ave : create a dBase table called "pflow.dbf" that contains the potential flow for each month and each watershed.

getwill.f : FORTRAN program to extract Willmott precipitation data for texas; this data is used to fill in precipitation over the Mexico portion of the Rio Grande; reads a control file called control.txt with the mapextent of data to be extracted and a variable which indicates whether geodetic or geocentric coordinates are being used. Outputs: point.txt and prec.txt.

mkgrid.aml and mkgrid2.aml : used to create/process precipitation grids. The main products are merged grids of Oregon St. and Willmott monthly values.

montomm.ave : script written to convert attributes in the table txmshdc3.pat from cfs to mm.

plotdrun.aml, plotflow.aml, plotrun.aml : AMLs used to create files for making maps of accumulated runoff (difference, actual, and expected runoff respectively).

preplot.aml, preplo2.aml : prepare runoff and evaporation grids for mapping with ArcView 2.1.

runoff2.aml : convert the annual rainfall grid to an annual runoff using the expected runoff function.

wrttext2.ave : export selected fields to a text file for graphing.

OTHER TEXT OR DBASE FILES:

bastotsn.txt : text file with basin totals of precip, evap, runoff, recharge.

control.txt : control file for getwill.f

pflow.dbf : potential flow in each watershed.

prec.txt : mean annual precipitation corresponding to each point where Willmott data is available.

precm.txt : monthly and annual precipitation from Willmott.

precip.avl : legend file for displaying precipitation.

whatidi, whatidi2, whatidi3 : descriptions of what I did with data in this directory. whatidi3 is simplified and most easily understood.

INFO FILES:

wprec.dat : file containing a point-id and the Willmott mean annual precipitation, to be joined to the coverage wprecpts

COVERAGES:

aoutflc : point coverage of all 166 outlets attributed with mean annual flows.

drunoutc : point coverage of major basin outlets attributed with values of druncfs.

drunxp : polygon version of druntxs used for display only.

runoutc : point coverage of major basin outlets attributed with expected runoff estimates.

stoutc : point coverage of outlets from major basins attributed with streamflow (estimates represent accumulated runoff values).

wprecpts : point coverage attributed with mean annual Willmott rainfall (geographic coordinates).

wprec2 : point coverage of Willmott points attributed with mean monthly and annual data (projected).

wthiess : Thiessen polygons made from wprec2; attributed with Willmott data.

GRIDS:

allann, alljan, allfeb, etc. : grids of monthly and annual precipitation for the entire study area. These grids include data from Willmott for areas not covered by the Oregon State grid.

arunoff : grid of actual runoff at a 500 m cell resolution.

aruntxs : actual runoff within Texas aggregated to 5 km cells for display.

drun0i: grid of differences between mean observed runoff and mean expected runoff (converted to integer to save space).

druntxs : difference between actual and expected runoff within Texas aggregated to 5 km cells for display

evap : grid of expected evaporation at a 500 m cell resolution.

evaptxs : expected evaporation within Texas aggregated to 5 km cells for display.

flowsac3 : grid of accumulated runoff ; see arun2.aml for creation details.

prectxs : precipitation within Texas, 5 km cell size.

rallann : allann resampled to a 500 m cell size so that the weighted flow accumulation can be determined.

runoff : expected runoff grid at 500 m resolution.

runoffs : expected runoff grid at 5 km resolution.

runtxs : expected runoff within Texas aggregated to 5 km cells.

txbprec : mean annual precipitation grid cut to the boundary of Texas.

txpann2 : grid of mean annual precipitation for Texas; portion of the U.S. grid obtained from Oregon St. U. (geographic coordinates).

txpann2p : projected version of txpann2 (5 km resolution)

txprec_r : resample precipitation for display.

wresamp : resampled wtprecg to the same size cells (5 km) as the Oregon St. grid (txpann2p)

wtprecg : Thiessen polygons (wthiess) attributed with mean annual precipitation converted to grid cells (50 km on a side).

RECHARGE

PROGRAMS:

calcrech.ave : convert DRASTIC ratings in rechpc into mm/year.

weight_r.aml : estimate mm/basin area/year of recharge for each basin; results are contained in the INFO file recharge.sta.

INFO Files:

recharge.sta : the field "sum-fr_recharge" contains mm/year of recharge averaged over each watershed; the field

COVERAGES:

rechpc : polygon version of rechp; fields min, max, and mean contain the minimum, maximum, and mean estimated mean annual recharge for each polygon.

rech_shd : recharge polygons intersected with delineated watersheds.

GRIDS:

rechp : grid of DRASTIC ratings for recharge; original data from University of North Texas; data has been converted to Arc/Info Grid format and projected.

REFERENCE

COVERAGES:

arcbasns : major basins in Texas from Smith, 1995, CD-ROM; national Albers projection.

arcbasnsp : major basins, Albers projection with TSMS parameters.

coastbc : coverage of coastal basins.

counties : coverage of Texas counties from ArcUsa.

huctxp : Texas HUICS, Albers projection with TSMS parameters.

majbtxc : major basins in Texas clipped by the polygon border of the State along the coast.

majbtxc2 : major basins in Texas clipped by the DEM along the coast.

txbnd : arc coverage of Texas boundary.

txbndp : polygon coverage of Texas boundary.

txbndp2 : polygon coverage of Texas boundary with islands eliminated.

txbound : generalized boundary of Texas in the national Albers projection.

txboundg : generalized boundary of Texas in geographic coordinates.

txcit2 : Texas cities in the national Albers projection.

txcit2p, txcities : Texas cities in an Albers projection with TSMS parameters.

GRIDS:

coastg1 : grid of coastal basins.

majbgrid : grid of major basins in Texas.

txbmsk : gridded mask of the Texas boundary defined by ArcUsa.

REPORT

wbtxpic2.doc : Microsoft Word 7.0 version of final report. An HTML version can be viewed at <http://www.ce.utexas.edu/prof/maidment/gishydro/seann/seann.htm>.

RF1

rf1txp : portion of EPA's River Reach File 1 that covers Texas. Attributes for this coverage are located in the ~/rf1/info.

SBUDGET

PROGRAMS:

c_whold.ave : compute the average water-holding capacity at center points of climate cells; adds a field to the point coverage txclimt called wholdavg.

getwillm.f : get the Willmott temperature and precipitation data for a geographic extent specified in the file "control.txt" and create the file point.txt suitable for creating a point coverage and prec.txt and temp.txt which can be joined to this point coverage in ArcView as needed.

getwhold.f, getwhol2.f : program to get water-holding capacity values for Texas from the global data set of Dunne and Willmott; writes text files used to create the coverage whold.

swbaltx.ave : run soil water balance algorithm described in Section 4.1; program prompts the user for a control file specifying input and output files; the control file for calculations made with Priestley-Taylor potential evaporation estimates is txbal2.ctl and the control file for calculations made with reservoir evaporation estimates is resev.ctl.

pevap.ave : computes potential evaporation using the Priestley-Taylor method; the control file texpev.ctl was used to specify inputs and outputs to this program for this study; output file is txpev.txt.

pevapre.ave : reformats reservoir evaporation data so that it can be used read by swbaltx.ave; output file is resevtx.txt.

selrad.aml : reselect polygons in the global net radiation coverage "tot" that are in and around the study area.

thiess.aml : used to generate map of 0.5 degree boundaries in projected space; program is general but was applied to txclim in this case.

tr_prec.ave : transpose the text file prec.txt so that it can be used by the soil-water balance program; result is prec_tr.txt.

transpose.ave : program used to transpose dBase tables.

wrtaml.ave : script used to write an AML to reselect specific cells in the global net radiation coverage (tot).

PROJECT FILES:

sbudget.apr : project used to make soil-water balance calculations and potential evaporation calculations; assumes all files are located in or below a directory names /export/home/seann/texas/sbudget.

OTHER TEXT OR DBASE FILES:

control.txt : control file for getwillm.f and getwhol2.f; specifies input parameters.

instruct.txt : summary of steps to create a temperature, precipitation, and water-holding capacity data set for any location in the world.

mresev.dbf : file containing mean monthly gross reservoir evaporation estimates for each quadrangle defined in /texas/evap/quadsp. Quadrangle ID's are field names and 12 records contain monthly values.

mresevtr.dbf : same data as mresev.dbf but with time as fields and quadrangle ID as records; in this form the data can be easily joined with /texas/evap/quadsp for display.

point.txt : text file for generating the coverage txclim.

prec.txt : Willmott precipitation data corresponding to points in txclim; 12 monthly values; records correspond to points and fields correspond to time.

prec_tr.txt : transposed version of prec.txt with 12 months as records and spatial units as fields; this text file can be used by swbaltx.ave.

resev.ctl : control file for soil water balance calculations made with swbaltx.ave using reservoir evaporation estimates.

resevtx.txt, resevtx.dbf : resevtx.txt is the output file from pevapre.ave and contains reservoir evaporation estimates for each climate cell; resevtx.dbf contains the same data.

resevtr.txt : contains monthly reservoir evaporation estimates for each 1 degree quadrangle defined by /texas/evap/quadsp; quad-ids are records and months are fields.

surpre.dbf, stre.dbf, dstre.dbf, evapre.dbf : output files of swbaltx.ave using resev.ctl. These are surplus, soil moisture storage, and actual evaporation respectively. 12 monthly values (records) for each climate cell (fields).

surpretr.dbf, stretr.dbf : same data as surpré.dbf and stre.dbf but with data transposed; months are fields and spatial units are records.

surptx0.dbf, sttx0.dbf, dsttx0.dbf, evaptx0.dbf : output files of swbaltx.ave using txbal2.ctl. These are surplus, soil moisture storage, and actual evaporation respectively. 12 monthly values (records) for each climate cell (fields).

temp.txt : Willmott temperature data corresponding to points in txclim; 12 monthly values.

txbal2.ctl : control file for soil water balance calculations made with swbaltx.ave using Priestley-Taylor potential evaporation estimates.

texpev.ctl : control file used with the script pevap.ave that computes potential evaporation using the Priestley-Taylor method.

txpev.txt : monthly potential evaporation estimates made using the Priestley-Taylor method; fields correspond to cells in txclim.

txpevtr.dbf : transposed version of txpev.txt.

whold.avl : ArcView legend file used for displaying water holding capacity.

whold.txt : text file used to create the grid of water-holding capacity for the world.

COVERAGES:

./shpfiles/txevap.shp : shapefile with cells where computations were made; computed evaporation attributes : "jan," "feb," "mar," . . . etc. have been joined to this table; units are mm.

./shpfiles/txrun2.shp, ./shpfiles/txrun.shp : cells on which soil-water balance was computed; important attributes are "wholdavg" (average water-holding capacity) and "satur" which indicates the mean annual saturation of the soil; created from txclim.

txclim : point coverage where Willmott temperature and precipitation data are available; one point at the center of each 0.5 degree cell in geographic coordinates.

txclimp : txclim projected into an Albers projection with Texas State Mapping System (TSMS) parameters.

txclimt : polygons of climate cells in projected space; these polygons were created using thiess.aml; an attribute "wholdavg" was added by c_whold.ave which is the average water holding capacity.

txradc : polygon coverage of ~2.5 degree cells covering Texas with attributed with 96 months of net radiation data (W/m²) and mean monthly radiation for this 8 year period; polygons were reselected from a global coverage.

txradp : projected version of txradc.

whold : point coverage of locations where water holding capacity estimates are available.

wholdp : whold coverage projected into an Albers projection with Texas State Mapping System (TSMS) parameters.

wholdt : polygons of cells where water-holding capacity estimates are available in projected space; water-holding capacity (mm) is stored in the field "whold"; these polygons were created using thuess.aml.

wholditx : coverage wholdt intersected with the border of Texas; the field "whold" is water-holding capacity and "areawh" is "area" * "whold."

GRIDS:

bowen3: grid of Bowen ratios, 5 km cell size.

density: grid of water density at mean annual temperature, 5 km cell size.

latheat : grid of latent heat of vaporization as a function of mean annual temperature, 5 km cell size.

radmm3 : approximate water equivalent of mean annual net radiation in mm, 5 km grid.

p5radg: mean annual net radiation grid in Texas; projected and resampled to 5 km cells.

tempg: mean annual temperature grid for Texas, resampled from 0.5° to 5 km cells.

wholdg : grid of water-holding capacity for the world.

SPRINGS

springsc : coverage of 127 major springs in geographic coordinates.

springsp : coverage of 127 major springs in TSMS Albers.

spring3.txt : selected spring characteristics.

spr_tots.ave : calculates the sum of the maximum observed springflows in each watershed and adds the fields max_spf,max_spfmm to the coverage txmshdc3 which have units of cfs and mm/year respectively.

STFLOW

PROGRAMS:



adjflows.ave : make adjustments to streamflows for stations with incomplete periods of record.

anntoafy.ave, convunit.ave : Avenue scripts for unit conversion on selected fields.

calcavg.ave : script used to extract a list of stations and certain bits of station information from a dBase file exported from the Hydrosphere ROM ; also calculates annual flows averaged over the 30 year period 1961-1990.

calcyavg.ave : calculates annual average flows and stores the value for each year, not just the 30 year period 1961 - 1990.

inflow.ave : write net measured and potential inflow for currently selected set of points to a file.

majout.aml : reselect only points that are outlets to major basins.

make_win.aml : display graphics in the vicinity of a selected point.

outflow.ave : write net measured and potential outflow for currently selected set of points to a file.

pot_flow.ave : unit conversion script.

restrapd.aml : reselects outlet points that are not "trapped."

select.aml : AML used to create the coverage 30plus.

selout.aml : AML that allows the user to interactively select watershed outlets given a point coverage and a link grid.

PROJECT FILES:

flows1c.apr : project used to compute net inflows to delineated watersheds ; project used to create shdflows.dat -- INFO file containing net inflow and outflow.

OTHER TEXT OR DBASE FILES:

id.txt, id2.txt, id3.txt : files containing station IDs used to ensure the correct attributes get linked to the correct stations.

plus_st.txt : list of stations for which flow adjustments were made.

COVERAGES:

30plus : point coverage of 185 stations considered for delineation; attributed with mean flow, drainage area, etc.; here are the definitions of important fields:

staname = station name

start_yr, last_yr = start year and end year

startmonth
 jan_mean, feb_mean, etc. = mean monthly flow (cfs)
 ann_meanwr = mean flow in water year (cfs)
 ann_mean = mean flow in calendar year (cfs)
 drainarea = drainage are reported by USGS (km2)
 contrb_area = contributing area (km2)
 nn30 = 30 year mean flow (cfs)
 mf_afy = 30 year mean flow (acre-ft / year)
 missmonth = # of months in 30 year period with missing records

30year : point coverage of 164 stations with a complete record for 1961-1990; important fields:

staname = station name
 staryr, last_yr = start year and end year
 startmonth
 jan_mean, feb_mean, etc. = mean monthly flow (cfs)
 ann_meanwr = mean flow in water year (cfs)
 ann_mean = mean flow in calendar year (cfs)
 drainarea = drainage are reported by USGS (km2)
 contrb_area = contributing area (km2)

out1maj : major outlets.

out2n : point coverage of watershed outlets.

plus : point coverage of 21 stations without complete records for 1961-1990; same attributes as 30year.

reserb60 : reservoirs built before 1960.

reserp : all reservoirs with attributes.

stations, stationp : stations coverages before reselecting those with the appropriate 30 year records in geographic and projected space respectively.

txstat : same as w2statp less one point that was way out of Texas

w2stat : coverage of streamflow stations in Texas.

w2statp : projected coverage of streamflow stations.
